

Imbibition Oil Recovery from Montney Core Plugs: The Interplay of Surfactants, Osmotic
Potential, and Wettability

by

Lin Yuan

A thesis submitted in partial fulfillment of the requirements for the degree of

Master of Science

in

Petroleum Engineering

Department of Civil & Environmental Engineering
University of Alberta

© Lin Yuan, Fall 2019

Abstract

Due to advances in hydraulic fracturing technology, hydrocarbon can now be produced at economic rates from unconventional resources with ultralow permeability and porosity. However, in general, over 90% of the original oil in place cannot be produced after hydraulic fracturing operations. Recent core analysis and wettability studies indicate that most of the remaining oil is trapped in sub-micron oil-wet pores, which can hardly be accessed by water. Subsequent EOR operations or re-fracturing jobs for producing the remaining oil are attractive but expensive and in some cases risky due to insufficient information on downhole completion conditions. In this study, we characterize rock-fluid properties such as wettability and pore size distribution to understand the mechanisms controlling oil recovery from tight rocks. We evaluate the idea of adding surfactants and nanoparticles in fracturing water to enhance its wetting affinity to oil-wet pores and to mobilize part of the oil during the extended shut-in periods.

In this study, we conducted a series of rock-fluid experiments to investigate 1) wettability of several core plugs from the Montney Formation and its correlations with other petrophysical properties such as pore-throat size distribution, and 2) the effects of wettability, salinity, microemulsion (ME) and nanoparticle additives of different concentrations on imbibition oil recovery. First, we evaluated wettability by conducting spontaneous imbibition experiments using reservoir oil and brine on six twin core plugs from the Montney Formation. In addition, we investigated the correlations between wettability and other petrophysical properties obtained from MICP data and tight-rock analyses. Second, we injected oil into partly brine-saturated core plugs to arrive at residual water saturation. Third, we performed soaking experiments on oil-saturated core plugs using fresh water, reservoir brine, and a ME system, and measured the volume of

produced oil with respect to time. The soaking fluids were characterized by measuring density, viscosity, surface tension (ST) and interfacial tension (IFT). We also evaluated nanoparticle-assisted imbibition oil recovery by conducting systematic contact-angle and counter-current imbibition tests under different conditions of brine salinity and nanoparticles concentration.

We observe faster and higher oil imbibition into the core plugs compared with brine imbibition, suggesting strong affinity of the samples to oil. The equilibrated normalized imbibed volume of oil (I_o^{eq}) positively correlates with the volume fraction of small pores, represented by the tail part of MICP pore-throat size distribution profiles. This suggests that the tight parts of the pore network which contain reservoir oil under in-situ conditions are preferentially oil-wet. The results of soaking experiments show that imbibition oil recovery positively correlates with the water-wet porosity measured by spontaneous brine imbibition into the dry core plugs. Fresh water imbibition results in around 3% (of initial oil volume in place) higher oil recovery compared with that of brine imbibition, possibly due to osmotic potential. Soaking the oil-saturated core plugs in ME solution after brine or fresh water soaking results in 1-2% incremental oil recovery. Soaking the oil-saturated core plugs immediately in ME solution results in faster oil recovery compared with the case when the plugs are first soaked in water and then in ME solution. Contact angle tests indicate that all the core plugs tend to be oil-wet in the presence of reservoir brine and fresh water. However, the results of dynamic contact angle measurements show that the nanoparticle additives in reservoir brine and fresh water make the rock water-wet by decreasing the water contact angle from more than 90 to less than 60. Wettability alteration is more pronounced in the presence of fresh water than reservoir brine. The imbibition oil-recovery tests show faster and higher oil recovery in the presence of the nanoparticle additives compared with the reference cases of brine

and fresh water, consistent with the results of contact-angle tests. The mechanism behind wettability alteration and oil recovery can be explained by structural disjoining pressure.

Preface

This thesis is an original work by Lin Yuan.

In Chapter 3, the tight rock analysis, mineralogy and rock-eval analysis (in 3.2.1, 3.2.2, 3.2.3 respectively) were conducted by commercial companies.

Chapter 3, 4 and 5 of this thesis has been published as Yuan, L., Dehghanpour, H., and Ceccanese, A. (2019, April). “Imbibition Oil Recovery from the Montney Core Plugs: The Interplay of Wettability, Osmotic Potential and Microemulsion Effects”. In SPE Western Regional Meeting. Society of Petroleum Engineers. I was responsible for conducting experiments, analyzing the experimental data, writing and editing this thesis. Ann Ceccanese, A was responsible for reviewing the paper and securing company approvals for publishing the paper. Hassan Dehghanpour was the supervisory author and was were responsible for reviewing the paper and providing technical feedbacks.

Dedication

To my dearest parents,

Mrs. Yunfang He, and Mr. Kunben Yuan.

Acknowledgements

I would like to express my sincere gratitude to my supervisor Dr. Hassan Dehghanpour for his patient and insightful guidance, continuous support, kind encouragement throughout my master study. He is like a light tower during my studying journey over the past years. My master study and research would not have been finished without his help. His kindness and guidance will have a profound influence on my future career and life.

I am deeply thankful to my parents Mr. Kunben Yuan and Mrs. Yunfang He for their moral support, continuous understanding and encouragement. They are always behind me with endless love whenever I meet difficulties.

I would like to give my special thanks to Dr. Mahmood Reza Yassin, Dr. Ali Habibi, and Dr. Obinna Ezulike for their valuable comments, suggestions and assistance on my master research. This dissertation could not have been completed without their help.

I am grateful to my past and present colleagues (Yanmin Xu, Yingkun Fu, Mingxiang Xu, Yue Shi, Ashkan Zolfaghari, Sara Eghbali, Maryam Eghbalvala, Mohammad Yousefi, Mohammad Hossein Doranehgard, Mohammad Sabbir Hossain, Son Tran, Tamer Moussa, Taregh Soleiman Asl, Momotaj Begum, Hamidreza Yarveicy, Shiyu Xu, and Yanze Zhang) for their insightful contributions and fruitful discussions.

I would also like to acknowledge the Natural Sciences and Engineering Research Council of Canada (NSERC) and Birchcliff Energy for providing the research funding for this study.

Tables of Contents

Abstract.....	ii
Preface.....	v
Dedication	vi
Acknowledgements	vii
List of Tables	xi
List of Figures.....	xiii
Chapter 1 Introduction.....	1
1.1 Background	1
1.2 Objectives of Research.....	4
1.3 Structure of Thesis	4
Chapter 2 Literature Review	6
2.1 Dual-Wet Behavior	6
2.1.1 Theory of Spontaneous Imbibition in Dual-Wet Systems.....	6
2.1.2 Previous Studies on Unconventional Rocks with Dual-Wet Behavior	7
2.2 Imbibition Oil Recovery	9
2.3 Surfactant Enhanced Oil Recovery	10
Chapter 3 Overview and Characteristics of Montney Tight Rocks	12
3.1 Background of Montney Formation.....	12
3.2 Core plugs from Montney Formation.....	14
3.2.1. Tight-Rock Analysis (TRA)	15
3.2.2. Mineralogy.....	16
3.2.3. Rock-Eval Pyrolysis	17

3.2.5. SEM Images	18
Chapter 4 Wettability Analysis and Pore Characterization of Montney Tight Oil Rocks..	20
4.1 Materials.....	20
4.1.1 Rock Samples	20
4.1.2 Fluid Samples	21
4.2 Methodology	22
4.2.1 Air-Liquid Contact-angle measurements.....	23
4.2.2 Spontaneous Imbibition on Dry Core Plugs	24
4.3 Results	25
4.3.1 Air-Liquid Contact-Angle Measurements	25
4.3.2 Spontaneous Imbibition on Dry Core Plugs.....	26
4.4 Discussions.....	28
4.4.1 Calculation of Wettability Index	28
4.4.2 Effective Porosity	29
4.4.4 Correlations between Imbibition and MICP Profiles	30
4.4.5 Correlation between Normalized Imbibed Volume of Oil (I_o) and $\phi_{\text{small-pore}}$	35
4.4.6 Correlations among Initial Oil Saturation (S_o), $\phi_{\text{small-pore}}$, and I_o	36
Chapter 5 Counter-current Imbibition Experiments on MT Samples: Evaluating Controlling Factors of Imbibition Oil Recovery	38
5.1 Materials.....	38
5.1.1 Core Samples	38
5.1.2 Fluid Samples	43
5.2 Methodology	45
5.2.1 Liquid-Liquid Contact Angle (CA)	45
5.2.2 Soaking Experiments	45

5.3 Results and Discussions	46
5.3.1 Liquid-Liquid Contact Angle	46
5.3.2 The Effect of Brine Effective Porosity (ϕ_{ew}) of Core Plugs on Oil Recovery	48
5.3.3 The Effect of Brine Salinity on Oil RF.....	50
5.3.4 The Impact of Surfactant on Imbibition Oil Recovery.....	55
5.3.5 Solvent Contribution to Oil Production.....	58
Chapter 6 Chemical EOR While Fracturing: Wettability Alteration by Nanoparticle Additives	60
6.1 Fluid samples.....	60
6.2 Methodology	61
6.2.1 Dynamic Liquid-liquid Contact-Angle (CA) Measurements	61
6.2.2 Soaking Experiments.....	62
6.3 Results and Discussions	62
6.3.1 Contact-Angle (CA) Measurements	62
6.3.2 Soaking tests.....	67
6.3.3 Effects of wettability on Imbibition Oil Recovery	70
Chapter 7 Conclusions and Recommendations for Future Study	73
7.1 Conclusions	73
7.2 Recommendations for Future Work.....	74
References	76
Appendix A: Dynamic Contact-Angle Measurements of Nanoparticle Solutions	82
Appendix B: Capillary-driven Imbibition Model	94

List of Tables

Table 3.1 Depth, original mass, diameter and length of the core plugs from the Montney Formation.	14
Table 3.2 Measured values of permeability, effective porosity, and grain density of the core samples.....	15
Table 3.3 Mineralogy of the core plugs determined from XRD method.....	16
Table 3.4 The results of rock-eval pyrolysis on offset samples.....	18
Table 4.1 Depth, original mass, diameter and length of the core plugs from the Montney Formation.	21
Table 4.2 Brine properties.....	21
Table 4.3 Oil properties.	22
Table 4.4 Air-liquid contact angles of oil and brine on the surface of fresh (dry) core samples..	25
Table 4.5 The equilibrated time, equilibrated imbibed volume and initial imbibition rate of oil and brine imbibition profiles.	28
Table 4.6 The values of WI_o for the 6 twin core plugs.	29
Table 4.7 Effective porosity of core plugs to oil and brine.	30
Table 4.8 The calculated small pore porosity ($\phi_{\text{small-pore}}$) ratio of oil capillary pressure to water capillary pressure for each twin core plug from imbibition data and Young-Laplace equation...	34
Table 5.1 Measured values of oil effective permeability and residual water saturation (end point).	42
Table 5.2 Depth, original mass, diameter and length of the core plugs from the Montney Formation.	43
Table 5.3 Properties of the aqueous fluids used for the soaking experiments.....	44

Table 5.4 The calculated capillary pressure during imbibition oil recovery process for different soaking fluid samples.....	57
Table 5.5 The calculated solvent which has been contacted with oil during ME soaking.	59
Table 6.1 Properties of the aqueous fluids used for the CA experiments.....	61
Table 6.2 The CA ranges of oil droplet on the surface of oil-saturated end pieces immersed into different aqueous fluids for the first 10 hours.....	63
Table 6.3 The calculated capillary pressure for different soaking fluid samples	67
Table 6.4 Capillary Pressure Inverse Bond Number Values for Different Soaking Fluid Samples	72
Table B.1 The ratio of oil capillary pressure to water capillary pressure for each twin core plug from imbibition data and Young-Laplace equation.....	96

List of Figures

Figure 2.1 Schematic view of (a) co-current spontaneous imbibition test and (b) non-piston-like oil and brine imbibition into the idealized bundle of capillaries (Shi et al., 2018 and 2019).....	7
Figure 2.2 Comparative spontaneous imbibition tests of oil (a, c) and brine (b, d) into the upper UMT and LMT samples (Lan et al., 2015).....	8
Figure 3.1 Location and depositional stratigraphy of Montney Formation. (NEB et al., 2013; Nieto et al., 2009)	13
Figure 3.2 Cross section of the Montney Formation. (NEB, 2013).....	13
Figure 3.3 Thin sections of core plugs taken from Well A at 2188.35 m (a and b), 2194.81 m (c and d), 2198.86 m (e and f), and 2216.24 m (g and h), under plane polarized light.	17
Figure 3.4 Cross-plots of (a) hydrogen index vs. oxygen index, and (b) production index vs. T_{max} . The Montney samples have type III kerogen and are immature except MT-B2 that is in oil window.	18
Figure 3.5 SEM images from core plug MT-B2. The pore network can be divided into large pores (> 100 nm) and small sub-micron pores (< 50 nm).	19
Figure 4.1 Mass loss (%) of heated plugs vs. time: (a) Well A samples, (b) Well B samples. The heating temperature is 90°C	23
Figure 4.2 Contact angle meter.....	24
Figure 4.3 Schematic of the imbibition setup.	24
Figure 4.4 Air-liquid contact angles of (a) brine and (b) oil droplets on polished surfaces of MT-A1.....	26
Figure 4.5 Profiles of normalized imbibed volume of (a) oil (I_o) and (b) brine (I_w) for 6 pairs of twin core plugs.....	27
Figure 4.6 Effective porosity measured by Boyle's law helium porosimetry versus effective porosity to (a) oil and (b) brine obtained by equilibrated imbibed volume of oil and brine.	30

Figure 4.7 The pore-throat size distribution of the core plugs. Cumulative intrusion volume (% of total intrusion volume) and percent intrusion (mL/g) vs. pore-throat radius (nm) for samples from Well A (a, c, e) and Well B (b, d, f).....	31
Figure 4.8 The Normallized imbibed oil volume (I_o) versus small-pore porosity ($\phi_{\text{small-pore}}$) for different values of pore-throat size cut-off.	35
Figure 4.9 R^2 of the fitted regression lines for different threshold values of pore-throat radius. We select 30 nm (having the highest R^2) as the threshold pore-throat radius for defining small pores.	35
Figure 4.10 (a) I_o (%PV) vs. $\phi_{\text{small-pore}}$; (b) $I_o - I_w$ (%PV) vs. $\phi_{\text{small-pore}}$	36
Figure 4.11 Correlation between (a) $\Phi_{\text{small-pore}}$ vs. S_o and (b) I_o vs. S_o of samples from Well A.	37
Figure 5.1 Vinci core-flooding system	39
Figure 5.2 Pressure difference profiles during oil flooding of core plugs of (a) MT-B1, (b) MT-B2, (c) MT-B3, (d) MT-A1, (e) MT-A2, and (f) MT-A3.....	40
Figure 5.3 Oil effective permeability versus water saturation at residual water saturation (end point) for different core plugs from Wells A and B.	42
Figure 5.4 The instrument used for physical properties measurements: (a) SIGMA 700 Tensiomer and (b) Brookfiled Viscometer	44
Figure 5.5 Spinning drop tensiometer.....	45
Figure 5.6 Amott cell used for soaking of oil-saturated core plugs in different soaking fluids. ..	46
Figure 5.7 The contact angles of oil droplets equilibrated on the surface of oil-saturated core sample MT-A1 immersed in (a) fresh water, (b) brine, (c) brine + ME, (d) fresh water + ME. (Experimental time =10 minutes).	48
Figure 5.8 Oil RF vs. time for 6 oil-saturated core plugs immersed in brine and ME solutions (brine with ME).....	49
Figure 5.9 The comparison between brine imbibition volume (V_b) and oil production volume (V_o). Generally, $V_b > V_o$ indicates that brine may imbibe into part of the hydrophilic pores to expel the oil out	50

Figure 5.10 Oil RF versus ϕ_{ew}	50
Figure 5.11 Comparison of oil recovery factor for Well B twin core plugs immersed in different soaking fluids (brine, fresh water, and ME solutions (brine with ME and fresh water with ME)).	51
Figure 5.12 SEM images from core plug MT-B2. The clay minerals are categorized as illite/mica.	53
Figure 5.13 The elemental spectrums determined by EDS analysis of area 1 & 2 in Fig 5.12 (b) & (c).	54
Figure 5.14 The Measured electrical conductivity profile when a dry end-piece of MT-B1 immersed in fresh water.....	55
Figure 5.15 Comparing oil recovery profiles for MT-A3 and the three core plugs of Well B immersed in fresh water and fresh water plus ME.	57
Figure 6.1 The Liquid-liquid contact angels of oil droplet on the oil-saturated end pieces immersed in (a) fresh water; (b) brine; (c) fresh water + additive 1 (5 wt%); (d) brine + additive 2 (1.89 cc/L); (e) brine + additive 1 (5 wt%); (f) fresh water + additive 1 (10 wt%); (g) brine + additive 2 (3.78 cc/L); (h) brine + additive 1 (10 wt%); (i) fresh water + additive 1 (35 wt%);(j) brine + additive 2 (7.56 cc/L); (k) brine + additive 1 (35 wt%)(time =10 minutes).	64
Figure 6.2 The structural disjoining pressure gradient mechanism at the wedge vertex drives the nanofluid spreading due to nanoparticle structuring in the wedge-film (from Wassan et al., 2011).	65
Figure 6.3 The oil recovery of MT-A1 (right side) soaked by fresh water with additive 1 and MT-A2 (left side) soaked by fresh water with additive 2. The soaking time is 45 days.	68
Figure 6.4 Oil RF vs. time for twin core plugs MT-A1 and MT-A2 immersed in brine and fresh water + nanoparticle solutions respectively.	69
Figure 6.5 Oil RF vs. time for MT-A1, MT-A2 and MT-A3 immersed in fresh water + nanoparticle additive 1, water + nanoparticle additive 2 and water + microemulsion (ME) solutions respectively.	70

Figure A.1 The CA changes of oil droplet with time on the surface of oil-saturated end piece immersed into brine. a) CA at 1 min; b) CA at 10 min; c) CA at 60 min; d) CA at 180 min; e) CA at 300min; a) CA at 600 min.....	82
Figure A.2 The CA changes oil droplet versus experimental time for oil-saturated end piece immersed into brine.	83
Figure A.3 The CA changes of oil droplet with time on the surface of oil-saturated end piece immersed into fresh water. a) CA at 1 min; b) CA at 10 min; c) CA at 60 min.....	83
Figure A.4 The CA changes of oil droplet with time on the surface of oil-saturated end piece immersed into fresh water with additive 1 (5 wt%). a) CA at 1 min; b) CA at 10 min; c) CA at 60 min; d) CA at 180 min; e) CA at 300min; a) CA at 600 min.	83
Figure A.5 The CA changes oil droplet versus experimental time for oil-saturated end piece immersed into fresh water with additive 1 (5 wt%).....	84
Figure A.6 The CA changes of oil droplet with time on the surface of oil-saturated end piece immersed into fresh water with additive 1 (10 wt%). a) CA at 1 min; b) CA at 10 min; c) CA at 60 min; d) CA at 180 min; e) CA at 300min; a) CA at 600 min.	85
Figure A.7 The CA changes oil droplet versus experimental time for oil-saturated end piece immersed into fresh water with additive 1 (10 wt%).....	86
Figure A.8 The CA changes of oil droplet with time on the surface of oil-saturated end piece immersed into fresh water with additive 1 (35 wt%). a) CA at 1 min; b) CA at 10 min; c) CA at 60 min; d) CA at 180 min; e) CA at 300min; a) CA at 600 min.	86
Figure A.9 The CA changes oil droplet versus experimental time for oil-saturated end piece immersed into fresh water with additive 1 (35 wt%).....	87
Figure A.10 The CA changes of oil droplet with time on the surface of oil-saturated core sample MT-A1 immersed into brine with nanoparticle additive 1 (5%wt). a) CA at 1 min; b) CA at 10 min; c) CA at 60 min; d) CA at 180 min; e) CA at 300min; a) CA at 600 min.....	87
Figure A.11 The CA changes oil droplet versus experimental time for oil-saturated end piece immersed into brine with additive 1 (5 wt%).	88

Figure A.12 The CA changes of oil droplet with time on the surface of oil-saturated core sample MT-A1 immersed into brine with additive 1 (10%wt). a) CA at 1 min; b) CA at 10 min; c) CA at 60 min; d) CA at 180 min; e) CA at 300min; a) CA at 600 min.	88
Figure A.13 The CA changes of oil droplet with time on the surface of oil-saturated core sample MT-A1 immersed into brine with additive 1 (35%wt). a) CA at 1 min; b) CA at 10 min; c) CA at 60 min.	89
Figure A.14 The CA changes oil droplet versus experimental time for oil-saturated end piece immersed into brine with additive 1 (35 wt%).	89
Figure A.15 The CA changes of oil droplet with time on the surface of oil-saturated end piece immersed into fresh water with additive 2 (1.89 cc/L). a) CA at 1 min; b) CA at 10 min; c) CA at 60 min; d) CA at 180 min; e) CA at 300min; a) CA at 600 min.	90
Figure A.16 The CA changes oil droplet versus experimental time for oil-saturated end piece immersed into fresh water with additive 2 (1.89 cc/L).	91
Figure A.17 The CA changes of oil droplet with time on the surface of oil-saturated end piece immersed into fresh water with additive 2 (3.78 cc/L). a) CA at 1 min; b) CA at 10 min; c) CA at 60 min; d) CA at 180 min; e) CA at 300min; a) CA at 600 min.	91
Figure A.18 The CA changes oil droplet versus experimental time for oil-saturated end piece immersed into fresh water with additive 2 (3.78 cc/L).	92
Figure A.19 The CA changes of oil droplet with time on the surface of oil-saturated end piece immersed into fresh water with additive 2 (7.56 cc/L). a) CA at 1 min; b) CA at 10 min; c) CA at 60 min; d) CA at 180 min; e) CA at 300min; a) CA at 600 min.	92
Figure A.20 The CA changes oil droplet versus experimental time for oil-saturated end piece immersed into fresh water with additive 2 (7.56 cc/L).	93
Figure B.1 Normalized imbibed volume of oil (a) and brine (b) into 6 pairs of twin core plugs vs. square root of time	96
Figure B.2 $(P_{co}/P_{cw})_{\text{Young-Laplace}}$ vs. $(P_{co}/P_{cw})_{\text{imbibition}}$	97

Nomenclature

A_c	Cross-sectional area of the core plug, L^2
$f_{small-pore}$	Tolome fraction of small pores (in % of total PV).
h	Film thickness, L
I_o	Normalized imbibed volume of oil
I_w	Normalized imbibed volume of oil at equilibrium state
I_o^{eq}	Normalized imbibed volume of water at equilibrium state
I_w^{eq}	Normalized imbibed volume of water
K	Fluid effective permeability, L^2
K_o	Effective permeability of oil at the end point, L^2
m_o	Imbibition slope of oil, t^{-1}
m_b	Imbibition slope of brine, t^{-1}
P_C	Capillary pressure, MLT^{-2}
ΔP	The pressure difference along the core plug (inlet pressure-outlet pressure), MLT^{-2}
Q_{oil}	Injection oil rate, $l^{-2}T^{-1}$
r	Pore radius, L
r_o	Average pore radius for oil imbibition flow, L
r_w	Average pore radius for water imbibition flow, L
S	Spreading coefficient
S_w	Water Saturation
S_o	Oil Saturation
S_f	Fluid saturation behind the imbibition front
V	Imbibed wetting fluid volume, L^3

WI_o	Wettability Index of oil
WI_w	Wettability Index of water
μ	Viscosity, $ML^{-1}t^{-1}$
μ_{oil}	Viscosity of oil, $ML^{-1}t^{-1}$
ρ	Density, ML^{-3}
σ	Surface tension or interfacial tension, Mt^{-2}
ϕ	Effective porosity
ϕ_{eo}	Effective porosity of the core plugs to oil
ϕ_{ew}	Effective porosity of the core plugs to brine
$\phi_{small-pore}$	Small-pores porosity
$\phi_{inaccessible}$	The porosity of inaccessible pores which cannot be invaded by Mercury
ϕ_{MICP}	The porosity of rock samples measured by MICP method
$\Pi(h)$	Disjoining pressure of a wetting film, MLT^{-2}

Abbreviations

CA	Contact Angle
EDS	Energy-Dispersive x-ray Spectroscopy
HI	Hydrogen index
ITA	Imbibition-Transient-Analysis
IFT	Interfacial Tension
MICP	Mercury Injection Capillary Pressure
ME	Microemulsion
NGL	Natural Gas Liquid
NMR	Nuclear Magnetic Resonance
OI	Oxygen Index
PSD	Pore Size Distribution
PV	Pore Volume
PI	Production Index
ST	Surface Tension
SEM	Scanning Electron Microscope
TOC	Total Organic Carbon
TRA	Tight Rock Analysis
USBM	US Bureau of Mines
Y-L	Young-Laplace
DLVO	Derjaguin, Landau, Verwey, and Overbeek Theory

Chapter 1 Introduction

1.1 Background

Due to worldwide growth in energy demand, unconventional resources (tight and shale reservoirs) have become important targets for hydrocarbon production (Cui et al., 2013; Khlaifat et al., 2011). Hydrocarbon in unconventional resources with ultralow permeability and porosity can be produced at economic rates by hydraulically-fractured horizontal wells (He et al., 2015). Efficient hydrocarbon recovery requires characterization of rock and fluid properties such as wettability, pore-throat size distribution (PSD), capillary pressure, and relative permeability for selecting optimal fracturing and EOR fluids (Kamari et al., 2014; Yassin et al., 2016). Rock wettability controls the distribution of fluid phases (oil, water, and gas) at pore scale which affects rock/fluid properties such as capillary pressure and waterflood behavior (Lan et al., 2015; Yassin et al., 2018; Morrow 1990). Wettability characterization is significant for 1) understanding fluid transport mechanisms, 2) selecting representative fluid-flow models (Yassin et al., 2017), and 3) selecting optimal fracturing fluid and EOR additives (Momotaj et al., 2017). Techniques for estimating rock wettability include equilibrium contact-angle measurements (Johnson and Dettre, 1969), spontaneous imbibition tests (Ma et al., 1999; Bobek et al., 1958), US Bureau of Mines (USBM) index (Donaldson et al., 1969), and nuclear magnetic relaxation (Brown and Fatt, 1956). Due to the low permeability and dual-wet pore network (Yassin et al., 2017) of tight rocks, it is challenging to use conventional methods such as USBM for evaluating their wettability.

Recent studies show that rock wettability can be characterized using comparative imbibition tests (Lan et al., 2015; Xu and Dehghanpour, 2014). Lan et al. (2015) measured and compared spontaneous imbibition of oil and brine in dry core plugs from the Montney tight-gas Formation.

They showed that imbibed oil volume is significantly higher than imbibed brine volume. They concluded that strong wetting affinity of the samples to oil is due to the abundant hydrophobic nanopores within or coated by solid bitumen. Yassin et al. (2017) extended Lan et al. (2015)'s work by analyzing scanning electron microscopy (SEM) images, energy-dispersive x-ray spectroscopy (EDS) images, mercury injection capillary pressure (MICP) measurements, and tight-rock analysis (TRA) results. SEM/EDS analyses showed the abundance of nanopores within organic matter. Based on these analyses, they proposed the dual-wet theory: nanopores within or coated by pyrobitumen/solid bitumen are strongly hydrophobic with negligible wetting affinity to the aqueous phase, while micropores bordered by inorganic minerals such as quartz and calcite are hydrophilic. However, they did not investigate the correlations between imbibition profiles and pore-throat size distribution of the core plugs.

During waterflooding in fractured reservoirs, water spontaneously imbibes into oil-saturated matrix and expels the oil out (Salehi et al., 2008; Kathel et al., 2013). Javaheri et al. (2018) conducted soaking tests on several Montney core plugs using produced brine. They found that oil-recovery curves follow the trend of brine-imbibition curves in the corresponding dry plugs, and that the oil recovery is always less than the volume of brine imbibed into the dry plugs. They argued that the oil produced during the soaking tests mainly comes from hydrophilic pores, which are accessible to the imbibing brine. The imbibition oil recovery is low in oil-wet reservoirs due to the weak driving capillary force (Mohan et al., 2011). Wettability alternation of the reservoir rock from an oil-wet state to a water-wet state can improve the performance of fracturing treatment and, consequently oil recovery factor (Alvarez et al., 2017). Rock wettability can be modified by different parameters such as pH, brine salinity, temperature, structure of surfactant, surfactant concentration (Wang et al., 2012; Yarveicy et al., 2017). Wettability can be favorably altered by

dissolving proper concentrations of surfactants in fracturing fluids (Salehi et al., 2008; Mohan et al., 2011). Wang et al. (2012) conducted wettability tests using four surfactant formulations on Bakken cores which were generally oil- or intermediate-wet. They concluded that the four surfactant formulations altered the wettability of Bakken shale cores from oil-wet to water-wet, having a substantial potential to imbibe into cores and expel oil out, leading to higher imbibition oil recovery. Alvarez et al. (2017) combined wettability alteration and IFT reduction to investigate and compare the imbibition capability of different surfactants in cores from unconventional liquid-rich reservoirs. They found that all surfactants at field-scale concentrations can change the wettability of cores from oil- and intermediate-wet to water-wet. Anionic surfactants better reduced IFT and better improved oil recovery from shale cores than non-ionic surfactants with lower contact angles. Yassin et al. (2018) measured wettability and characterized pore networks of shale samples from the Duvernay Formation to investigate oil-recovery mechanisms by imbibition of different soaking fluids including water with surfactant or clay stabilizer. They found that soaking fluids with lower IFT yield higher oil recovery factor (RF) since they can wet a larger part of the dual-wet pore network. However, the investigations on the effects of salinity and initial water saturation on oil recovery are still not very clear.

In the first part of the study, we present petrophysical properties, mineralogy, and rock-eval pyrolysis results of several core plugs from two wells (Wells A and B in condensate and oil windows, respectively) drilled in the lower Montney Formation. We conduct contact-angle and co-current spontaneous-imbibition tests to evaluate wettability and its dependence on PSD curves obtained from MICP tests. In the second part, we conduct counter-current imbibition experiments (soaking tests) on oil-saturated core plugs using brine, fresh water and a microemulsion solution, and investigate the dependence of the measured oil recovery on wettability of the core plugs and

properties of the soaking fluids. We also evaluate nanoparticle-assisted imbibition oil recovery during the shut-in time by conducting systematic contact-angle and counter-current imbibition tests under different conditions of brine salinity and nanoparticles concentration

1.2 Objectives of Research

The objectives of this study are as follows:

- 1) Characterize the wettability of Montney tight rocks and investigate its dependence on other petrophysical properties.
- 2) Investigate possible correlations between imbibition (oil and water) curves and pore-throat size distribution profiles from MICP tests.
- 3) Investigate the effects of wettability, salinity, initial water and ME on imbibition oil recovery.
- 4) Investigate the effects of nanoparticle additives on imbibition oil recovery and wettability change by conducting systematic contact-angle and counter-current imbibition tests under different conditions of brine salinity and nanoparticles concentration

1.3 Structure of Thesis

Chapter 1 briefly introduces the research background, research gap and objectives of this study.

Chapter 2 reviews previous studies on rock-fluid interactions and water flooding.

Chapter 3 briefly introduces the Montney Formation and describes the mineralogy, porosity, permeability, SEM analysis and MICP profiles of Montney samples.

Chapter 4 presents the results of contact-angle measurements and spontaneous imbibition experiments. The wettability analysis and pore characterization are analyzed based on imbibition and MICP results.

Chapter 5 investigates the factors controlling imbibition oil recovery including salinity of soaking fluid, initial water saturation, and ME solution by conducting counter-current imbibition experiments (soaking experiments) on Montney oil-saturated samples.

Chapter 6 presents the evaluation of nanoparticle-assisted imbibition oil recovery during the shut-in time by conducting systematic contact-angle and counter-current imbibition tests under different conditions of brine salinity and nanoparticles concentration.

Chapter 7 summarizes the main findings and conclusions of this study and provides recommendations for future studies.

Chapter 2 Literature Review

2.1 Dual-Wet Behavior

2.1.1 Theory of Spontaneous Imbibition in Dual-Wet Systems

Shi et al. (2018 and 2019) proposed an imbibition-transient-analysis (ITA) technique to characterize dual-wet pore networks, in which larger pores are hydrophilic while small pores are hydrophobic (see **Fig 2.1**). They considered the pore network as a bundle of tortuous capillaries with different diameters (**Fig 2.1b**). The idealized pore network is considered as a dual-wet system, where larger pores are among hydrophilic inorganic minerals while smaller pores are mainly within hydrophobic organic materials. Oil can imbibe into both large inorganic pores and small organic pores while brine can only imbibe into inorganic pores.

For spontaneous imbibition tests by using oil and brine (**Fig 2.1a**), all pores are considered to be in contact with the wetting liquid at the bottom part of the rock sample. The imbibition process in all the pores starts simultaneously. The Lucas-Washburn (L-W) Equation (Lucas, 1918; Washburn, 1921) can be used to describe the imbibition of wetting liquid into tortuous capillaries under laminar flow conditions. According to the L-W equation, the imbibition height and mass versus time is proportional to the square root of pore diameter. Therefore, the imbibing liquid fills the larger capillaries first, and thus the imbibition process is a non-piston-like displacement. Schembre et al. (1998) and Gruener et al. (2016) observed the non-piston-like liquid front by neutron imaging and X-ray computerized tomography scanning, respectively.

Fig 2.1b shows the non-piston-like oil and brine imbibition into idealized bundle of capillaries. At Stage 1, the dry rock samples are saturated with air initially (initial water saturation, $S_w = 0$). At Stage 2, oil imbibe into most of the pores while brine can only imbibe into large hydrophilic pores.

The imbibition rate of oil is higher than that of brine since higher number of pores are accessible to oil. At Stage 3, oil in large pores has reached the top of core plug and only small pores are imbibing oil since the imbibition rate is higher in larger pores. For brine imbibition, brine has reached the equilibrated state since brine can only imbibe into the larger hydrophilic pores. At Stage 4, oil imbibition has also reached the equilibrated state. As discussed above, non-piston-like liquid imbibition into the idealized bundle of capillaries can explain the results of the imbibition tests for the Montney rock samples with dual-wet characteristics.

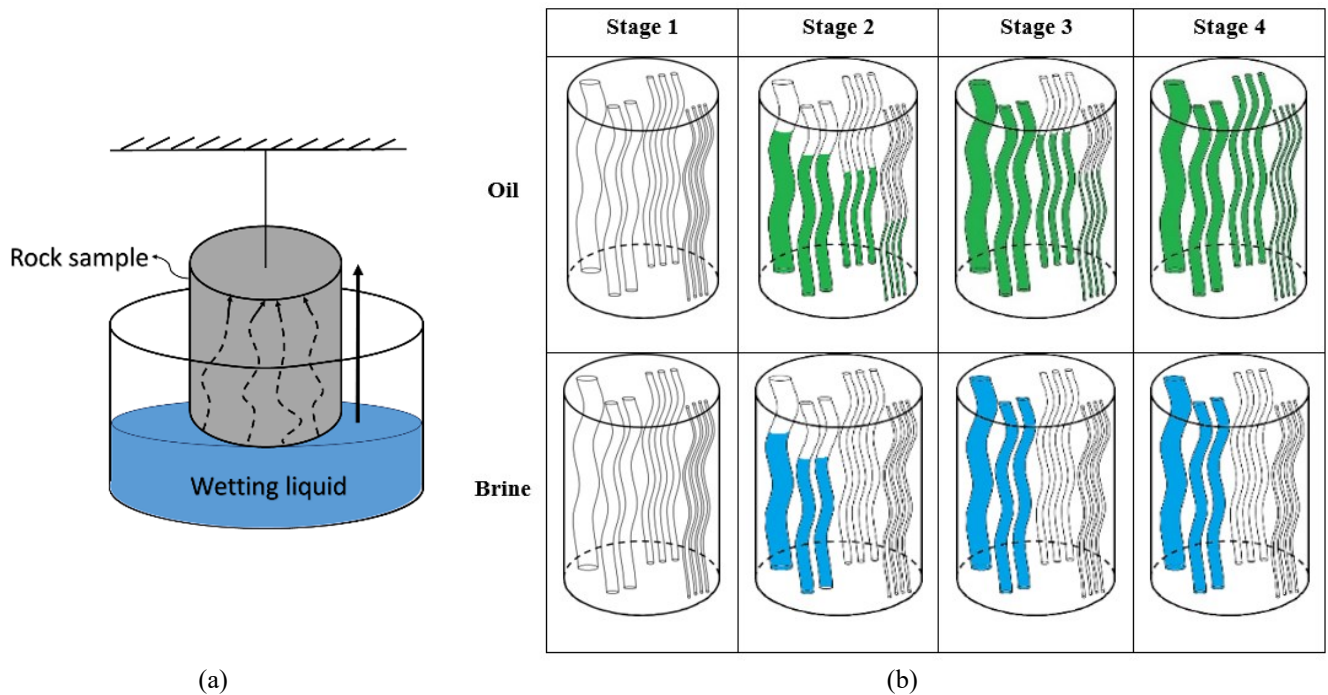


Figure 2.1 Schematic view of (a) co-current spontaneous imbibition test and (b) non-piston-like oil and brine imbibition into the idealized bundle of capillaries (Shi et al, 2018 and 2019).

2.1.2 Previous Studies on Unconventional Rocks with Dual-Wet Behavior

Lan et al. (2015) conducted spontaneous imbibition experiments on core plugs from different depths of a well drilled in the Montney formation. They placed the dry core plugs inside imbibition cells filled with oil or brine by exposing only the bottom face of plugs to the wetting liquid. The weight gains of core plugs were measured periodically.

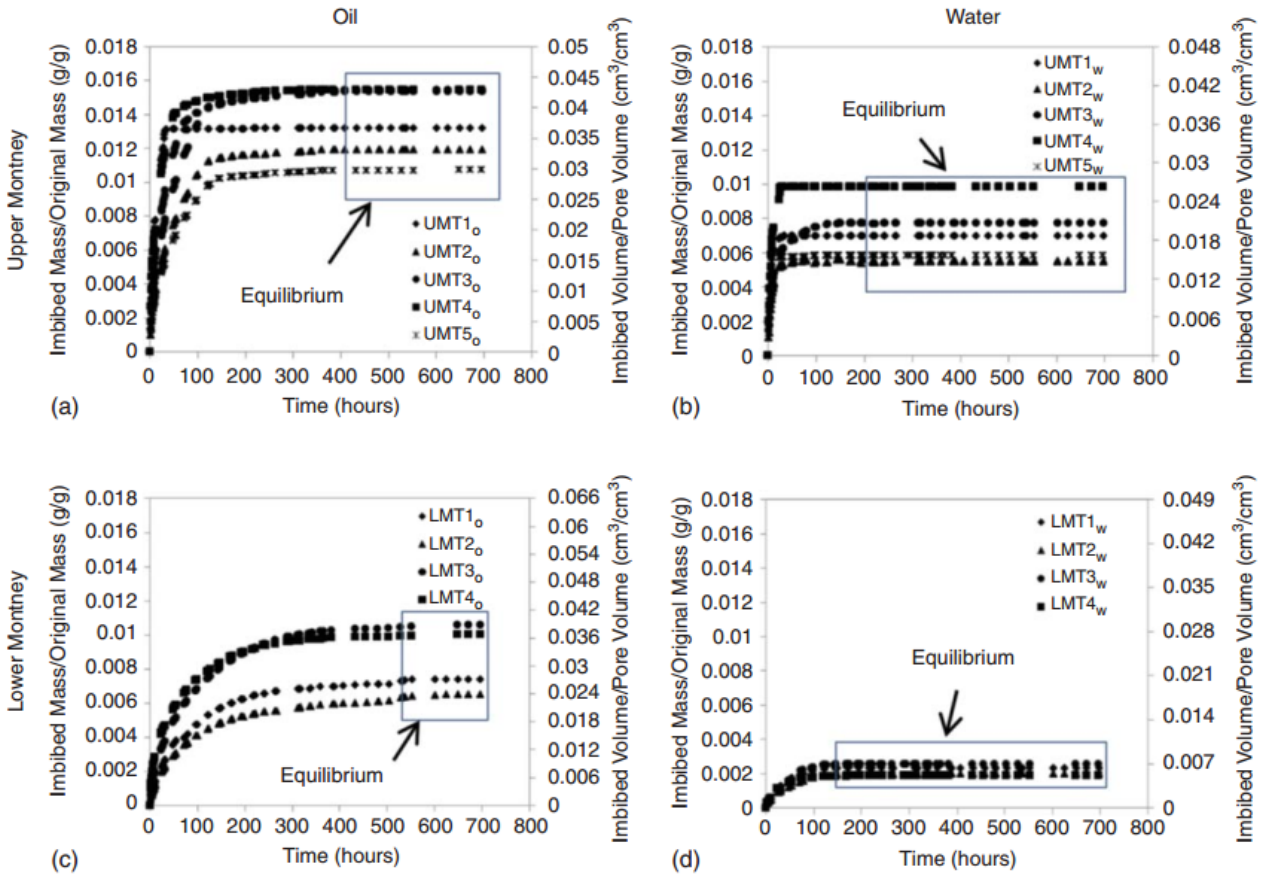


Figure 2.2 Comparative spontaneous imbibition tests of oil (a, c) and brine (b, d) into the upper UMT and LMT samples (Lan et al., 2015).

Fig. 2.2 compares the normalized mass and volume of oil and brine imbibed into core plugs from the upper Montney (UMT) and the lower Montney (LMT) rock samples. The normalized imbibed mass/volume of oil is significantly higher than that of water for all the samples, indicating the wetting affinity of these samples to oil is higher than that to water. Lan et al. (2015) explain this dual-wettability behavior using the adsorption of oil on the surface presence of organic matter as strong driving forces for the oil uptake in addition to the surface tension. This organic matter could be solid bitumen.

Yassin et al. (2016) extended Lan et al. (2015)'s work by analyzing scanning electron microscopy (SEM) images, energy-dispersive x-ray spectroscopy (EDS) images, mercury injection capillary pressure (MICP) measurements, and tight-rock analysis (TRA) results. SEM/EDS analyses

showed the abundance of nanopores within organic matter. Based on these analyses, they proposed the dual-wet theory: nanopores within or coated by pyrobitumen/solid bitumen are roving oil recovery with surfactantstrongly hydrophobic with negligible wetting affinity to the aqueous phase, while micropores bordered by inorganic minerals such as quartz and calcite are hydrophilic.

2.2 Imbibition Oil Recovery

Water imbibes into oil-saturated matrix spontaneously and expels the oil out during waterflooding in fractured reservoirs (Kathel et al., 2013). Javaheri et al. (2018) conducted soaking tests on several Montney core plugs using produced brine. They found that oil-recovery curves follow the trend of brine-imbibition curves in the corresponding dry plugs, and that the oil recovery is always less than the volume of brine imbibed into the dry plugs. They argued that the oil produced during the soaking tests mainly comes from hydrophilic pores, which are accessible to the imbibing brine. The forces which contribute to oil production include capillary, gravity and viscous forces (Alvarez et al., 2017). The major driving force to displace oil during soaking process is capillary pressure (P_c) described by Young-Laplace (1805) equation:

$$P_c = \frac{2 \times \sigma \times \cos\theta}{r} \quad 2.1$$

where σ is the interfacial tension between soaking fluid and oil (N/m), θ is the contact angle of soaking fluid (degree), and r is the pore radius (m).

The relative significance of capillary and gravity forces are related by the inverse Bond number (N_B^{-1}) (Schechter et al., 1994):

$$N_B^{-1} = C \frac{\sigma \times \sqrt{\frac{\phi}{k}}}{(\Delta \rho)gh} \quad 2.2$$

where ϕ is core porosity, k is the core permeability (m^2), $\Delta \rho$ is density difference of two immiscible fluids (kg/m^3), g is the gravitational acceleration (m/s^2), h is the length of the core (m) and C is 0.4 for the capillary tube model. Schechter et al. concluded that capillary forces dominate imbibition when $N_B^{-1} > 5$ and gravity forces which drives vertical flow dominate imbibition when $N_B^{-1} < 1$. When $1 < N_B^{-1} < 5$, the recovery of the nonwetting phase is faster due to the combination of capillary and gravity forces. Alvarez et al. (2017) calculated capillary pressure and inverse Bond number, they concluded that the dominated force in imbibition oil recovery for ultralow permeability of Bakken plugs is capillary pressure.

2.3 Surfactant Enhanced Oil Recovery

The main driving force, capillary pressure is not strong enough for spontaneous imbibition process in oil or intermediate-wet reservoirs and consequently result in low oil recoveries (Salehi et al., 2008). Surfactant formulations were used for wettability alternation to make the reservoir rocks to be more water-wet and therefore increase the oil production (Wang et al. 2012).

Wang et al. (2012) conducted wettability tests using four surfactant formulations on Bakken cores which were generally oil- or intermediate-wet. They concluded that the four surfactant formulations alerted the wettability of Bakken shale cores from oil-wet to water-wet, having a substantial potential to imbibe into cores and expel oil out, leading to higher imbibition oil recovery. Alvarez et al. (2017) combined wettability alternation and IFT reduction to investigate and compare the imbibition capability of different surfactants in cores from unconventional liquid-rich reservoirs. They found that all surfactants at field-scale concentrations can change the wettability of cores from oil- and intermediate-wet to water-wet. Anionic surfactants better reduced IFT and better improved oil recovery from shale cores than nonionic surfactants with lower contact angles.

Yassin et al. (2018) measured wettability and characterized pore networks of shale samples from the Duvernay Formation to investigate oil-recovery mechanisms by imbibition of different soaking fluids including water with surfactant or clay stabilizer. The results of imbibition oil recovery shows that soaking fluids with lower IFT yield higher oil recovery factor (RF). They explained the results by the reduction in contact angle of the soaking fluid with lower IFT, which indicate stronger wettability of rock to soaking fluid and lead to higher oil imbibition recovery consequently. They concluded that adding surfactant may alter the wettability of organic pores which are hardly displaced by soaking fluid to less-oil-wet conditions, leading to higher oil recovery.

Chapter 3 Overview and Characteristics of Montney Tight Rocks

3.1 Background of Montney Formation

The Montney Formation is a stratigraphic unit of Lower Triassic age in the Western Canadian Sedimentary Basin (WCSB) that trends northwest from Alberta to northeastern British Columbia (Nieto, 2009), as shown in **Fig 3.1**. The Montney Formation is covering 130,000 km² areally with a thickness ranging from 100m to 300m typically (NEB, OGC, & MNGD, 2013). The Montney Formation is as an important source of oil and gas in Canada and has considerable unconventional petroleum potential. The marketable natural gas, natural gas liquids (NGLs) and oil of the Montney Formation are estimated at 12,719 billion m³ (449 Tcf), 2,308 million m³ (14,521 million barrels) and 179 million m³ (1,125 million barrels) respectively (NEB et al., 2013).

This Formation generally comprises calcareous and dolomitic siltstones with minor shales (Wood 2013). It varies from very fine-grained sandstone landward in the east to dolomitic siltstone basinward in the west (Kendall, 1999). Based on depth and unit composition, the Formation can be divided into Upper Montney which is characterized as light brown siltstone interlaminated with fine grained sandstone, and Lower Montney which contains dark grey, dolomitic siltstone with interbedded (Davies, 1997). **Fig 3.2** shows the cross section of the Montney Formation (NEB, 2013). In Alberta, the siltstone near the bottom of the Doig Formation was included with the Montney Formation because the stratigraphy of this unit is equivalent to Upper Montney in British Columbia (NEB, 2013).

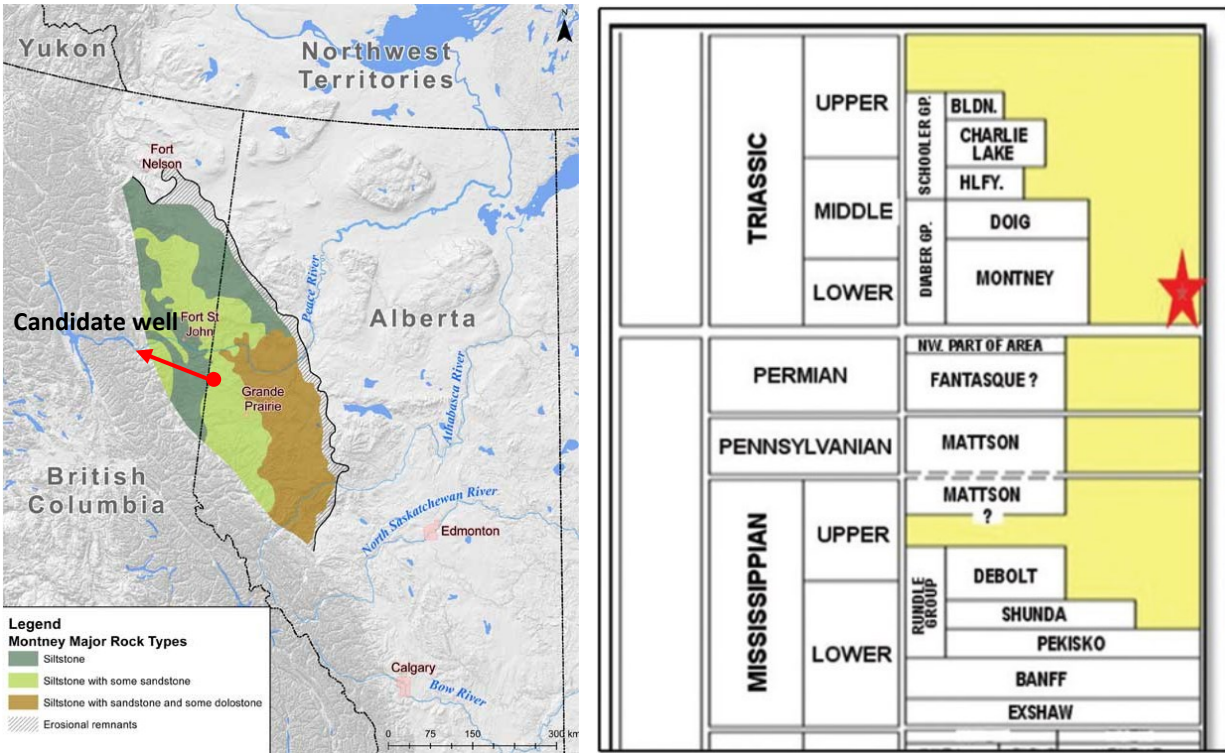


Fig 3.1:

Figure 3.1 Location and depositional stratigraphy of Montney Formation. (NEB et al., 2013; Nieto et al., 2009)

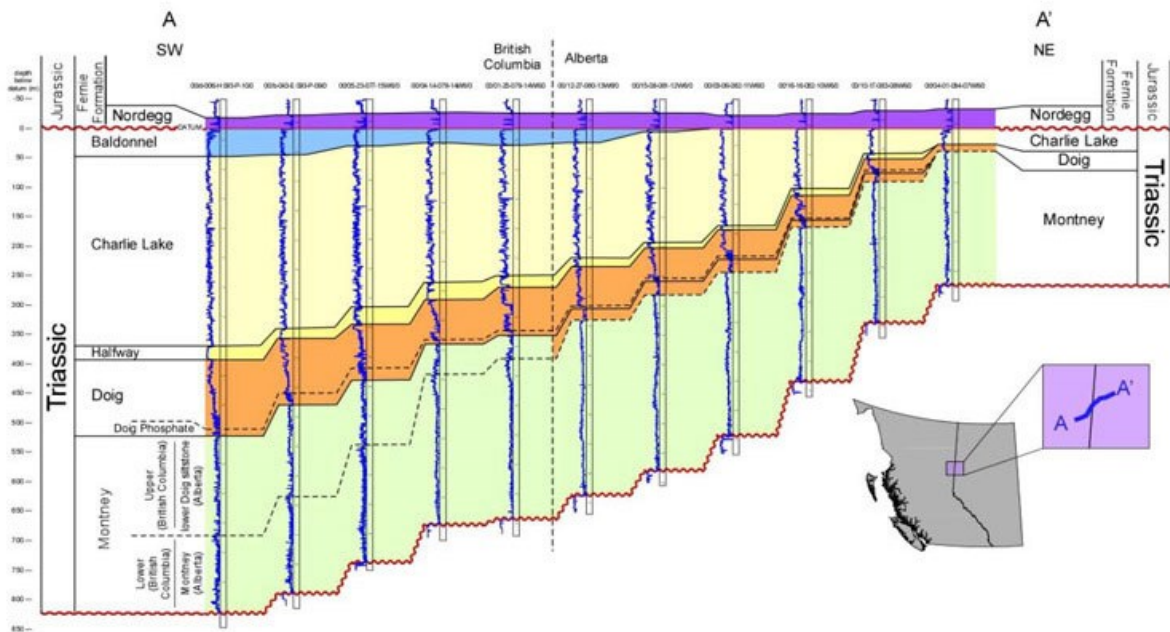


Figure 3.2 Cross section of the Montney Formation. (NEB, 2013).

3.2 Core plugs from Montney Formation

Here, we present the results of tight-rock analysis (TRA), X-ray diffraction (XRD) analysis, rock-eval pyrolysis, and SEM/thin section images of the Montney core plugs used in this study.

We used 6 pairs of twin core plugs that are drilled from two wells (Well A and Well B) completed in the lower Montney Formation. Well B is situated in the oil window while Well A is in the wet-gas (condensate) window. Both wells are over-pressured (>10 kPa/m) and their location is shown in **Fig 3.1**. **Table 3.1** summarizes the depth, original mass, diameter, and length of these plugs. The core plugs are drilled using dry-cut technology to avoid contamination with coring fluids. The plugs are not fully preserved and mainly saturated with air because the original oil and brine have partly or completely evaporated. We tested all samples as received and did not use toluene or methanol to clean them.

Table 3.1 Depth, original mass, diameter and length of the core plugs from the Montney Formation.

Well	Sample ID	Pair	Depth (m)	Mass (g)	Diameter (cm)	length (cm)
Well A	MT-A1	MT-A1-1	2,274.70	159.4	3.78	5.53
		MT-A1-2	2,274.66	167.8	3.77	5.86
	MT-A2	MT-A2-1	2,285.12	173.0	3.78	5.97
		MT-A2-2	2,285.16	173.8	3.79	5.99
	MT-A3	MT-A3-1	2,287.30	176.0	3.79	6.05
		MT-A3-2	2,287.34	174.5	3.79	5.93
Well B	MT-B1	MT-B1-1	2,188.13	187.6	3.79	6.62
		MT-B1-2	2,188.18	173.7	3.79	6.12
	MT-B2	MT-B2-1	2,196.90	186.9	3.79	6.49
		MT-B2-2	2,196.94	185.5	3.79	6.43
	MT-B3	MT-B3-1	2,200.76	186.0	3.79	6.52
		MT-B3-2	2,200.80	182.4	3.79	6.37

3.2.1. Tight-Rock Analysis (TRA)

Table 3.2 lists the values of permeability, porosity, and grain density corresponding to the offset samples near the twin plugs listed in **Table 3.1**. In general, the samples from Well A are less porous and permeable than those from Well B. Porosity and grain density are measured using Boyle's Law helium porosimetry method. This is combined with a calibration technique for improved accuracy (Handwerger et al., 2011). The measured effective porosity ranges from 2.79% to 6.61% of bulk volume (BV). The grain density ranges from 2.67 g/cm³ to 2.7 g/cm³. For the offset samples from Well A, the permeability is measured at a hydrostatic net confining pressure of 5520 kPa. The pressure decay of Helium gas across the sample over time is measured and extrapolated to the infinite mean pore pressure. This is then used to calculate Klinkenberg corrected permeability (Wu et al., 1998). The air permeability of Well A samples ranges from 5.05 μD to 9.02 μD and the Klinkenberg permeability ranges from 1.02 μD to 2.01 μD. For offset samples drilled from Well B, their permeabilities are measured by steady-state method at 5000 Kpa pressure difference and therefore require no Klinkenberg correction. The air permeability for Well B samples is from 20 to 40 μD, which is larger than that of Well A samples.

Table 3.2 Measured values of permeability, effective porosity, and grain density of the core samples.

Sample ID	Depth of offset sample (m)	Permeability, k_{air} (μD)	Klinkenberg Permeability (μD)	Porosity (%BV)	Grain density(g/cm ³)
MT-A1	2274.38	9.02	2.01	4.51	2.68
MT-A2	2285.92	5.25	1.02	2.79	2.67
MT-A3	2286.96	7.28	1.55	4.74	2.7
MT-B1	2188.33	40	/	6.14	2.68
MT-B2	2196.74	20	/	4.31	2.71
MT-B3	2201.52	40	/	6.61	2.68

3.2.2. Mineralogy

Table 3.3 lists the core samples' mineralogy as determined by X-ray diffraction (XRD) analysis.

The dominant clay mineral is a mixture of illite/mica (7.6 to 12.8 wt%), and the dominant non-clay minerals are quartz (31.7 to 43.5 wt%), K-feldspar (12.7 to 16.7 wt%) and dolomite (8.2 to 18.9 wt%).

For thin-section analysis, we cut thin slivers from rock samples and make them optically flat by grinding. Then, we mount them on glass slide and ground them smooth until the thin slivers are only 30 μm thick. Different minerals have different optical properties, altering the color and intensity of light. **Fig 3.3** shows thin-section images taken under plane polarized light. Quartz, carbonates, and feldspars, appear as white, gray, and yellow, respectively, while pores appear as pink areas. The black areas may represent pyrite, organic matter, or clay minerals.

Table 3.3 Mineralogy of the core plugs determined from XRD method.

Sample ID	Quartz	Feldspar		Carbonates			Clays		Sulphides		Apatite
		Albite	K-feldspar	Calcite	Dolomite	Ankerite	illite/mica	Chlorite	Pyrite	Marcasite	
MT-A1	43.1	12.4	14.4	2.9	9.3	6.2	7.6	2.3	0.9	0.3	0.5
MT-A2	31.7	10.6	14	2	17	12.9	8.9	1	1.1	0.4	0.5
MT-A3	40.6	13.3	15.7	2.9	8.2	6.3	9.3	1.6	1.3	0.3	0.6
MT-B1	43.5	11.7	13.9	0.1	12	6.3	9.6	0.9	1.2	0.3	0.6
MT-B2	37.3	12.9	16.7	1.8	8.9	4.9	12.8	2.3	1.6	0.5	0.2
MT-B3	36.3	11.5	12.7	0.1	18.9	8.4	9.5	0.9	1.1	0.2	0.5

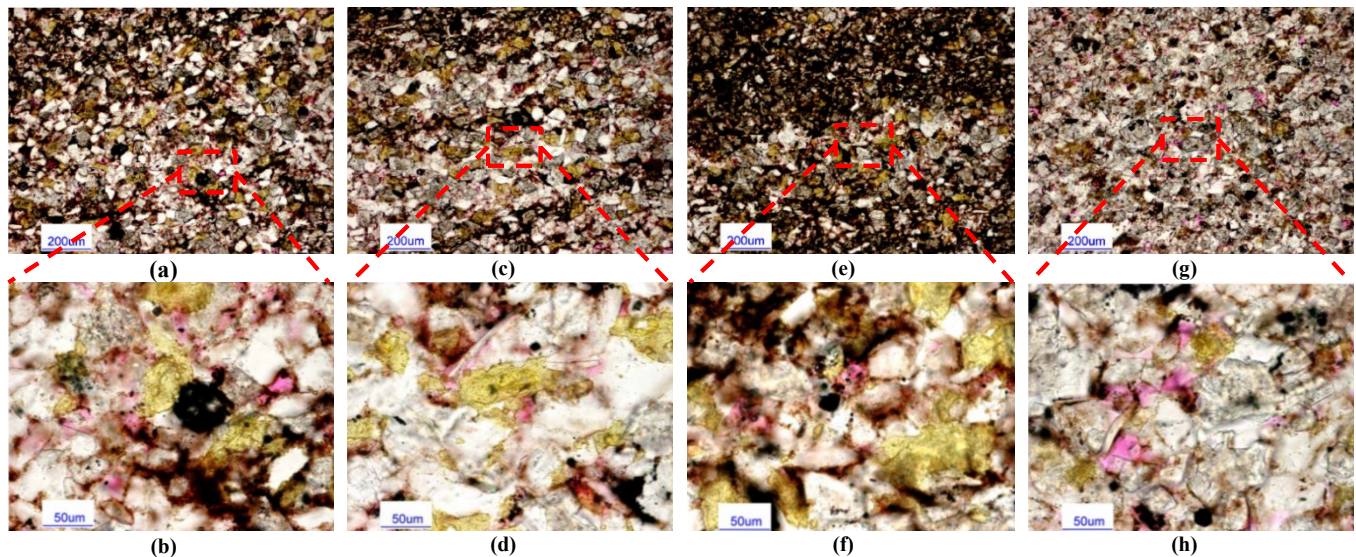


Figure 3.3 Thin sections of core plugs taken from Well A at 2188.35 m (a and b), 2194.81 m (c and d), 2198.86 m (e and f), and 2216.24 m (g and h), under plane polarized light.

3.2.3. Rock-Eval Pyrolysis

Table 3.4 lists the results of rock-eval pyrolysis on offset samples. They include TOC (total organic carbon), S_1 , S_2 , S_3 , T_{max} , hydrogen index (HI), oxygen index (OI), and production index (PI). TOC content is used to evaluate the hydrocarbon potential of source rocks (Baskin, 1997; Peters and Cassa, 1994). The TOC content of the samples varies from 1.06 to 1.32 wt%. In addition, since S_2 is smaller than 1.0 mg/g, the TOC is categorized as “poor”. However, this TOC should be lower than the actual value because the rock-eval pyrolysis was run on samples after organic-solvent extraction. The Van Krevelen diagram (HI vs. OI crossplot in **Fig 3.4a**) indicates that the Montney samples have Type III kerogen (Krevelen et al., 1950) which has a predominant gas potential. The PI vs. T_{max} crossplot in **Fig 3.4b** shows the level of kerogen maturity (Law, 1999). It indicates that all the samples are immature except MT-B2 which is in oil window, based on T_{max} values. However, the core samples of Well B are situated in the oil window while those of Well A are in the wet-gas (condensate) window. Therefore, T_{max} is not reliable here due to the poor S_2 peak.

Table 3.4 The results of rock-eval pyrolysis on offset samples.

Sample ID	Depth (m)	T _{max} (°C)	S ₁ (mg/g)	S ₂ (mg/g)	S ₃ (mg/g)	PC (%)	PI	S ₂ /S ₃	S ₁ /TOC	TOC (%)	HI	OI
MT-A1	2274.38	432	0.38	0.16	0.40	0.04	0.70	0.40	0.34	1.13	14	35
MT-A2	2285.92	430	0.36	0.17	0.33	0.04	0.68	0.52	0.32	1.14	15	29
MT-A3	2286.96	428	0.43	0.15	0.29	0.05	0.74	0.52	0.41	1.06	14	28
MT-B1	2188.33	424	1.31	0.94	0.37	0.19	0.58	2.54	0.99	1.32	72	28
MT-B2	2196.74	454	0.78	0.66	0.3	0.12	0.54	2.2	0.58	1.34	49	22
MT-B3	2201.52	428	0.5	0.39	0.39	0.07	0.56	1	0.46	1.08	36	36

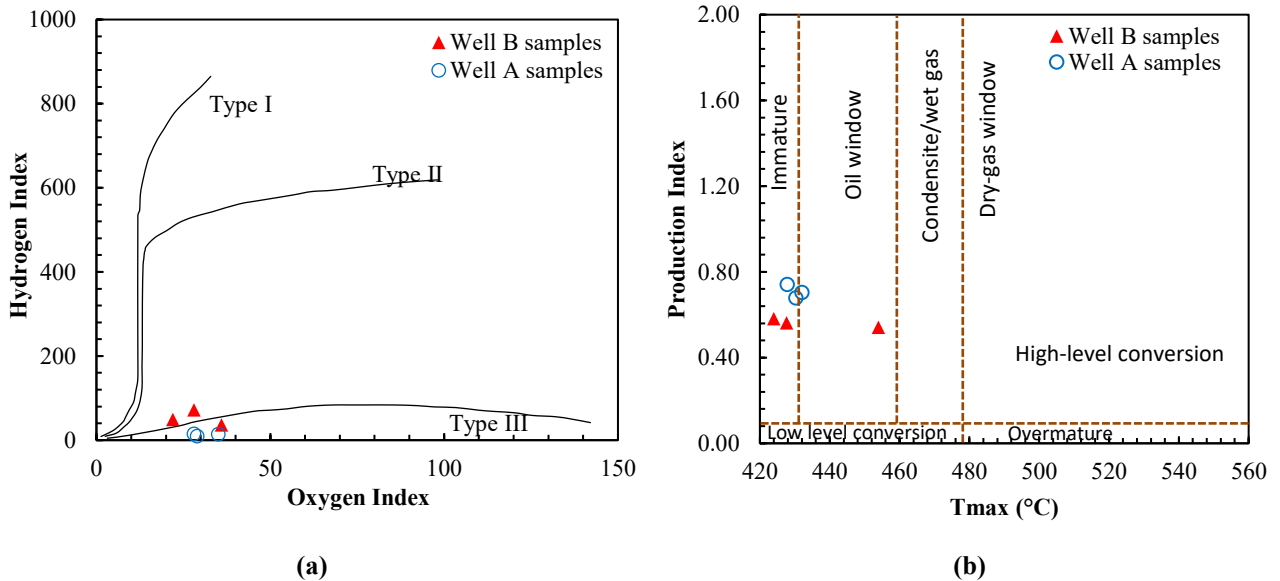


Figure 3.4 Cross-plots of (a) hydrogen index vs. oxygen index, and (b) production index vs. T_{max}. The Montney samples have type III kerogen and are immature except MT-B2 that is in oil window.

3.2.5. SEM Images

For SEM analysis, we polished end pieces of the core plugs to get smooth surfaces, and then, coated the surface with carbon to eliminate the charging effects affecting the image resolution.

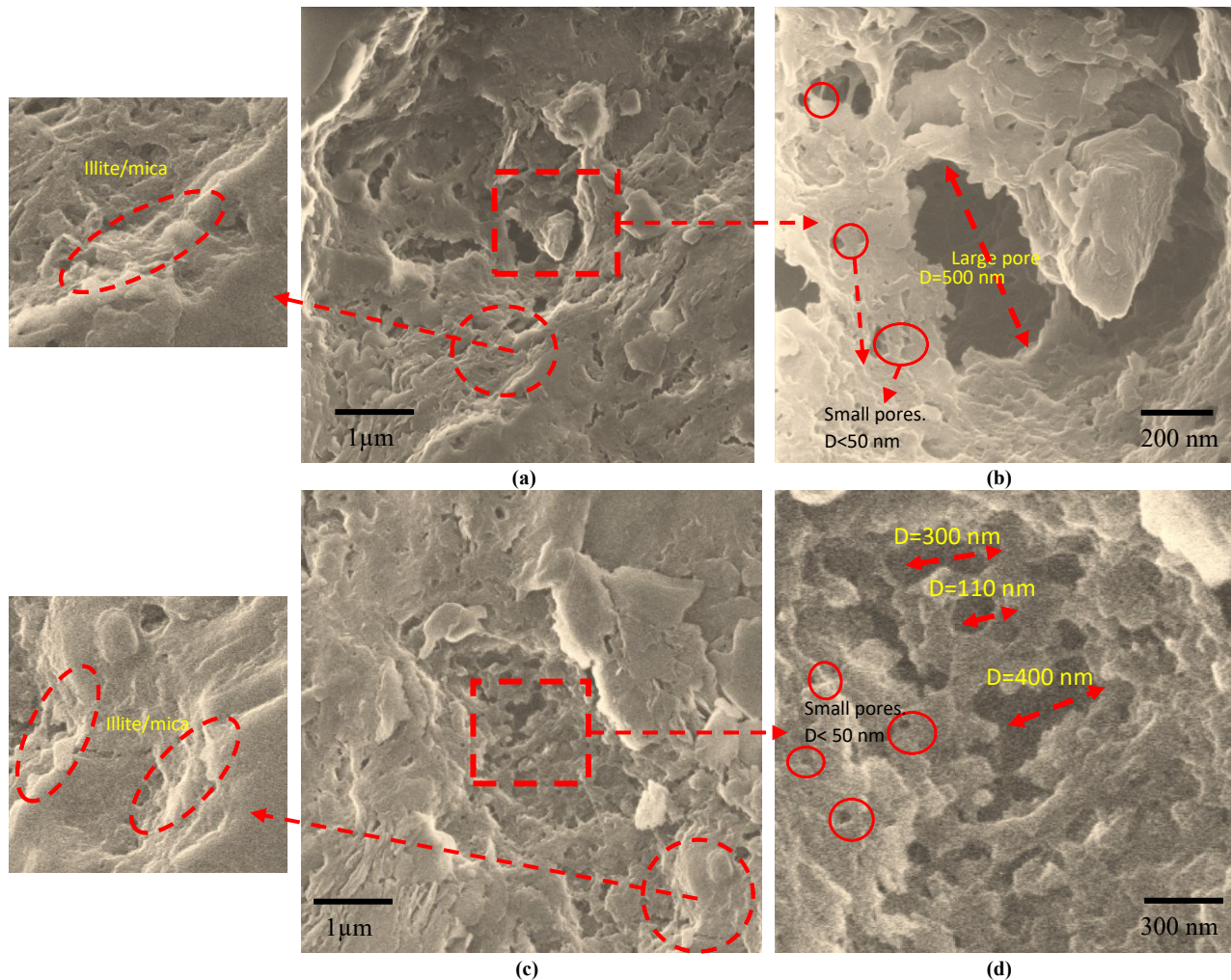


Figure 3.5 SEM images from core plug MT-B2. The pore network can be divided into large pores (> 100 nm) and small sub-micron pores (< 50 nm).

Fig 3.5 shows the SEM images from core plug MT-B2. We observe two kinds of pores: 1) large pores greater than 100 nm and 2) small sub-micron pores smaller than 50 nm. Also, **Fig 3.5** shows the existence of clay minerals. Illite ribbons grow and coalesce to thin, platy crystals which tend to be planar and laminated (Keller et al., 1986). The edges of illite flakes are scalloped due to the non-uniform growth of illite ribbons (Keller et al., 1986). We can observe crystal layers and flakes, and the edges of the coalesced flakes are scalloped in the SEM images. These clay minerals can be categorized as illite/mica.

Chapter 4 Wettability Analysis and Pore Characterization of Montney Tight Oil Rocks.

This section presents the results of contact-angle measurements and spontaneous imbibition experiments. Here, we analyze wettability of core samples to oil and water, characterize their pores based on imbibition and MICP results, and investigate correlations among petrophysical properties.

4.1 Materials

4.1.1 Rock Samples

We used 6 pairs of twin core plugs that are drilled from two wells (Well A and Well B) completed in the lower Montney Formation. Well B is situated in the oil window while Well A is in the wet-gas (condensate) window. Both wells are over-pressured (>10 kPa/m). **Table 4.1** lists the depth, mass, diameter, length, porosity, permeability and TOC of the six pairs of twin plugs from Montney Formation. The other petrophysical properties of the core plugs have been introduced in Chapter 3.

Table 4.1 Depth, original mass, diameter and length of the core plugs from the Montney Formation.

Well	Sample ID	Pair	Depth (m)	Mass (g)	Diameter (cm)	length (cm)	Porosity (%BV)	Permeability, k_{air} (μ D)
Well A	MT-A1	MT-A1-1	2,274.70	159.4	3.78	5.53	4.51	9.02
		MT-A1-2	2,274.66	167.8	3.77	5.86		
	MT-A2	MT-A2-1	2,285.12	173.0	3.78	5.97	2.79	5.25
		MT-A2-2	2,285.16	173.8	3.79	5.99		
	MT-A3	MT-A3-1	2,287.30	176.0	3.79	6.05	4.74	7.28
		MT-A3-2	2,287.34	174.5	3.79	5.93		
Well B	MT-B1	MT-B1-1	2,188.13	187.6	3.79	6.62	6.14	40
		MT-B1-2	2,188.18	173.7	3.79	6.12		
	MT-B2	MT-B2-1	2,196.90	186.9	3.79	6.49	4.31	20
		MT-B2-2	2,196.94	185.5	3.79	6.43		
	MT-B3	MT-B3-1	2,200.76	186.0	3.79	6.52	6.61	40
		MT-B3-2	2,200.80	182.4	3.79	6.37		

4.1.2 Fluid Samples

We conduct spontaneous imbibition experiments using reservoir oil and brine. The oil utilized in this study is from Well B. **Tables 4.2** and **4.3** list the properties of reservoir brine and oil respectively.

Table 4.2 Brine properties.

Property	Quantity
Total dissolved solids (mg/L)	130,000
Relative density (g/cc)	1.101
Surface tension (mN/m)	67
Refractive index	1.356
Conductivity (μ S/m)	159,000
Resistivity (ohm-m) @25°C	0.06
Total hardness as CaCO ₃ (mg/L)	22,000
Total Alkalinity as CaCO ₃ (mg/L)	110
Observed PH	6.89
H ₂ S spot test	Absent
Viscosity (cp)	1.18

Table 4.3 Oil properties.

Property	Quantity
Relative density (g/cc)	0.74
Absolute density (kg/m ³)	738.0
API	46.8
Surface tension (mN/m)	25.5
Viscosity (cp)	3.56
Total sulphur (mass percent) ASTM D4294	0.107

4.2 Methodology

In this section, we present the experiments that we conduct for wettability evaluation of the plugs: air-liquid contact angle measurements and spontaneous imbibition experiments. The six twin core plugs are as-received samples which may be partly saturated with oil or formation water. Here, in order to exclude the effect of initial oil and water saturation on wettability evaluation, we heated the six samples at 90°C until there is no mass loss anymore. Then we assume that after heating, the oil and water saturations of the core plugs are negligible.

Fig 4.1 shows the mass loss (%) of the six core plugs vs. time, calculated by dividing the mass by initial mass:

$$\text{Mass loss (\%)} = \frac{\text{Heated mass} - \text{Initial mass}}{\text{Initial mass}} \times 100$$

Here we assume that after heating the oil or water saturations of the heated samples are negligible.

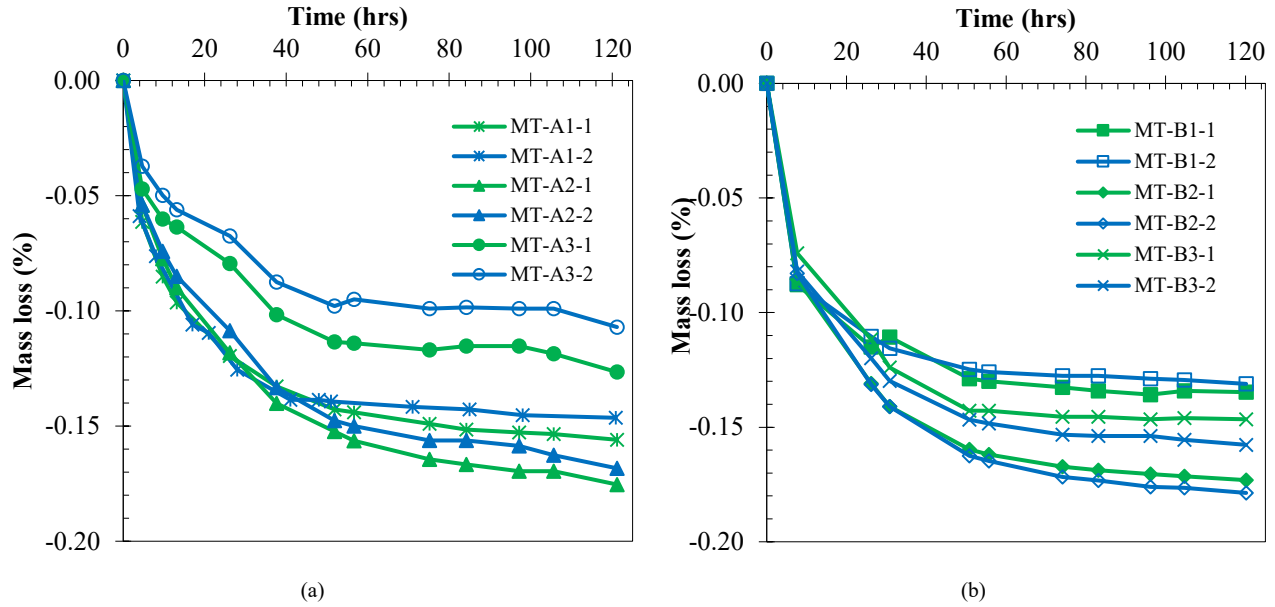


Figure 4.1 Mass loss (%) of heated plugs vs. time: (a) Well A samples, (b) Well B samples. The heating temperature is 90°C

4.2.1 Air-Liquid Contact-angle measurements

We polish the end pieces of the dry core plugs to get smooth surfaces for measuring air-liquid contact angle using a high-resolution camera (see Fig 4.2). For air-liquid contact measurement, the dry end piece is placed on the stage of contact angle meter, then an oil droplet or brine droplet is placed on the rock surface by a syringe needle. The contact angle of oil or brine droplet is captured by the camera and measured by the software till the equilibrium state.

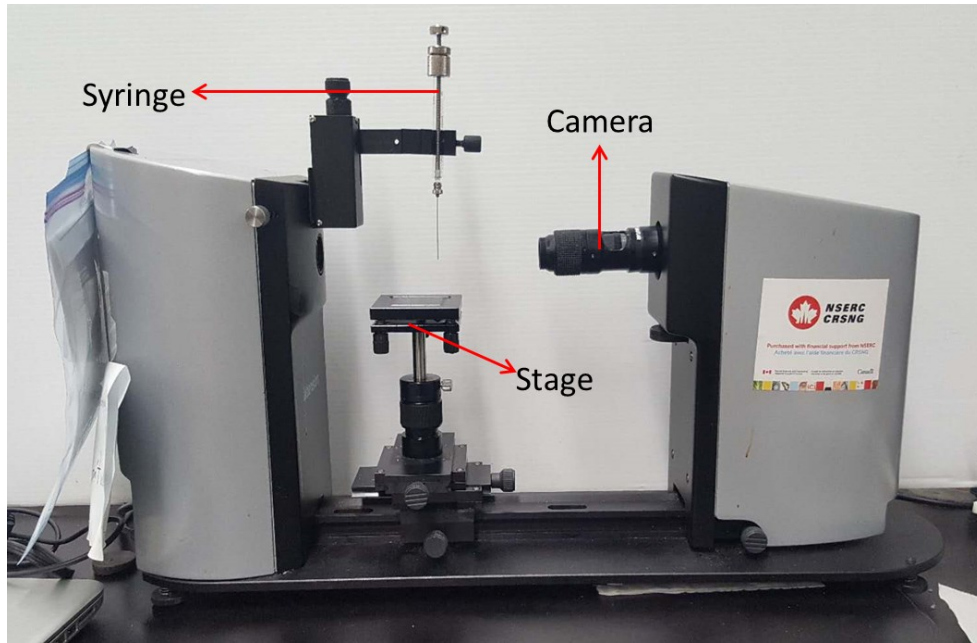


Figure 4.2 Contact angle meter.

4.2.2 Spontaneous Imbibition on Dry Core Plugs

We evaluate wetting affinity of oil and brine by measuring spontaneous imbibition of reservoir oil and brine into six pairs of twin core plugs, at room pressure and temperature. We place each core plug on a mesh screen inside the imbibition cell partly filled with brine or oil with only the plug's bottom face in contact with the wetting liquid (as shown in **Fig 4.3**). As oil or brine imbibes into the plug, we record its mass gain periodically. Since the depth difference between the twin plugs is less than 5 cm, we assume that they have similar petrophysical properties.

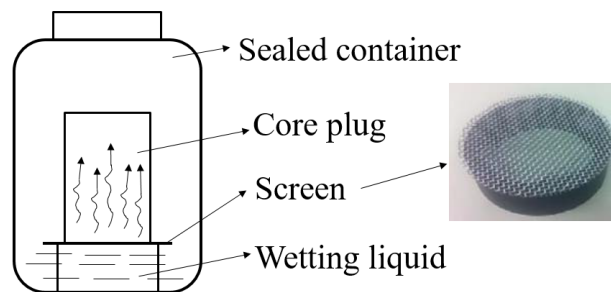


Figure 4.3 Schematic of the imbibition setup.

4.3 Results

This section presents the results of contact-angle measurements and spontaneous imbibition experiments.

4.3.1 Air-Liquid Contact-Angle Measurements

Figs 4.4a and **4.4b** show the contact angles of brine and oil on polished surface of the end piece of MT-A1. We observe that the brine remains a droplet with contact angle of 32° while oil completely spreads on the rock surface. **Table 4.4** lists the measured air-liquid contact angles of oil and brine for all the samples. The contact angles of brine vary from $32^\circ \pm 3^\circ$ to $45^\circ \pm 5^\circ$. There are no contact angles for oil since its droplet completely spreads on the rock surface. The measured air-liquid contact angles can be used to interpret the results of water and oil imbibition into dry samples later. The results of air-liquid contact-angle measurements on dry end pieces suggest that in the presence of air, the wetting affinity of the rock samples to oil is stronger than that to brine. The similar observations were reported in a previous study (Lan et al., 2013).

Table 4.4 Air-liquid contact angles of oil and brine on the surface of fresh (dry) core samples.

Sample ID	Oil contact angle	Brine contact angle
MT-A1		$32^\circ \pm 4^\circ$
MT-A2		$35^\circ \pm 5^\circ$
MT-A3	Complete spreading on all rock samples	$35^\circ \pm 3^\circ$
MT-B1		$34^\circ \pm 5^\circ$
MT-B2		$37^\circ \pm 6^\circ$
MT-B3		$45^\circ \pm 5^\circ$



Figure 4.4 Air-liquid contact angles of (a) brine and (b) oil droplets on polished surfaces of MT-A1.

4.3.2 Spontaneous Imbibition on Dry Core Plugs

Figs. 4.5a and **4.5b** show the normalized imbibed volume of oil (I_o) and brine (I_w) versus time. We calculate I_o and I_w by dividing the imbibed volumes of oil and brine by pore volume (PV) of the core plugs. The PV of each core plug is calculated by multiplying its bulk volume by the measured porosity of the corresponding offset sample (Table 2). **Table 4.5** lists the equilibrated time, equilibrated normalized imbibed volume and the imbibition rate of oil and brine. We define imbibition rate as normalized imbibed volume divided by imbibition time, during the first 50 hours of imbibition process. The spontaneous imbibition of both oil and brine into the core plugs indicates a dual-wet pore system.

At equilibrium state, $I_o^{eq} > I_w^{eq}$ for all the core plugs. I_o^{eq} and I_w^{eq} vary from 97.4% to 119.51% and from 24.87% to 57.7% of total PV, respectively. For sample MT-B1 and MT-B2, I_o^{eq} is over 100% of total PV. This is because we used predicted porosities from offset samples to calculate PV of the core plugs. These predicted porosities may differ from the actual porosity of the plugs used for imbibition tests. The spontaneous imbibition results indicate that all the core plugs are oil-wet. I_o^{eq} for all core plugs is close to 100%, suggesting that oil can fill most of the pore networks, while I_w is from 24.87% to 57.7%, suggesting that brine can only imbibe into portion of pores.

Brine imbibition into the cores reaches equilibrated state before 600 hours while oil imbibition continues after 800 hours. During the first 150 hours, the average oil imbibition rate for different samples varies from 0.298% hr⁻¹ to 0.482% hr⁻¹ while the average brine imbibition rate varies from 0.095% hr⁻¹ to 0.209% hr⁻¹. The oil imbibition rate here is defined as the ratio of total imbibed volume (%PV) to the imbibition time. The initial imbibition rate of oil is higher than that of brine for all the samples. Lan et al. (2015) reported similar observations for core samples from a different part of the Montney Formation. This observation is consistent with Yue's imbibition analysis theory (2018). Higher imbibition rate of oil as well as late equilibrium of oil can be explained by the hydrophobic pores available for oil imbibition. Brine has low wetting affinity in these hydrophobic pores and cannot fill them spontaneously.

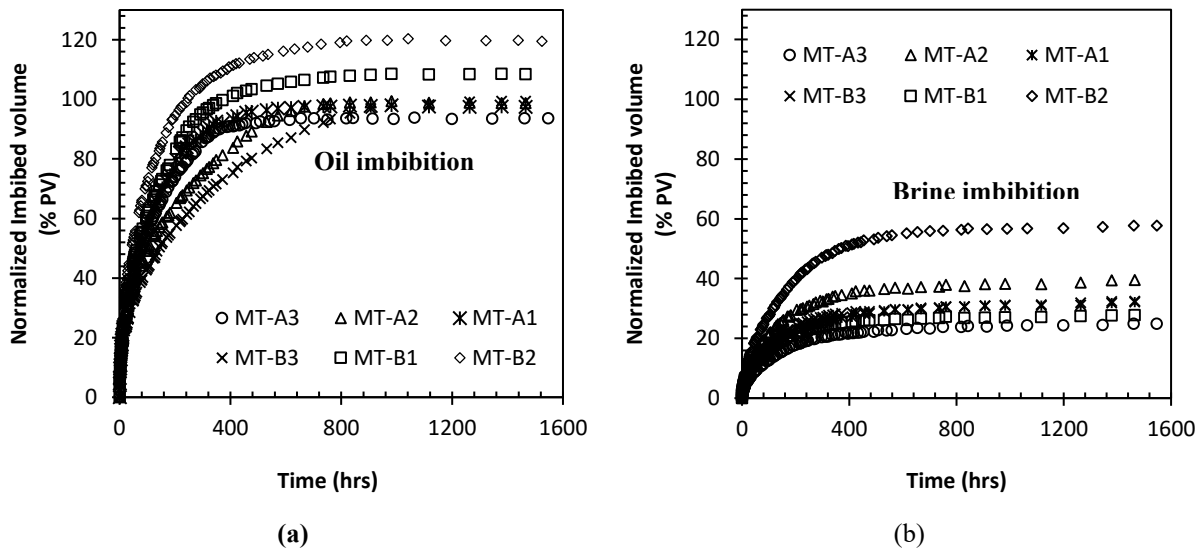


Figure 4.5 Profiles of normalized imbibed volume of (a) oil (I_o) and (b) brine (I_w) for 6 pairs of twin core plugs.

Table 4.5 The equilibrated time, equilibrated imbibed volume and initial imbibition rate of oil and brine imbibition profiles.

Sample ID	Equilibrated time for oil (hrs)	Equilibrated time for brine (hrs)	I_o^{eq} (% PV)	I_w^{eq} (% PV)	Imbibition rate of oil (% hr ⁻¹)	Imbibition rate of brine (% hr ⁻¹)
MT-A1	850	580	97.429	32.105	0.393	0.120
MT-A2	900	600	98.719	39.477	0.337	0.159
MT-A3	850	650	93.338	24.870	0.392	0.095
MT-B1	1000	576	108.151	28.284	0.423	0.116
MT-B2	1100	650	119.516	57.755	0.482	0.209
MT-B3	1200	780	99.391	32.434	0.298	0.130

4.4 Discussions

Here, we analyze wettability of the core samples to oil and water, characterize their pores based on imbibition and MICP results, and correlate their petrophysical properties.

4.4.1 Calculation of Wettability Index

To compare the wetting affinity of the Montney plugs to oil and brine, the wettability index defined by Lan et al. (2014c) is used:

$$WI_o = I_o^{eq} / (I_o^{eq} + I_w^{eq}) \quad 4.1$$

Here, I_o^{eq} and I_w^{eq} are the normalized imbibed volumes of oil and brine at equilibrium conditions. WI_o quantifies the comparative capacity of the rock for oil and brine imbibition. Here, we assume that all the twin plugs have similar petrophysical properties. **Table 4.6** lists the calculated values of WI_o . WI_o ranges from 0.674 to 0.790 with an average of 0.746. The average value of WI_o is higher than 0.5, suggesting that the wetting affinity of the plugs to oil is higher than that to brine, under dry conditions.

Table 4.6 The values of WI_o for the 6 twin core plugs.

Sample ID	WI_o
MT-A1	0.752
MT-A2	0.714
MT-A3	0.790
MT-B1	0.794
MT-B2	0.674
MT-B3	0.754

4.4.2 Effective Porosity

Lan et al. (2015) define effective porosity of the core plugs to oil and brine (ϕ_{eo} and ϕ_{ew}) as the ratio of imbibed volume of oil and brine at equilibrium conditions to bulk volume. The effective porosity of each plug is obtained by analyzing the measured porosity of the offset samples using Boyle's law helium porosimeter. **Table 4.7** lists the calculated ϕ_{eo} and ϕ_{ew} . The average value of ϕ_{eo} (5.34%) is three times higher than that of ϕ_{ew} (1.82 %). In **Fig. 4.6**, we plot ϕ_{eo} and ϕ_{ew} versus effective porosity and observe that ϕ_{eo} is close to the effective porosity and ϕ_{ew} is almost three times lower than the total porosity. This suggests that oil imbibe into most pores while brine can only imbibe into part of the pore network. The SEM images presented in **Fig 3.5** show two kinds of pores: large pores (> 100 nm) and sub-micron pores (< 50 nm). Similar to previous studies (Yassin et al., 2018; Yue et al., 2018) we conclude that oil can imbibe into both large and small pores while brine mainly tends to imbibe into large pores.

Table 4.7 Effective porosity of core plugs to oil and brine.

Sample	ϕ_{co} (%)	ϕ_{ew} (%)
MT-A1	4.48	1.48
MT-A2	4.34	1.74
MT-A3	4.57	1.22
MT-B1	6.70	1.74
MT-B2	5.26	2.54
MT-B3	6.66	2.17

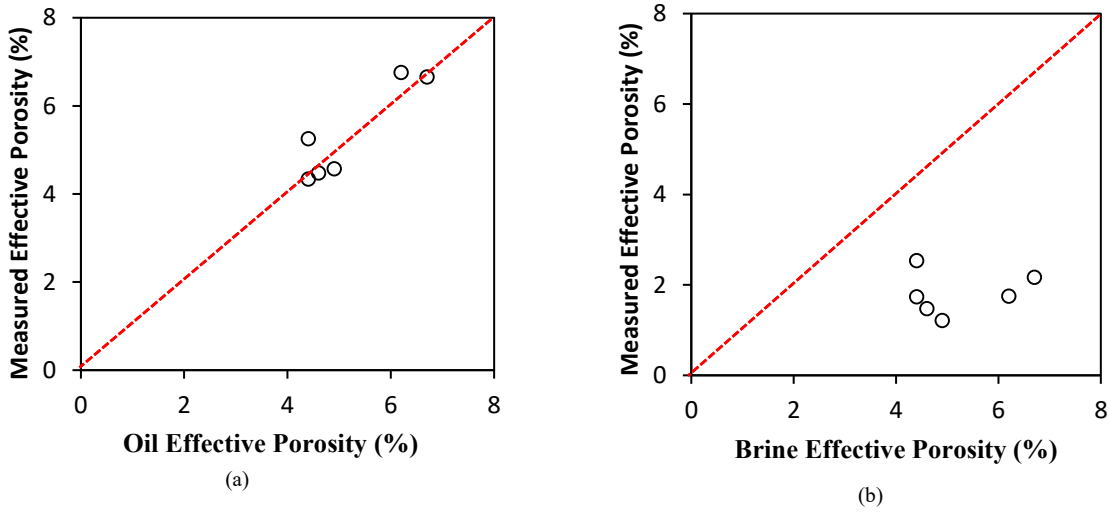


Figure 4.6 Effective porosity measured by Boyle’s law helium porosimetry versus effective porosity to (a) oil and (b) brine obtained by equilibrated imbibed volume of oil and brine.

4.4.4 Correlations between Imbibition and MICP Profiles

The measured imbibition results of the Montney core plugs are consistent with dual-wet theory (Shi et al., 2019). During imbibition process, oil spontaneously fills most of the pores while brine only fills the hydrophilic pore. Here, we may argue that oil can imbibe into all the pores while brine can only imbibe into hydrophilic pores, in the presence of air.

4.4.4.1 Mercury Injection Capillary Pressure (MICP) Data

Fig. 4.7 shows the PSD profiles from MICP measurements on the Montney core plugs. The y-axes represent the intrusion volume which is normalized based on the final intruded volume of Mercury at 400 Mpa (% total intrusion volume), and the incremental P (mL/g) invaded by mercury.

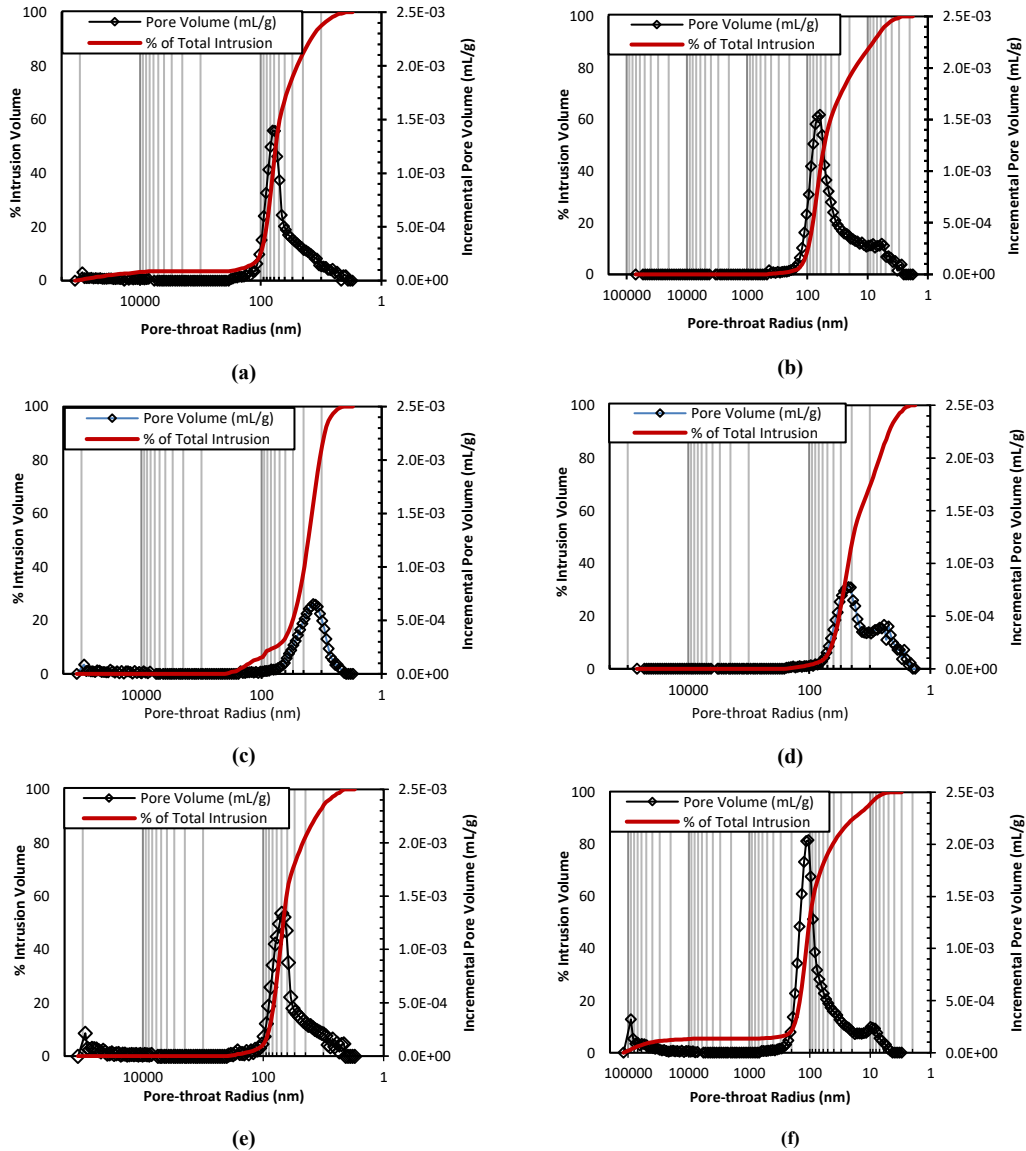


Figure 4.7 The pore-throat size distribution of the core plugs. Cumulative intrusion volume (% of total intrusion volume) and percent intrusion (mL/g) vs. pore-throat radius (nm) for samples from Well A (a, c, e) and Well B (b, d, f).

The porosity invaded by mercury (ϕ_{MICP}) is lower than the porosity determined using Boyle's Law helium porosimetry method (**Table 2**). The reason for this is that mercury cannot access the nanopores with diameters < 3 nm since an extremely high pressure (> 400 Mpa) is required (Al Hinai et al., 2014; Yue et al., 2019, Zolfaghari et al., 2017). The PSD profiles consist of two parts: a bell-shaped part representing large pores and a tail part representing very small pores. Lan et al. (2015) and Yassin et al. (2016) reported similar observations in terms of two different parts by analyzing core plugs from the Montney Formation. **Fig 4.7a** shows a well-developed peak at about 67-nm radius and a tail extending from about 30 nm to 1 nm for sample MT A-1. The mercury intrusion volume corresponding to the small pores with pore radius < 30 nm is 27% of the total intrusion volume.

4.4.4.2 Estimating Small-Pore Porosity ($\phi_{small-pore}$)

Figs 4.7a through **4.7f** show the PSD profiles from MICP measurements of the core plugs. For the Montney tight rocks with permeability in the order of microDarcy, mercury cannot invade the entire pore volume due to the presence of extremely-small pores (Lan et al., 2015; Yassin et al., 2017). For the samples in this study, mercury cannot invade the pores with diameters < 3 nm. The porosity of rock samples measured by MICP method (ϕ_{MICP}) is smaller than that measured by helium porosimeter. The inaccessible porosity is calculated by $\phi_{inaccessible} = \phi - \phi_{MICP}$. ϕ is the predicted porosity from the porosity of the offset samples measured by Boyle's Law helium porosimetry method.

Therefore, the small-pores porosity can be calculated by

$$\phi_{small-pore} = \phi_{inaccessible} + \phi_{MICP} \times f_{small-pore} \quad 4.2$$

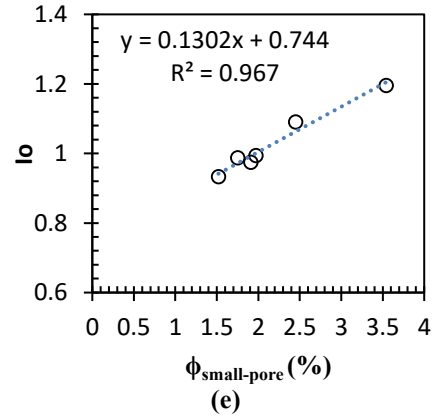
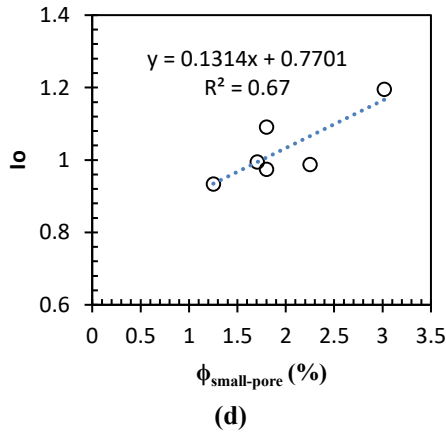
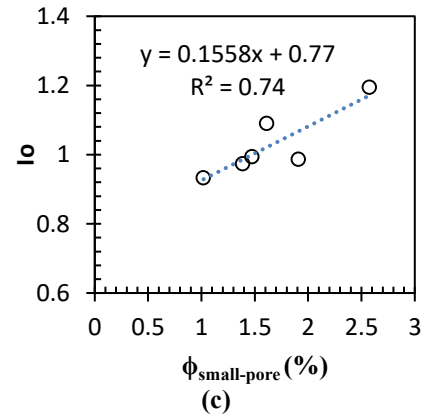
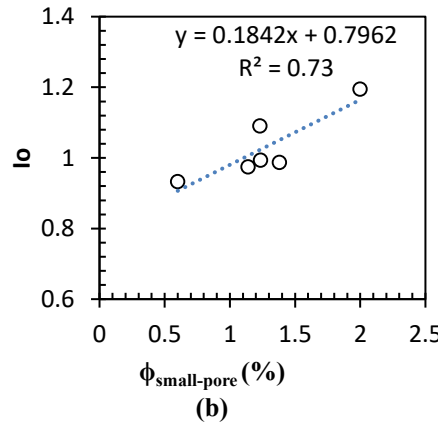
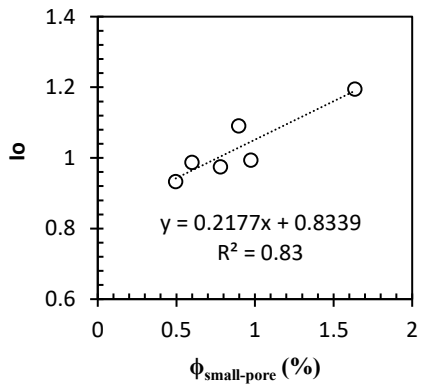
where $\phi_{\text{small-pore}}$ is the small-pores porosity, $\phi_{\text{inaccessible}}$ is the porosity of inaccessible pores which cannot be invaded by Mercury, and $f_{\text{small-pore}}$ is the volume fraction of small pores (in % of total PV).

4.4.4.2 Determination of R² Values

According to the dual-wet theory presented in **Fig 2.1b**, we hypothesize that the imbibed oil volume is proportional to the volume fraction of small pores. In order to calculate $\phi_{\text{small-pore}}$, we determine the optimum threshold value of pore-throat size for small pores by comparing the R² values of the correlations between I_o and $\phi_{\text{small-pore}}$ for different values of cut-off pore-throat size, varying from 10 to 40 nm with 5 nm interval. At a specific pore-throat size, we determine $f_{\text{small-pore}}$ from MICP profiles and calculate $\phi_{\text{small-pore}}$ using Eq 4.2. **Table 4.8** lists the calculated $\phi_{\text{small-pore}}$ of core samples when selecting different threshold value of pore-throat radius from 10 to 40nm. Then we plot the normalized imbibed volume of oil (I_o) versus small pore porosity ($\phi_{\text{small-pore}}$) to determine the optimum threshold value. **Fig 4.8** shows the normalized imbibed volume of oil (I_o) versus small pore porosity when we select (a) 10 nm, (b) 15, (c) 20 nm, (d) 25 nm, (e) 30 nm, (f) 35 nm, and (g) 40 nm as threshold pore-throat radius of small pores. In **Fig 4.9** we compare the R² values for threshold values of pore-throat-size varying from 10 to 40 nm that we got from **Fig 4.8** The results show that 30 nm threshold value has the highest R², and thus, we choose 30 nm as the cutoff, and classify pore-throat radii less than 30 nm as micropores and those greater than 30 nm as comparatively large pores.

Table 4.8 The calculated small pore porosity ($\phi_{\text{small-pore}}$) ratio of oil capillary pressure to water capillary pressure for each twin core plug from imbibition data and Young-Laplace equation.

Well	Threshold value Sample ID	Small pore porosity (% Pore Volume)						
		10nm	15nm	20nm	25nm	30nm	35nm	40nm
Well A	MT-A1	0.78	1.08	1.39	1.7	1.91	2.53	3.22
	MT-A2	0.6	1.38	1.91	2.22	1.75	2.52	2.54
	MT-A3	0.5	0.77	1.02	1.25	1.52	1.7	1.93
Well B	MT-B1	0.9	1.31	1.61	1.83	2.45	2.27	2.51
	MT-B2	1.64	2.07	2.58	3.02	3.54	3.74	3.98
	MT-B3	0.97	1.24	1.47	1.7	1.97	2.24	2.42



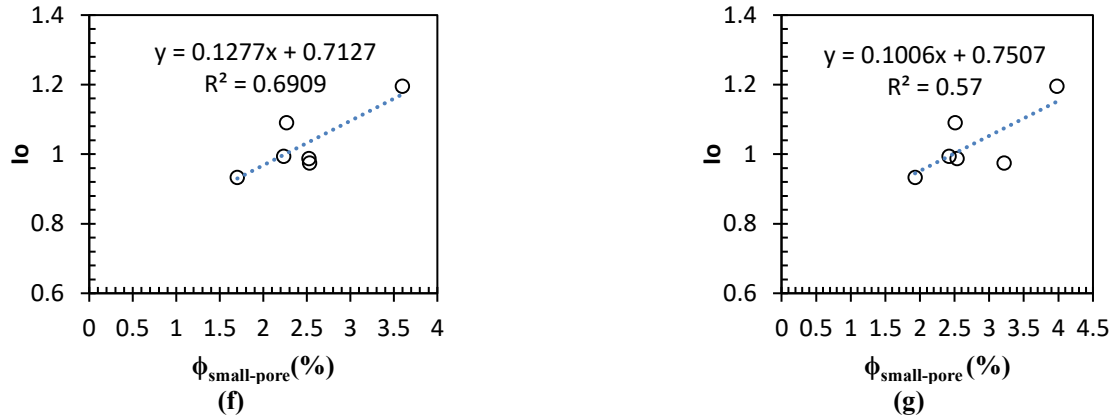


Figure 4.8 The Normalized imbibed oil volume (I_o) versus small-pore porosity ($\phi_{\text{small-pore}}$) for different values of pore-throat size cut-off.

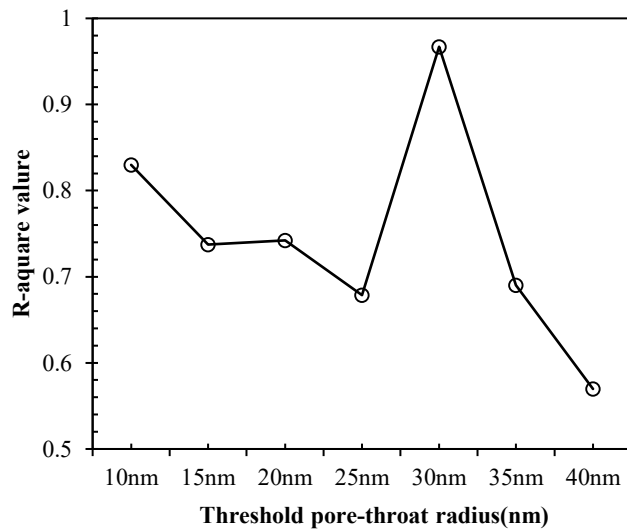


Figure 4.9 R^2 of the fitted regression lines for different threshold values of pore-throat radius. We select 30 nm (having the highest R^2) as the threshold pore-throat radius for defining small pores.

4.4.5 Correlation between Normalized Imbibed Volume of Oil (I_o) and $\phi_{\text{small-pore}}$

Fig 4.10a plots I_o which represents the pores accessible for oil imbibition versus $\phi_{\text{small-pore}}$ and Fig 4.10b plots $I_o - I_w$ which represents pores fraction only accessible for oil but not accessible for water (water repellent) versus $\phi_{\text{small-pore}}$. $\phi_{\text{small-pore}}$ is determined by setting 30 nm as the threshold value for small pores. The positive correlation observed in Fig 4.10a indicates that the samples with higher fraction of small pores imbibe more oil and that observed in Fig 4.10b

suggests that the samples with higher fraction of small pores have more water repellent (hydrophobic) pores. This result is consistent with the late equilibrium times of oil-imbibition profiles compared with brine-imbibition profiles, suggesting that oil imbibes into small pores which tend to be water repellent. It is believed that such small pores are filled with hydrocarbon under in-situ conditions which is consistent with field observation that there is more oil production from the wells located in the tighter (lower permeability) parts of the target reservoir.

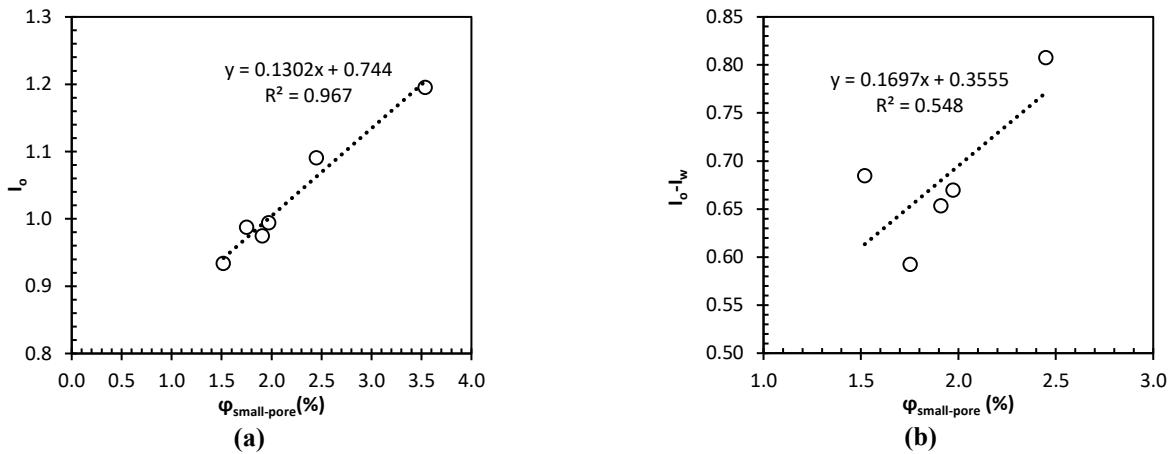


Figure 4.10 (a) I_o (%PV) vs. $\phi_{small-pore}$; (b) $I_o - I_w$ (%PV) vs. $\phi_{small-pore}$

4.4.6 Correlations among Initial Oil Saturation (S_o), $\phi_{small-pore}$, and I_o .

To find critical factors controlling the initial oil saturation of our samples, we plot $\phi_{small-pore}$ and I_o versus initial oil saturation (S_o) (Fig 4.11). $\phi_{small-pore}$ has a strong positive correlation with S_o (Fig 4.11a), suggesting the initial oil saturation in rocks mainly depends on the small pores. Small pores are hydrophobic and trend to imbibe oil, therefore the core plugs with higher $\phi_{small-pore}$ have higher oil saturation. Moreover, Fig 4.11b shows that I_o and is positively correlated with S_o . This correlation can be explained by the positive correlation between I_o and small $\phi_{small-pore}$ which we have discussed. By using the relationship between $\phi_{small-pore}$ and

S_o , we find a possible way to identify sweet spots with high oil saturation in the field by analyzing imbibition data (I_o) and MICP profiles ($\phi_{small-pore}$).

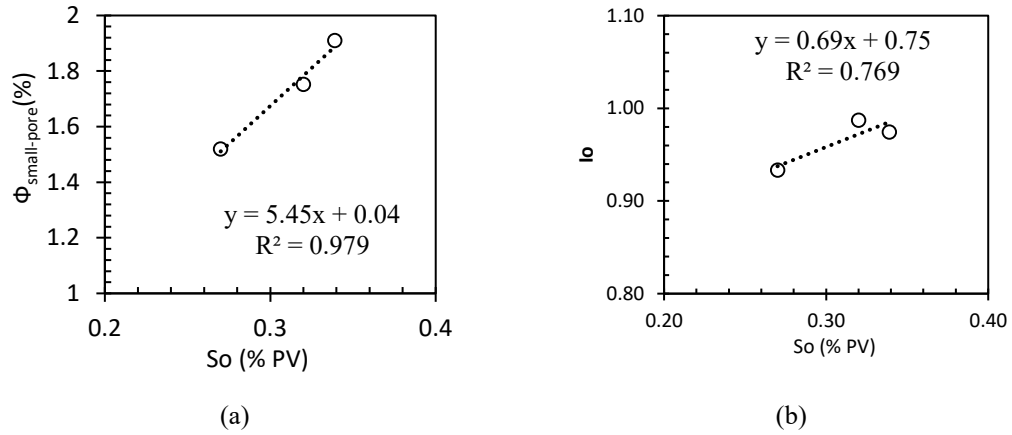


Figure 4.11 Correlation between (a) $\Phi_{small-pore}$ vs. S_o and (b) I_o vs. S_o of samples from Well A.

Chapter 5 Counter-current Imbibition Experiments on MT Samples:

Evaluating Controlling Factors of Imbibition Oil Recovery

In this chapter, we conduct liquid-liquid contact angle measurements and counter-current imbibition experiments (soaking experiments) on Monteny oil-saturated samples. Here, we investigate the factors controlling imbibition oil recovery including salinity of soaking fluid, initial water saturation, and ME solution.

5.1 Materials

5.1.1 Core Samples

After spontaneous-imbibition experiments, six of the core plugs are partly oil-saturated and the other six are partly brine-saturated. Then we inject oil into the partly brine-saturated core plugs by using a core-flooding system until the core plugs reach residual water saturation. The pressure difference profiles during oil flooding and the calculation of effective permeability of oil (K_o) is presented here.

Using a core-flooding system (**Fig 5.1**), we inject oil into the partly brine-saturated core plugs at a constant inlet pressure and wait for equilibrium state, when the plugs reach residual water saturation and no more brine is produced from the system outlet. After reaching the equilibrium state, we stop constant pressure injection and inject oil at different constant rates and record the change of differential pressure along the core plug (i.e. inlet pressure – outlet pressure, where outlet pressure is 0 psig).



Figure 5.1 Vinci core-flooding system

Fig 5.2 shows pressure difference (inlet pressure- outlet pressure) versus flooding time of the core plugs. Initially we inject oil at a constant pressure until the core plugs reach residual water saturation. Then, we start injecting oil at constant flow rate. As we can see in **Fig 5.2**, the pressure difference generally decreases over time until it plateaus. For example, the initial oil injection pressure for sample MT-B3 (**Fig 5.2c**) is 1,800 psig. After the core plug reaches its residual water saturation, the constant pressure oil injection is changed to constant rate oil injection. Oil is injected at 0.003 cc/min initially. The pressure difference decreases until it plateaus at 1,580 psig. Then we change the oil injection rate to 0.002 cc/min. The pressure difference decreases again until it plateaus at 1,310 psig.

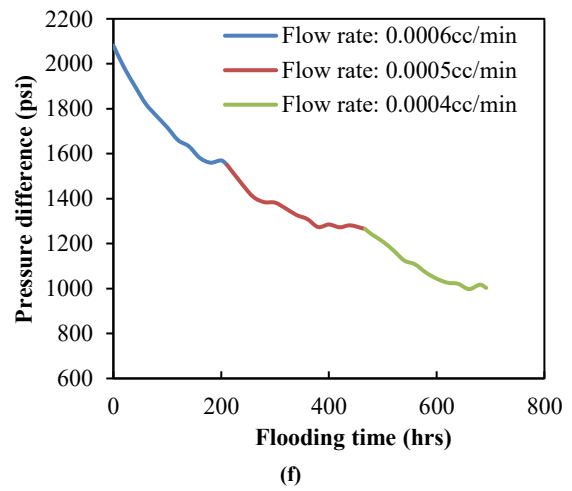
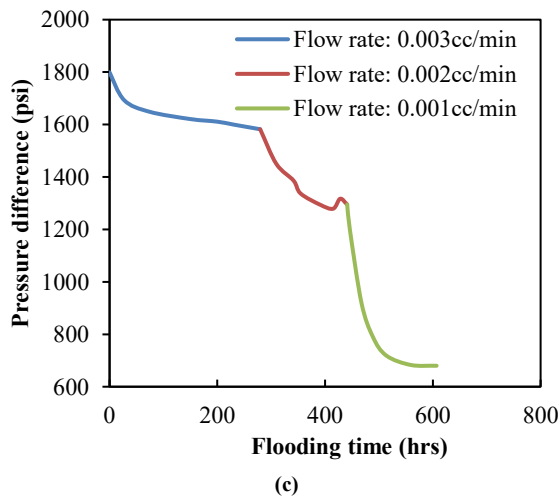
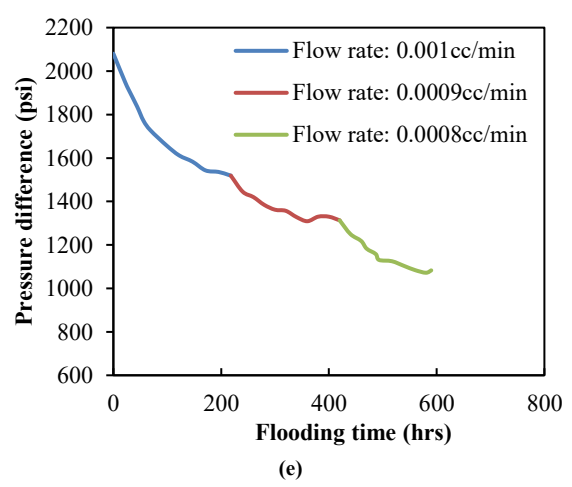
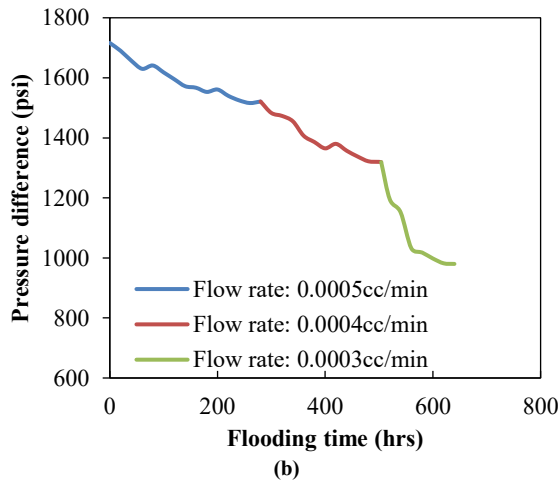
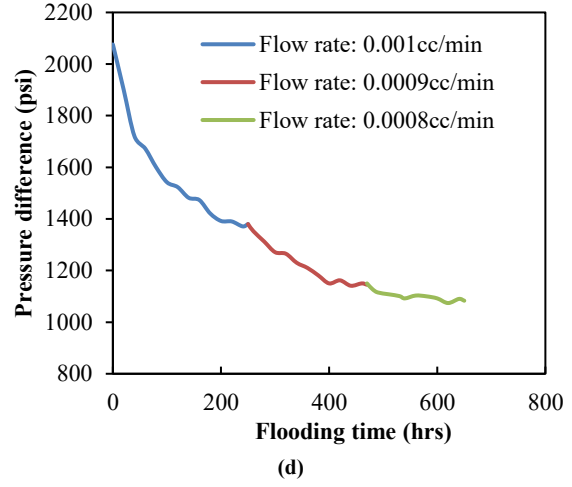
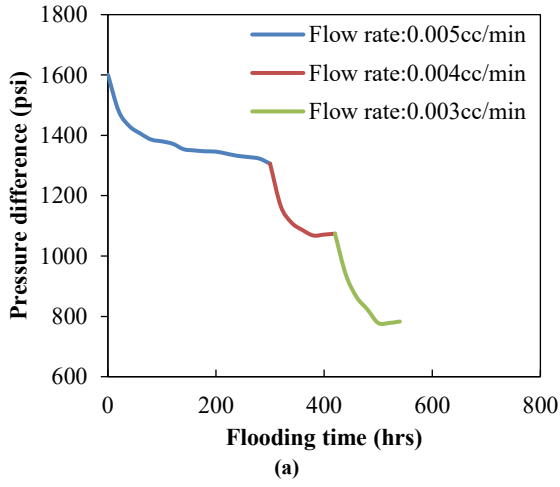


Figure 5.2 Pressure difference profiles during oil flooding of core plugs of (a) MT-B1, (b) MT-B2, (c) MT-B3, (d) MT-A1, (e) MT-A2, and (f) MT-A3.

5.1.1.1 Oil Effective Permeability (K_o) for Core Plugs

Effective permeability is the ability of a rock to transmit one fluid phase when it contains multiple fluid phases (Satter et al., 2015). Based on Darcy's law (Whitaker et al., 1986), the calculation of effective permeability of oil in this study is:

$$K_o = \frac{Q_{oil}\mu_{oil}L}{A_c\Delta P} \quad 5.1$$

where K_o is effective permeability of oil at the end point, Q_{oil} is injection oil rate, μ_{oil} is the viscosity of oil, L is the length of the core plug, A_c is the cross-sectional area of the core plug, ΔP is the pressure difference along the core plug (inlet pressure-outlet pressure).

Results of our core flooding tests show that pressure difference along the core plug reaches equilibrium when we inject oil at a constant flow rate (**Fig 5.2**). The value of L , A_c and μ_{oil} are known. Therefore, we calculate effective permeability of oil using the value of equilibrated pressure difference and constant flow rate. For one core plug, K_o is calculated three times since we inject oil at three flow rates. We average K_o to reduce measured errors. **Table 5.1** shows the average K_o for The Montey core plugs. K_o of Well B samples is typically higher than that of Well A samples.

Table 5.1 lists the effective permeability of oil at residual water saturation for all the core plugs, which is determined by injecting oil into partly brine-saturated plugs using a core-flooding system. The oil effective permeability calculated using the core-flooding data and steady-state Darcy's

equation is significantly lower than the measured air permeability listed in **Table 3.2**. **Fig 5.3** shows the oil effective permeability versus residual water saturation for different core plugs.

Table 5.1 Measured values of oil effective permeability and residual water saturation (end point).

Sample ID	Depth (m)	End-point oil effective permeability (μD)	End-point water saturation (%PV)
MT-A1	2274.66	0.381	4.86
MT-A2	2285.16	0.317	10.92
MT-A3	2287.34	0.180	15.74
MT-B1	2188.18	1.791	8.96
MT-B2	2196.94	0.155	31.19
MT-B3	2200.80	0.802	16.84

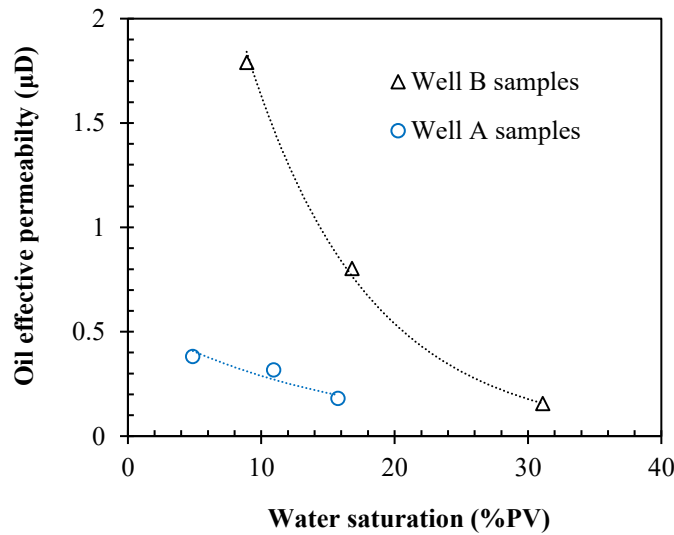


Figure 5.3 Oil effective permeability versus water saturation at residual water saturation (end point) for different core plugs from Wells A and B.

Therefore, after spontaneous imbibition experiment and core flooding experiment, half of the core plugs are oil-saturated ($S_w=0$) and the other half are oil-saturated with residual brine ($S_w \neq 0$). **Table 5.2** shows the depth, S_w , permeability and porosity of the core plugs for soaking experiments.

Table 5.2 Depth, original mass, diameter and length of the core plugs from the Montney Formation.

Sample ID	Pair	Depth (m)	S_w (%PV)	Permeability, k_{air} (μD)	Porosity (%BV)
MT-A1	MT-A1-1	2,274.70	0	9.02	4.51
	MT-A1-2	2,274.66	4.86		
MT-A2	MT-A2-1	2,285.12	0	5.25	2.79
	MT-A2-2	2,285.16	10.92		
MT-A3	MT-A3-1	2,287.30	0	7.28	4.74
	MT-A3-2	2,287.34	15.74		
MT-B1	MT-B1-1	2,188.13	0	40	6.14
	MT-B1-2	2,188.18	8.96		
MT-B2	MT-B2-1	2,196.90	0	20	4.31
	MT-B2-2	2,196.94	31.19		
MT-B3	MT-B3-1	2,200.76	0	40	6.61
	MT-B3-2	2,200.80	16.84		

5.1.2 Fluid Samples

Different soaking fluids are used to evaluate the imbibition oil recovery by conducting soaking tests. Here, we present the properties of reservoir brine, fresh water and a microemulsion (ME) solution. ME refer to a structured and spontaneous solution of surfactant, solvent and water (Hoar et al., 1943). The ME additive here is composed of nonionic surfactants and solvent (citrus terpene with concentration in the range of 7-13 wt%). This additive is thermodynamically stable and dilutable in a wide range of brines, from fresh water up to 300,000 mg/L brines. Table 6.2 shows the physical properties of the aqueous fluids used for the soaking experiments including surface tension, viscosity and interfacial tension (IFT). We measured density and surface tension of fluids

and interfacial tension between oil and brine with SIGMA 700 Tensiometer (as shown in **Fig 5.4a**). We also measured viscosity of fluids with viscometer (as shown in **Fig 5.4b**). All the tests are conducted under room temperature. Each test is repeated three times and an average is recorded in **Table 5.3**.

The interfacial tension between oil and different aqueous fluids were also measured by spinning drop tensiometer (**Fig 5.5**). The IFT values can be measured by Young-Laplace Equation or Vonnegut Equation (for ultra-low IFT values).

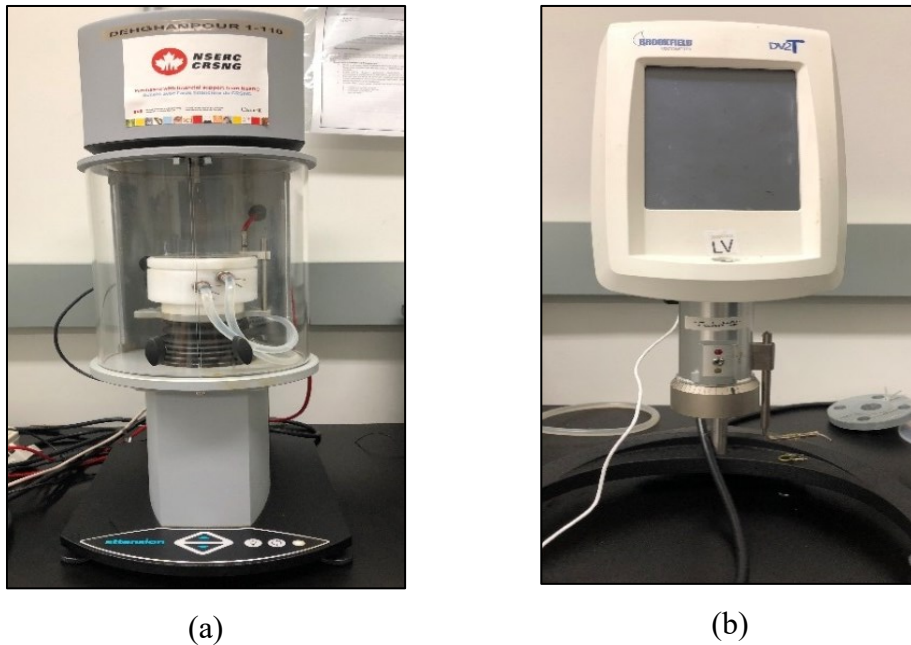


Figure 5.4 The instrument used for physical properties measurements: (a) SIGMA 700 Tensiometer and (b) Brookfield Viscometer

Table 5.3 Properties of the aqueous fluids used for the soaking experiments.

Fluid sample	Density (g/cc)	Surface tension (mN/m)	Viscosity (cp)	IFT (mN/m)
Brine	1.1	65.6	1.18	2.04
Fresh water	1.01	72.6	1.27	2.15
Brine with ME	1.09	22.5	0.90	0.06
Fresh water with ME	1.00	25.3	0.92	0.09



Figure 5.5 Spinning drop tensiometer.

5.2 Methodology

5.2.1 Liquid-Liquid Contact Angle (CA)

We polish the end pieces of the core plugs to get smooth surfaces for measuring liquid-liquid contact angle on oil-saturated end pieces by using a high-resolution camera (**Fig 4.1**). For CA measurement, the oil-saturated end piece is placed into a glass cell which is filled with the fluid samples we use, then an oil droplet is dropped by a J-shape syringe needle on the rock surface.

5.2.2 Soaking Experiments

After imbibition experiments on as-received core plugs, we soak the partly oil-saturated plugs ($S_w = 0$) in brine-filled Amott cells (**Fig 5.6**) and measure the volume of produced oil. Following core flooding tests, we place the plugs saturated with oil and residual brine in fresh-water-filled Amott cells. We then periodically record the volume of oil accumulating at the top of Amott cell (**Fig.**

5.6). When oil production stops, we add ME additives into brine or fresh water (1 cc/L) and record the additional oil production over time. Also, to investigate the impact of use Sequence of ME, we place one oil-saturated plug immediately in water with ME solution. Then, we compare its oil RF with that of the samples which are immersed first in water and then in ME solution.

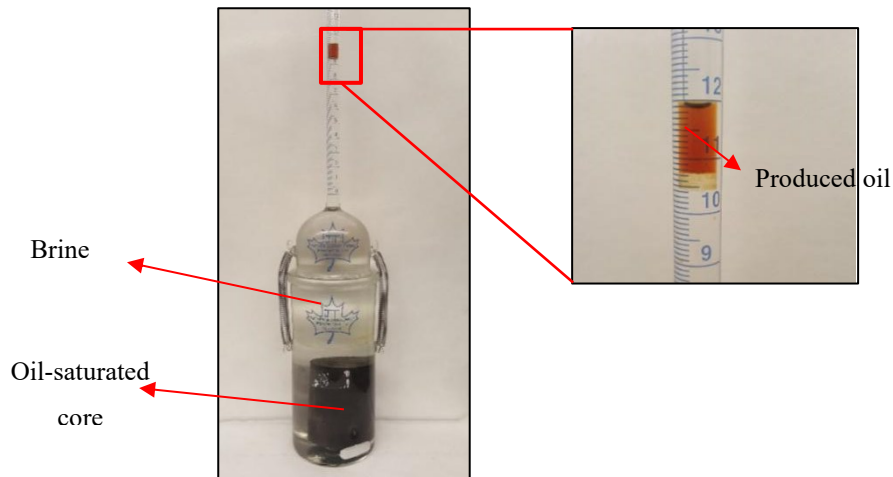


Figure 5.6 Amott cell used for soaking of oil-saturated core plugs in different soaking fluids.

5.3 Results and Discussions

Here, we present the results of liquid-liquid contact angles of oil and the results of soaking experiments on oil-saturated core plugs immersed in soaking fluids with different compositions. We investigate the factors controlling imbibition oil recovery including salinity of soaking fluid, initial water saturation, and ME solution.

5.3.1 Liquid-Liquid Contact Angle

Figs 5.7 show the contact angles of oil on the polished surface of oil-saturated core end pieces immersed in different soaking fluids (fresh water, brine, fresh water with ME, and brine with ME). The oil contact angles in fresh water and brine are less than 90° , which are 85° and 80° respectively), indicating the oil-saturated rock surface is more oil-wet in these two cases. However, the oil

contact angles in fresh water with ME and brine with ME are larger than 90° , which are 138° and 119° respectively, indicating the oil-saturated rock surface is more water-wet in ME solutions. The results indicate that 1) increasing salinity of water reduces the affinity of the core plugs to water; 2) adding ME may alter the oil-wet rock surface to water-wet. We use Young equation (1805) to describe oil contact angles in different soaking fluids shown in Figs. 6.4:

$$\cos(\theta) = \frac{\gamma_{sl} - \gamma_{so}}{IFT} \quad (6.1)$$

Here, θ is the measured oil contact angle on rock surface, γ_{sl} is the interfacial tension between solid surface and soaking liquid, γ_{so} is the interfacial tension between solid surface and oil, and IFT is the interfacial tension between oil and soaking fluid. γ_{so} is the same for different tests if we assume the surface chemistry is homogenous, but γ_{sl} may change with different soaking fluids due to altering composition and properties. When θ is smaller than 90° , which means $0 < \cos(\theta) < 1$, $\gamma_{sl} > \gamma_{so}$ consequently. When θ is larger than 90° , which means $-1 < \cos(\theta) < 0$, $\gamma_{sl} < \gamma_{so}$. The interfacial tension between rock surface and ME solutions is lower than that between rock surface and water. Adding ME to tap water or brine increases the oil contact angle and alters the wettability of rock surface to more water-wet.



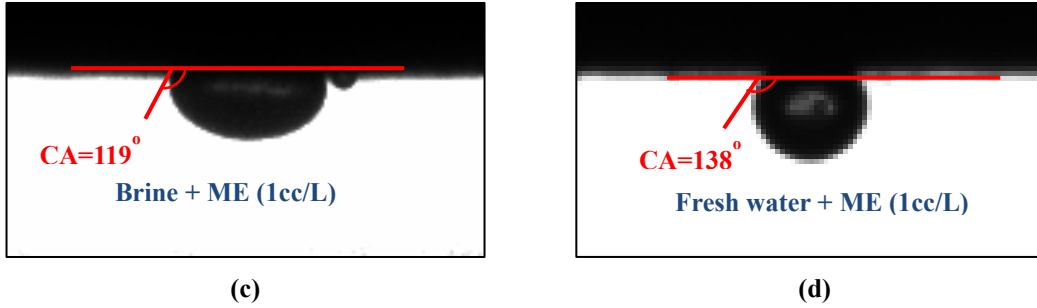


Figure 5.7 The contact angles of oil droplets equilibrated on the surface of oil-saturated core sample MT-A1 immersed in (a) fresh water, (b) brine, (c) brine + ME, (d) fresh water + ME. (Experimental time =10 minutes).

5.3.2 The Effect of Brine Effective Porosity (ϕ_{ew}) of Core Plugs on Oil Recovery

After spontaneous imbibition experiments, we immerse six oil-saturated core plugs in brine and record the volume of produced oil accumulating on the top of Amott cell. The oil recovery factor (RF) is defined as the produced oil volume divided by the initial oil volume in the core plugs. **Fig 5.8** shows the profiles of oil RF versus soaking time for the six oil-saturated core plugs soaked in brine and then in brine with ME. The oil RF for the core plugs immersed in brine varies from 6.02% to 10.42% and the equilibrium time (when no more oil is produced) is 60 to 70 days. In order to investigate the pores invaded by brine, we compare the brine imbibition value (V_b) and oil production volume (V_o) as shown in **Fig 5.9**. Based on our spontaneous imbibition tests, oil imbibe into both hydrophobic and hydrophilic pores while brine imbibe only into hydrophilic pores. **Fig 5.9** shows that brine imbibition volume (V_b) is higher than oil production volume (V_o), indicating that brine may only imbibe into a portion of the hydrophilic pores to expel the oil out, which means part of the hydrophilic pores are not accessible for brine imbibition during soaking tests. **Fig 5.10** shows the oil RF versus ϕ_{ew} , representing brine effective porosity. The oil RF is positively correlated with ϕ_{ew} , suggesting that oil expelled out is mainly from the water-wet pores. Here we conclude that most initial oil cannot be expelled and still remain in pores of the core plugs.

This is because the main driving force, capillary pressure, is not strong enough to displace the oil out of small pores (which are often oil-wet). Also, it may be due to snap-off mechanism, which traps oil in large water-wet pores.

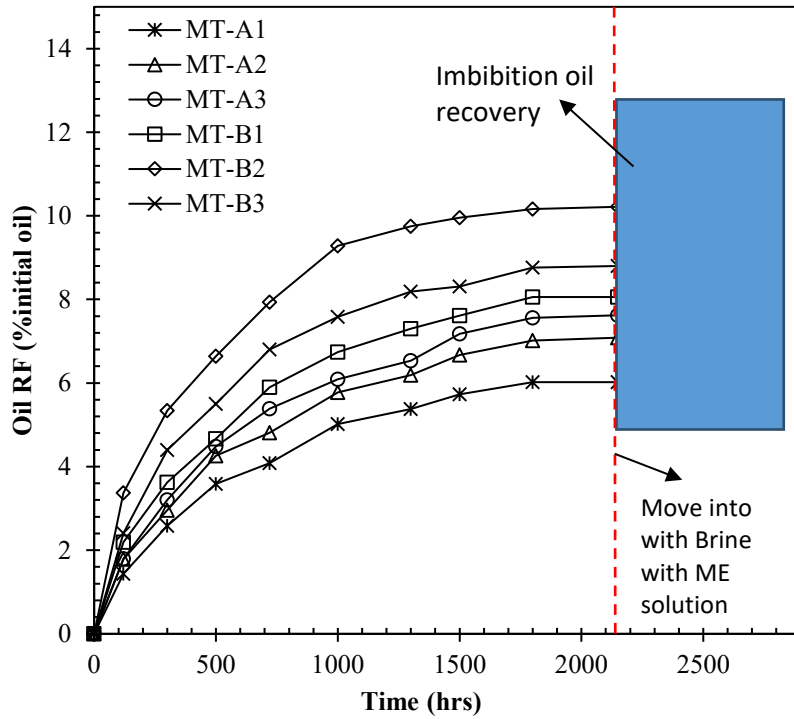


Figure 5.8 Oil RF vs. time for 6 oil-saturated core plugs immersed in brine and ME solutions (brine with ME)

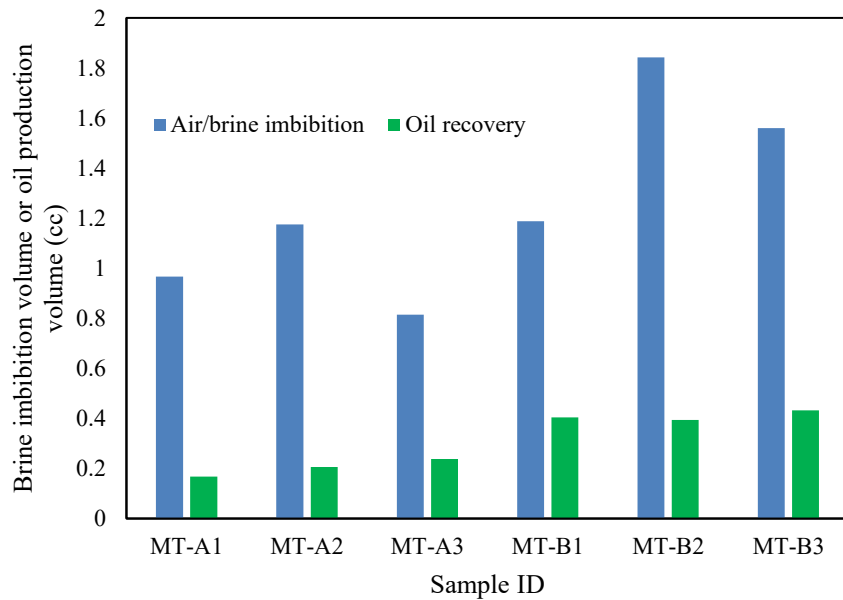


Figure 5.9 The comparison between brine imbibition volume (V_b) and oil production volume (V_o). Generally, $V_b > V_o$ indicates that brine may imbibe into part of the hydrophilic pores to expel the oil out

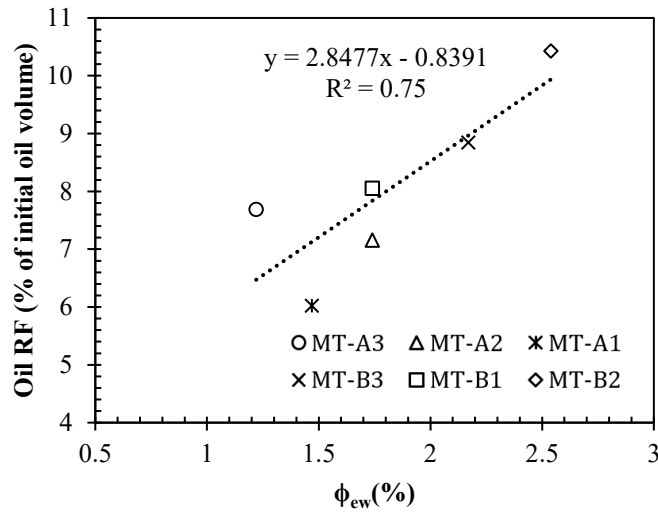


Figure 5.10 Oil RF versus ϕ_{ew} .

5.3.3 The Effect of Brine Salinity on Oil RF

After core-flooding experiments, the brine-saturated core plugs are saturated with oil at residual water saturation. Then, we immerse them in fresh water and record the oil recovery over time. **Fig 5.11** compares the oil recovery profiles of twin core plugs soaked in brine or fresh water, and then in brine (or fresh water) with ME.

In **Fig 5.11** we observe higher oil RF for plugs immersed in fresh water (avg. RF=11%) compared with those in brine (avg. RF=9%). Furthermore, the imbibition rate of fresh water into the plugs is higher than that of brine. **Fig 5.11** shows that oil RF by fresh water soaking is higher than that by brine soaking. The two possible mechanisms responsible for higher imbibition of fresh water compared with brine into the oil-saturated core plugs are i) osmotic effect (Kemper et al., 1966; Neuzil et al., 2000) and ii) presence of water film covering the rock surface before soaking tests due to the existence of residual water in the pores (Salathiel et al., 1973). iii) Water with lower salinity has higher affinity of the core plugs to water based on contact-angle measurements.

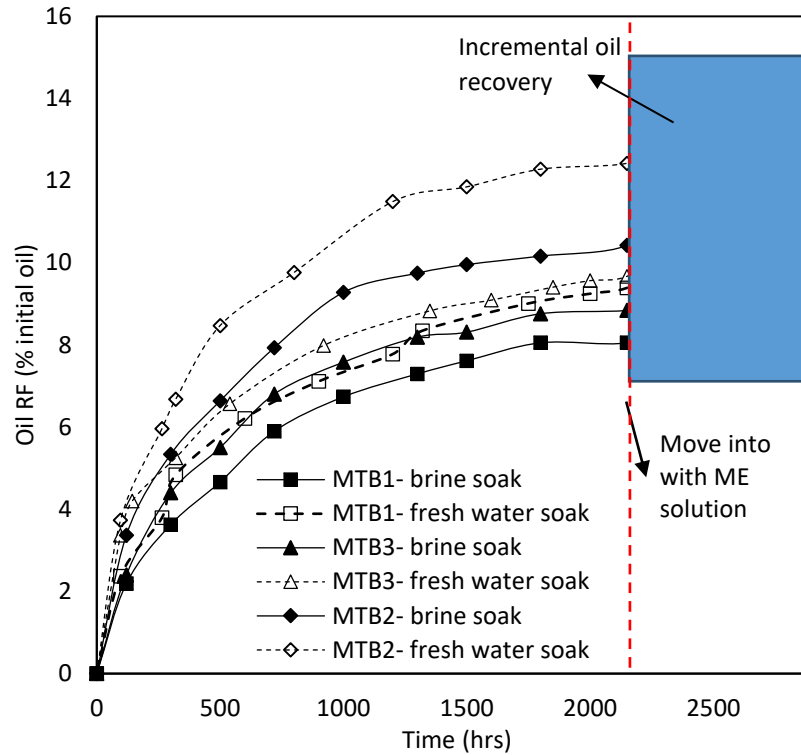
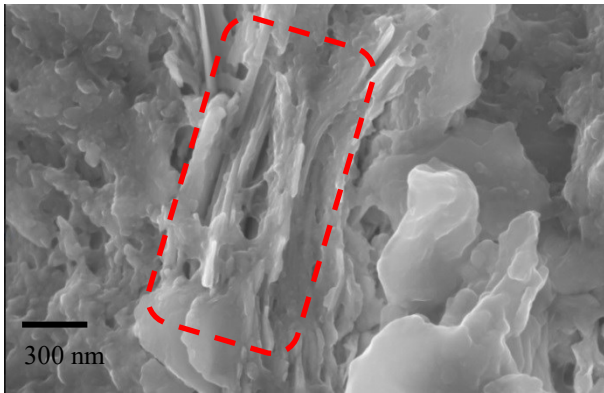


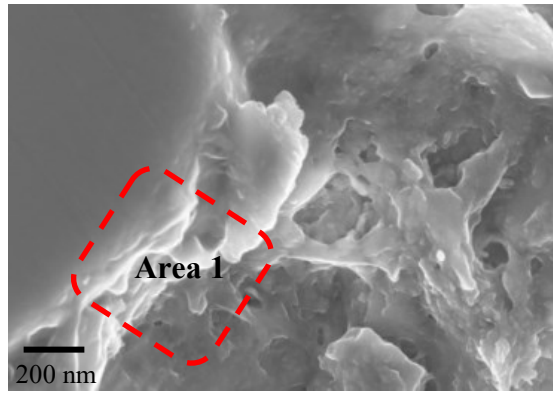
Figure 5.11 Comparison of oil recovery factor for Well B twin core plugs immersed in different soaking fluids (brine, fresh water, and ME solutions (brine with ME and fresh water with ME)).

From **Fig 3.5**, we can observe clay minerals like illite/mica. The transport of water through a semi-permeable membrane (e.g. clay minerals) from a region of low salinity to a region of high salinity equilibrates ions concentration on both sides of the membrane (Greenberg et al., 1973; Kemper et al., 1966; Neuzil et al., 2000). In other words, initial water saturation inside the rock usually has high salinity due to the dissolution of precipitated salt, cation exchange from clays, and dissolution of rock minerals (Kemper et al., 1966). To meet the thermodynamic equilibrium conditions, chemical potential of each ion in the pore space and outside of the core plugs should be the same. Therefore, fresh water (salinity < 500mg/L) imbibes more into the core plugs compared with high salinity reservoir brine (130,000 mg/L), resulting in higher oil displacement from core plugs. Zhang et al. (2007b), Lager et al. (2007), Webb et al. (2005) and Morrow et al. (2011) concluded that oil recovery increases by performing a tertiary low-salinity waterflood process.

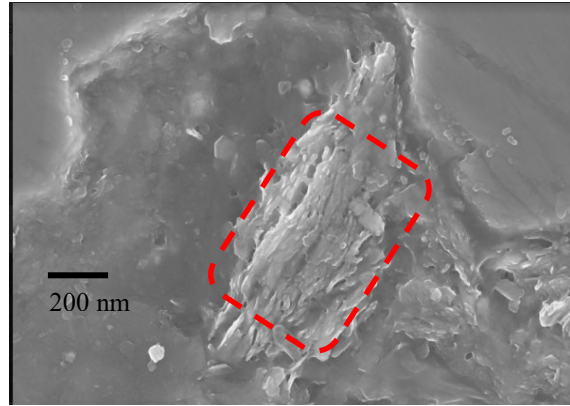
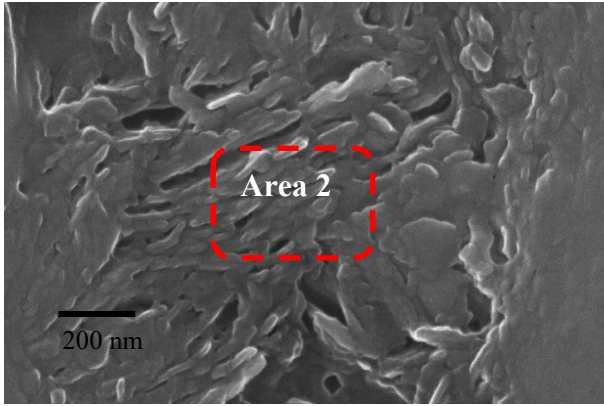
Except SEM analysis, we also conducted EDS analysis to confirm the existence of clay minerals. **Fig 5.12** shows the SEM images from core plug MT-B2. Clay minerals can be observed in SEM images. Illite ribbons grow and coalesce to thin, platy crystals which tend to be planar and laminated (Keller et al., 1986). The edges of illite flakes are scalloped due to the non-uniform growth of illite ribbons (Keller et al., 1986). We can observe crystal layers and flakes, and the edges of the coalesced flakes are scalloped in the SEM images. These clay minerals can be categorized as illite/mica. In order to confirm the elemental analysis or chemical characterization of these areas, we conducted EDS analysis to get elemental spectrums as shown in **Fig 5.13**. From the elemental spectrums, we find the main elements are silicon, oxygen, and aluminum, representing clay minerals. There are also some minor elements such magnesium, iron and potassium. The existence of potassium elemental spectrum of the areas represents non-kaolinite clay minerals. These clays can be categorized as illite/mica base on the crystal layers and coalesced edges of flakes from **Fig 5.12**.



(a)



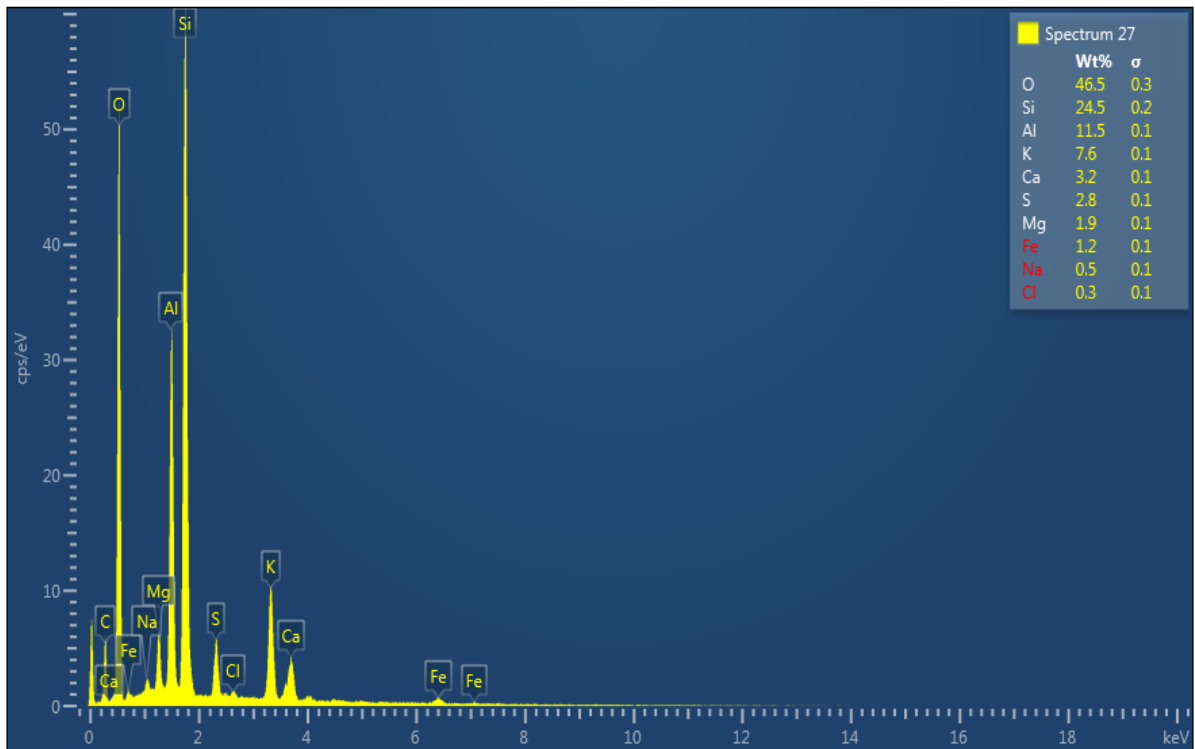
(b)



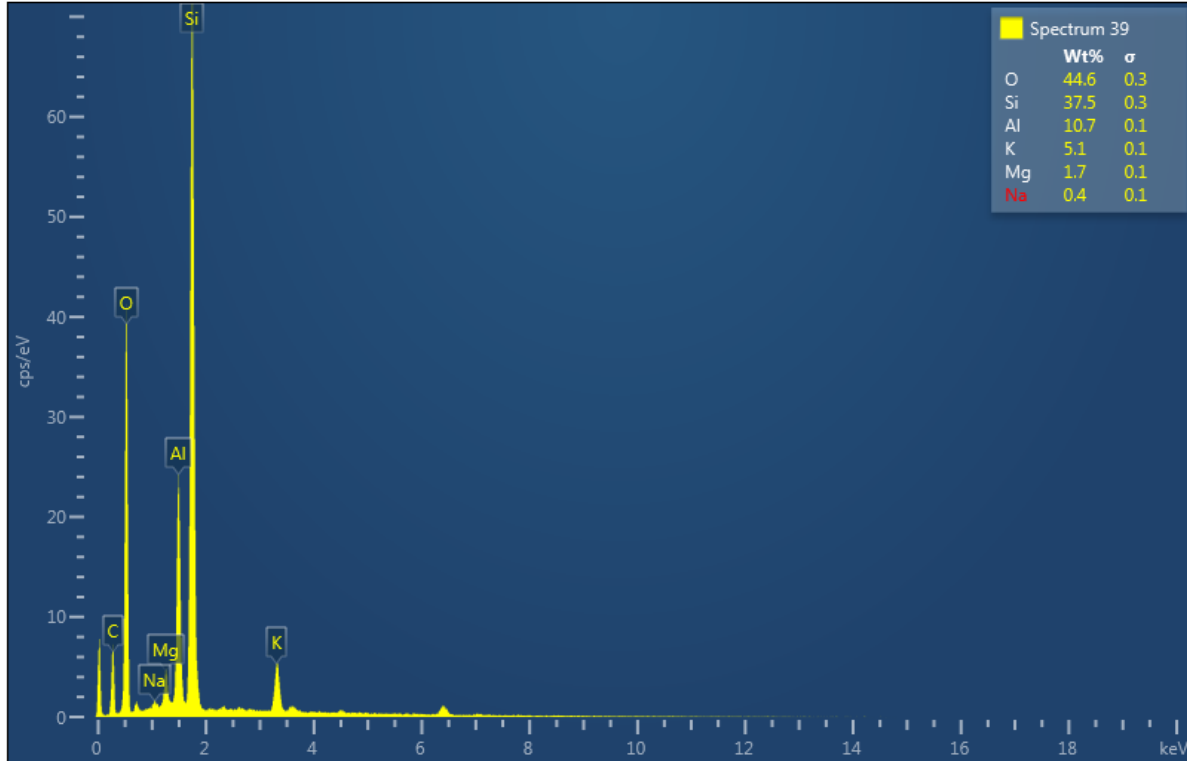
(c)

(d)

Figure 5.12 SEM images from core plug MT-B2. The clay minerals are categorized as illite/mica.



(a)



(b)

Figure 5.13 The elemental spectrums determined by EDS analysis of area 1 & 2 in Fig 5.12 (b) & (c).

To confirm the existence of salts precipitated in the pore space of as-received core plugs, we perform the electrical conductivity measurements. An end-piece of core plug is immersed in fresh water and electrical conductivity is measured during the imbibition process. Fig 5.14 shows the measured electrical conductivity versus time. We observe that the electrical conductivity increases over time during the imbibition process, indicating that water imbibe into the rock and salt diffuses out of the rock. This observation suggests the presence of salt precipitated in the pore space. The difference between ions concentration in the pores space and that in the imbibing water (out of the core plugs) leads to a chemical-potential difference. To reach the equilibrium conditions, it is expected to observe higher imbibition of fresh water into the core plugs compared with high-salinity brine. Therefore, osmotic potential can provide an additional driving force for water

imbibition and expelling the oil out of the core plugs. Similarly, Xu et al. (2014) investigated the role of osmotic potential on water imbibition by comparing the imbibition rates of deionized water and brine with salinities of 10 and 20 wt% for core samples from the Horn River Basin. Their results showed that fresh water imbibition is significantly higher than brine imbibition.

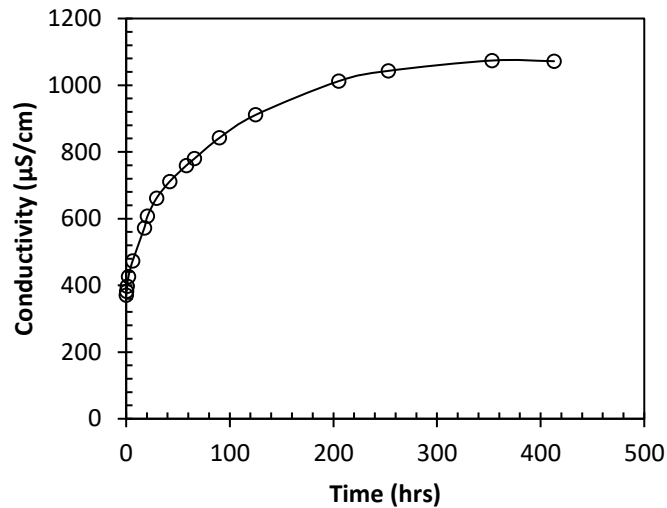


Figure 5.14 The Measured electrical conductivity profile when a dry end-piece of MT-B1 immersed in fresh water.

5.3.4 The Impact of Surfactant on Imbibition Oil Recovery

Here, we evaluate the effects of ME solution on imbibition oil recovery:

Set-1 (representing surfactant-EOR after fracturing): The oil-saturated core plugs are first soaked in brine or fresh water until oil production is stopped. Then, the core plugs are removed from the cell and soaked in another cell filled with the brine (or fresh water) plus ME solution. **Figs 5.8 and 5.11** show that oil production due to brine and fresh water soaking ends before 2150 hours. After soaking the plugs in ME solution, we observe incremental oil recovery ranging from 1.1% to 1.9%.

Set-2 (representing surfactant-EOR while fracturing): We immersed an oil-saturated core plug (MT-A3) immediately in fresh water plus ME solution and the measured oil recovery factor is

plotted versus time in **Fig 5.15**. In the same figure, we plot the oil recovery profiles of the three samples of Well B (with porosity and permeability values higher than that of MT-A3) which were first soaked in fresh water and then in fresh water plus ME solution. Interestingly, the rate of oil recovery for MT-A3 with lower porosity and permeability is higher than those for the other three samples. This is possibly caused by the sequence of surfactant addition. Some large hydrophilic pores contain brine or fresh water when soaking a plug in a fluid without surfactant. Subsequent addition of surfactant to the soaking fluid does not significantly improve oil RF since many of the pore networks already have water occupying them. Here, we may argue that surfactant or ME EOR techniques are better deployed as a part of the initial fracturing or at the onset of a waterflood versus in the later stages as a remedial soaking.

Calculation of Capillary Pressure. The major driving force to displace oil during soaking process is capillary pressure (P_c) described by Young-Laplace (1805) equation (Eq. 2.1). Based on our liquid-liquid contact angle measurements, the oil contact angle in fresh water or brine is less than 90° while that in ME solutions is larger than 90° , indicating the oil-saturated rock surface is more water-wet in ME solutions. According to Eq. 2.1, capillary pressure can be calculated by using oil CA, IFT and pore radius. Here we assume the average pore radius in the calculation is 30nm.

Table 5.4 lists the calculated capillary pressure during imbibition oil recovery process for different soaking fluid samples. P_c is negative when using brine and fresh water as soaking fluids but positive for ME solutions. Here, when adding ME in base cases, P_c changes from negative to positive and the wettability of rock alters from oil-wet to water-wet. Negative capillary pressure presents soaking fluids from imbibing into bypassed zone while positive capillary pressure promote soaking fluid enter bypassed zones (Sharma and Mohanty, 2011). Therefore as capillary

change in ME solutions, the oil can be mobilized easier during counter-current imbibition. Here we may conclude that the increased oil recovery when using ME solutions as soaking fluids is dominated by the effect of wettability alternation. However, we notice that as the main driving force for imbibition oil recovery, the calculated P_c here is too small since the IFT of ME solutions is very low. Therefore the calculation of P_c may not suitable for this case.

Table 5.4 The calculated capillary pressure during imbibition oil recovery process for different soaking fluid samples

Fluid sample	IFT (mN/m)	Oil CA (degree)	P_c (psi)
Brine	2.04	81	-2.79
Fresh water	2.15	85	-1.72
Brine with ME	0.06	119	0.28
Fresh water with ME	0.09	138	0.65

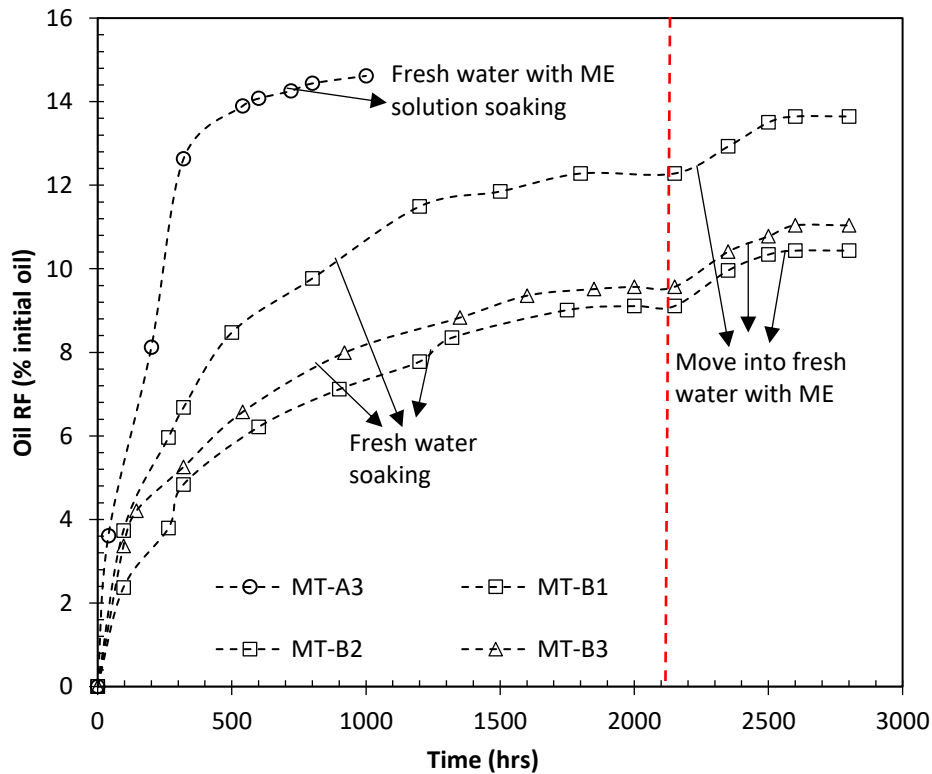


Figure 5.15 Comparing oil recovery profiles for MT-A3 and the three core plugs of Well B immersed in fresh water and fresh water plus ME.

5.3.5 Solvent Contribution to Oil Production

When using ME solutions to conduct counter-current imbibition experiments, the solvent in solutions may dissolve some part of the oil components and accumulate on the top of Amott cell with the produced oil droplets, which may cause measured errors of produced oil volume. Here, in order to figure out the possible solvent contribution to oil production during soaking process, we assume 20% pore volume of core plugs can be contacted with solvent since the oil RF for all the cases is lower than 20%. The ME additive here is composed of nonionic surfactants and solvent with concentration in the range of 7-13 wt%. Here we use 10 wt% as the concentration of solvent in ME additive. The calculated solvent which has been contacted with oil is shown in **Table 5.5**. The solvent contacted with oil is much lower than produced oil of all samples immersed in ME solutions. Also, most of the samples except MT-A3-2 were immersed into base cases (brine or fresh water) first and then moved to ME solutions. The pore volume contacted with solvent may be much lower than 20% in real cases. Therefore, the solvent contribution to oil production can be ignored.

Table 5.5 The calculated solvent which has been contacted with oil during ME soaking.

Sample ID	Pair	Pore Volume (cc)	Solvent contacted with oil (cc)	Produced oil (cc)
MT-A1	MT-A1-1	2.80	0.056	0.22
	MT-A1-2	2.95	0.059	Nanoparticle solution soaking
MT-A2	MT-A2-1	1.87	0.037	0.24
	MT-A2-2	1.89	0.038	Nanoparticle solution soaking
MT-A3	MT-A3-1	3.24	0.065	0.28
	MT-A3-2	3.17	0.063	0.3
MT-B1	MT-B1-1	4.58	0.092	0.47
	MT-B1-2	4.24	0.085	0.44
MT-B2	MT-B2-1	3.15	0.063	0.476
	MT-B2-2	3.12	0.062	0.38
MT-B3	MT-B3-1	4.86	0.097	0.486
	MT-B3-2	4.75	0.095	0.42

Chapter 6 Chemical EOR While Fracturing: Wettability Alteration by Nanoparticle Additives

Core analysis and wettability studies indicate that most of the remaining oil is trapped in sub-micron oil-wet pores which can hardly be accessed by water. Subsequent EOR operations or re-fracturing jobs for producing the remaining oil are attractive but expensive and in some cases risky due to insufficient information regarding the downhole completion conditions. Instead, in this chapter, we evaluate the idea of adding nanoparticles in fracturing water to enhance its wetting affinity to oil-wet pores and to mobilize part of the oil during the extended shut-in periods.

6.1 Fluid samples

We analyze the performance of two different nanoparticle additives on core plugs collected from the Montney Formation. Additive 1 is a colloidal dispersion with highly surface-modified nanoparticles and additive 2 is a micellar dispersion with silicon dioxide nanoparticles, solvents and surfactants. We mix reservoir brine or fresh water with additive 1 or 2 of different concentrations for more than 24 hours to prepare aqueous phases in this study. **Table 6.1** lists the measured properties of the aqueous fluids, including density, surface tension (mN/m) and IFT (mN/m). This table shows that the solutions with nanoparticle additives have lower IFT compared with the base cases (brine and fresh water). The IFT decreases with the increase of the concentration of nanoparticle additive generally.

Table 6.1 Properties of the aqueous fluids used for the CA experiments.

Sample name	Density (g/cc)	Surface tension (mN/m)	IFT (mN/m)
Brine	1.101	65.60	1.842
Fresh water	1.009	72.6	2.046
Brine with additive 1 (5 wt%)	1.089	24.03	0.267
Brine with additive 1 (10 wt%)	1.086	26.93	0.242
Brine with additive 1 (35 wt%)	1.083	27.54	0.190
Fresh water with additive 1 (5 wt%)	1.002	29.16	0.447
Fresh water with additive 1 (10 wt%)	1.003	30.28	0.373
Fresh water with additive 1 (35 wt%)	1.082	32.25	0.344
Fresh water with additive 2 (1.89 cc/L)	0.998	28.55	0.186
Fresh water with additive 2 (3.78 cc/L)	0.999	28.75	0.211
Fresh water with additive 2 (7.56 cc/L)	0.999	29.30	0.260

6.2 Methodology

6.2.1 Dynamic Liquid-liquid Contact-Angle (CA) Measurements

We conducted liquid-liquid contact-angle measurements to characterize the natural wettability of oil-saturated end pieces by using different aqueous phases in **Table 6.1**. For liquid-liquid contact-angle measurements, the oil-saturated end piece is placed into a glass cell which is filled with the fluid samples we use, then an oil droplet is dropped by a J-shape syringe needle on the rock surface. We record the dynamic The CA changes for 10 hours have been recorded.

6.2.2 Soaking Experiments

We performed imbibition oil-recovery tests using Amott cells to investigate if adding nanoparticle additives in fracturing fluid can enhance spontaneous imbibition of aqueous phase and improve the oil displacement from the oil-saturated core plugs. Here, we used two oil-saturated core plugs: (i) the core plug MT-A1 was immersed into fresh water with additive 1 (10 wt%) and (ii) the core plug MT-A2 was immersed into fresh water with additive 2 (3.78 cc/L).

6.3 Results and Discussions

6.3.1 Contact-Angle (CA) Measurements

6.3.1.1 CA Results.

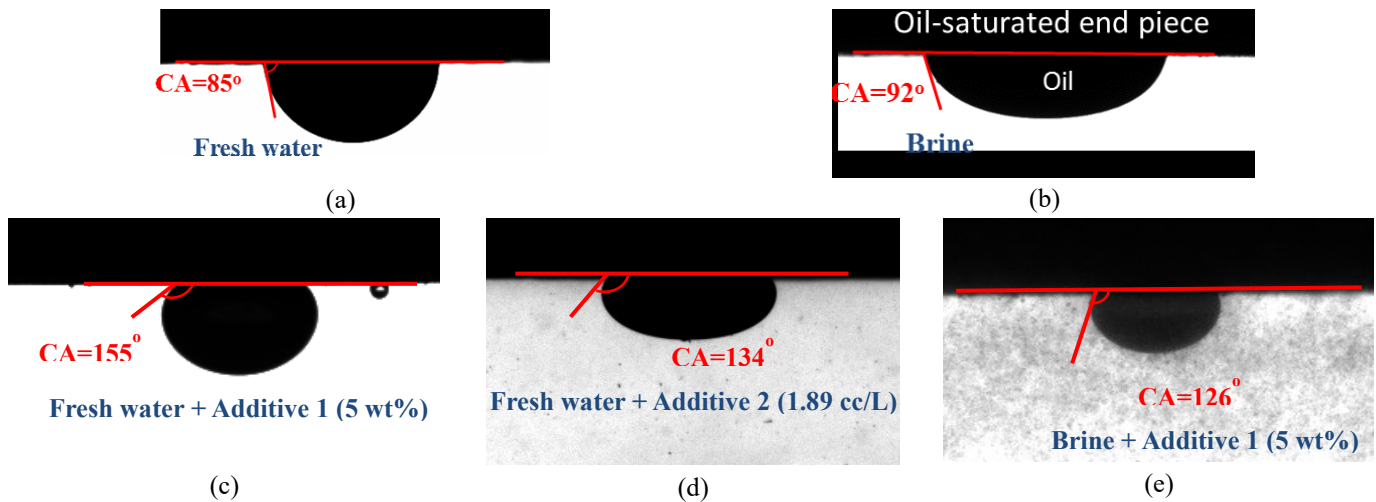
The detailed dynamic contact angle measurements and contact angles changing profiles versus time are presented in **Appendix A. Table 6.2** lists the measured contact angles of oil droplet on the surface of oil-saturated end pieces which were immersed into different aqueous fluids. **Fig 6.1** shows the liquid-liquid contact angles of oil droplet on the oil-saturated end pieces immersed in different solutions when the experiment time is 10 minutes. The CA results could be used as a qualitative way to describe wettability change of rock surface.

From **Table 6.2**, we can find the oil droplet CA changes from 102° to 79° in brine, and 90° to 72° in fresh water, which indicate that the oil-saturated rock is oil-wet in reservoir brine. When brine or fresh water was mixed with nanoparticle additive 1 or additive 2 of different concentrations, the CA oil droplet increases to more than 90° , indicating the rock surface is more water-wet. Based on the results shown in Table 6.2, there is no clear correlations between additive concentration and contact angle change. For fresh water with different concentrations of additive 1, the oil droplet CA is very similar for different additive concentrations. For fresh water with additive 2 with

different concentrations of additive 2, the oil droplet CA is highest when the concentration is 1 3.78 cc/L, which is varying from 146° to 135°.

Table 6.2 The CA ranges of oil droplet on the surface of oil-saturated end pieces immersed into different aqueous fluids for the first 10 hours.

Aqueous fluids	Contact angle of oil droplet on oil-saturated rock surface (for first 10 hours)
Brine	102°-79°
Tap water	90° to 72°
Brine with additive 1 (5 wt%)	133°-112°
Brine with additive 1 (10 wt%)	140°- ?° (too cloudy to measure for software)
Brine with additive 1 (35 wt%)	139°- ?° (too cloudy to measure for software)
Fresh water with additive 1 (5 wt%)	150°-163°
Fresh water with additive 1 (10 wt%)	148°-137°
Fresh water with additive 1 (35 wt%)	160°-118°
Fresh water with additive 2 (1.89 cc/L (0.5gpt))	137°-125°
Fresh water with additive 2 (3.78 cc/L (1gpt))	146°-135°
Fresh water with additive 2 (7.56 cc/L (2gpt))	120°-95°



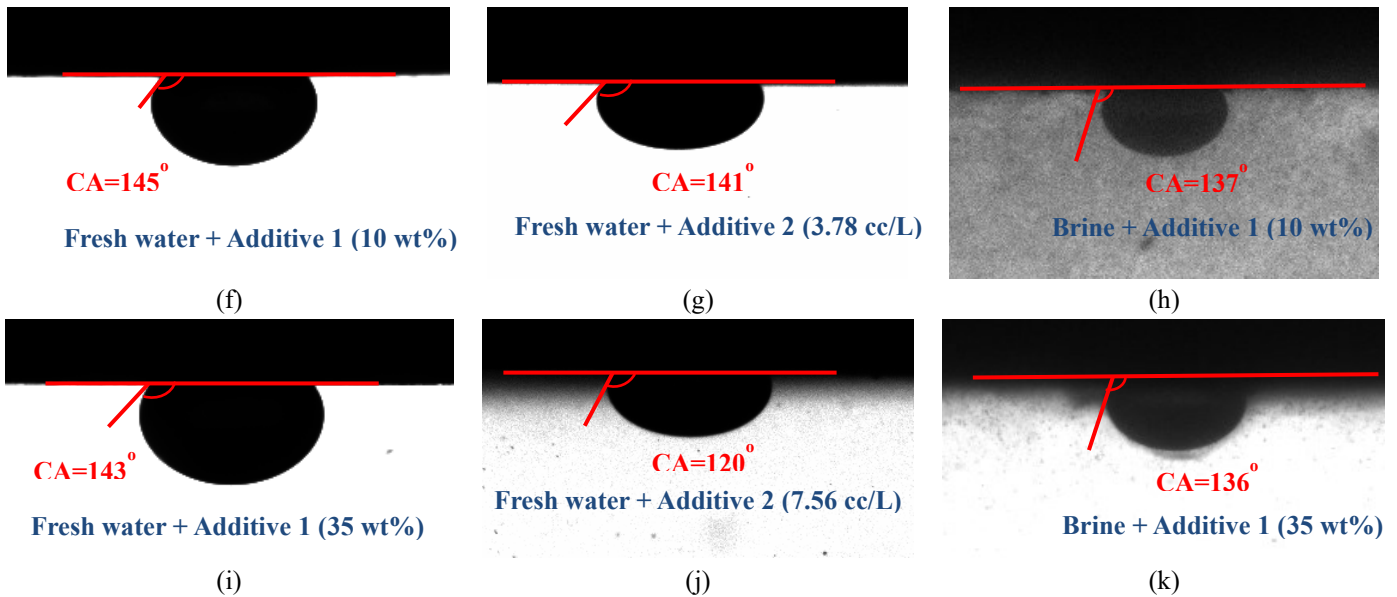


Figure 6.1 The Liquid-liquid contact angles of oil droplet on the oil-saturated end pieces immersed in (a) fresh water; (b) brine; (c) fresh water + additive 1 (5 wt%); (d) brine + additive 2 (1.89 cc/L); (e) brine + additive 1 (5 wt%); (f) fresh water + additive 1 (10 wt%); (g) brine + additive 2 (3.78 cc/L); (h) brine + additive 1 (10 wt%); (i) fresh water + additive 1 (35 wt%);(j) brine + additive 2 (7.56 cc/L); (k) brine + additive 1 (35 wt%)(time =10 minutes).

6.3.1.2 Mechanisms behind Wettability Change.

Based on the CA results, we may conclude that the additive 1 and additive 2 can change the wettability of oil-saturated rock surface to make it more water-wet. The extent of wettability alteration is more pronounced in the presence of fresh water compared with reservoir brine.

The mechanism behind wettability alternation and oil recovery can be explained by structural disjoining pressure: nanoparticles have a tendency to create wedge-like film driven by Brownian motion and diffusion described by disjoining pressure. The spreading of nanofluids can be enhanced by the in-layer particle structuring (Wasan et al., 2011, Hendraningrat et al., 2013).

Presence of nanometer-sized particles can create an in-layer particle structuring (a wedge-like film) in three-phase contact region (Wasan et al., 2011, Hendraningrat et al., 2013). Wasan and Nikolov (2003) and Wasan et al. (2011) investigated the oil recovery mechanism using suspension of nanometer-sized particles. They revealed the effects of particle structure formation and disjoining

pressure on spreading nanofluids on solid surface utilizing de Gennes theory (1985) was used in their study:

$$S = \Pi(h)h + \int_0^h \Pi(h)dh \quad (6.1)$$

where S is spreading coefficient, $\Pi(h)$ is disjoining pressure of a wetting film, h is film thickness.

They found that the structural disjoining pressure gradient toward the vertex of the wedge-film is the driving force for spreading the nanofluids (Fig 6.2). Their calculations showed that the spreading coefficient increases as film thickness decreases towards the wedge vertex, indicating the spreading of nanofluids can be enhanced by the in-layer particle structuring.

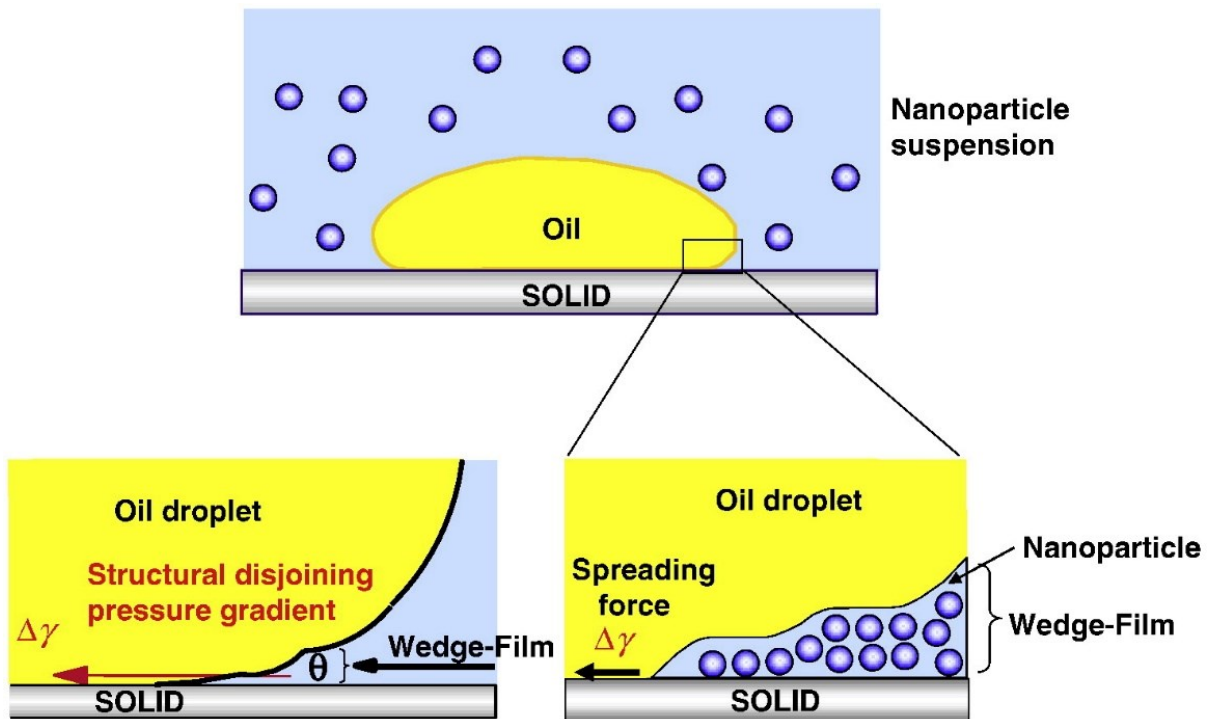


Figure 6.2 The structural disjoining pressure gradient mechanism at the wedge vertex drives the nanofluid spreading due to nanoparticle structuring in the wedge-film (from Wassan et al., 2011).

6.3.1.3 The Effect of Wettability Change on P_c .

According to Eq 2.1, capillary pressure can be calculated by using oil CA, IFT and pore radius (assuming 30nm here in calculation). **Table 6.3** lists the calculated capillary pressure during imbibition oil recovery process for brine, fresh water and the base cases with nanoparticle additives of different concentrations. P_c is negative when using brine and fresh water as soaking fluids but positive for all the nanoparticle solutions. Negative capillary pressure presents soaking fluids from imbibing into bypassed zone while positive capillary pressure promote soaking fluid enter bypassed zones (Sharma and Mohanty, 2011). The soaking fluids can imbibe into pores easier during counter-current imbibition and consequently result in higher oil production. Higher oil CA indicates higher wetting affinity to water and results in higher P_c . The core plugs with higher wetting affinity toward water have stronger P_c during counter-current imbibition process for oil production. P_c is the main driving force for oil production. Here, we get the conclusion that the wettability alternation when adding nanoparticles in soaking fluids may enhance the oil recovery. However, if we compare the concentration of nanoparticle additives with oil CA or P_c , no clear correlations between additive concentrations with oil CA or P_c can be found. Therefore there is no guarantee that additional oil recovery can be produced with the increase of nanoparticle concentrations.

Table 6.3 The calculated capillary pressure for different soaking fluid samples

Fluid samples	IFT (mN/m)	Oil CA (degree)	P _c (psi)
Brine	1.842	81	-5.57
Tap water	2.046	85	-3.45
Brine with additive 1 (5 wt%)	0.267	126	0.91
Brine with additive 1 (10 wt%)	0.242	137	1.03
Brine with additive 1 (35 wt%)	0.19	136	0.79
Fresh water with additive 1 (5 wt%)	0.447	155	2.35
Fresh water with additive 1 (10 wt%)	0.373	145	1.77
Fresh water with additive 1 (35 wt%)	0.344	143	1.59
Fresh water with additive 2 (1.89 cc/L)	0.186	134	0.75
Fresh water with additive 2 (3.78 cc/L)	0.211	141	0.95
Fresh water with additive 2 (7.56 cc/L)	0.26	120	0.75

6.3.2 Soaking tests

Sample MT-A2 was immersed into the nanoparticle additive 2 (3.78 cc/L) solution and sample MT-A1 was immersed into the nanoparticle additive 1 (10 wt%) solution to conduct soaking experiments.

Fig 6.3 shows the final results of soaking tests on MT-A2 (left side) and MT-A1 (right side) when the soaking time is around 45 days (no more oil produced anymore). In **Fig 6.3** we can observe accumulated oil on the top of the Amott cell and there are some small oil droplets attached on the rock surface. However, the actual oil RF should be higher than the calculated oil RF, because there are small oil droplets attached on the rock surface or the Amott cell surface, which didn't accumulate on the top of Amott cell. In order to get these oil droplets, a magnet was put into Amott

cell and used for stirring the soaking fluid to make these droplets detached from rock surface. The final produced oil for MT-A2 and MT-A3 are 0.38cc and 0.30cc, and the corresponding oil RF is 16.5% and 11.3% respectively, suggesting the nanoparticle additive 2 (3.78 cc/L) can lead to higher oil RF compared to nanoparticle additive 1 (10 wt%).

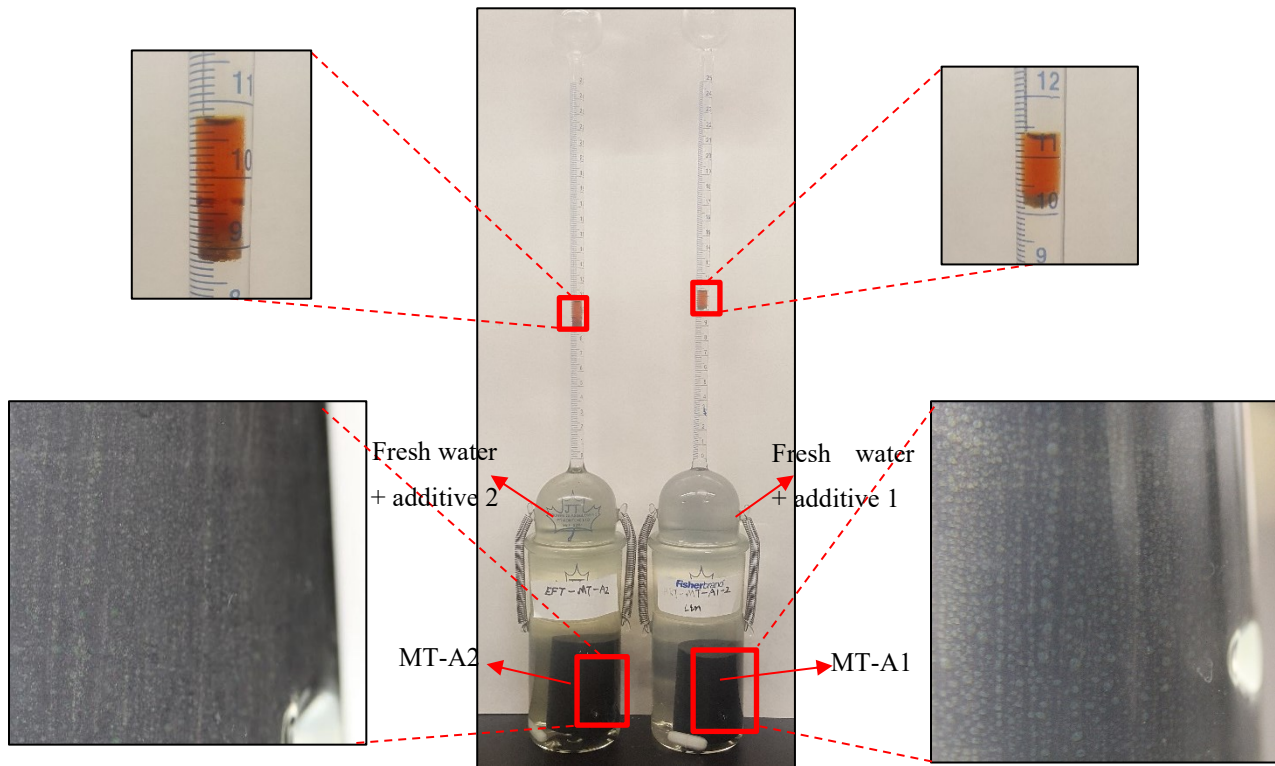


Figure 6.3 The oil recovery of MT-A1 (right side) soaked by fresh water with additive 1 and MT-A2 (left side) soaked by fresh water with additive 2. The soaking time is 45 days.

Fig 6.4 shows the Oil RF vs. time for twin core plugs MT-A1 and MT-A2 immersed in brine and nanoparticle solutions respectively. We can observe that the samples immersed into fresh water with nanoparticle additive 1 and fresh water with nanoparticle additive 2 have higher and faster oil RF compared to the samples immersed into brine. The fresh water+ additive 2 can lead to higher oil RF compared to fresh water+ additive 2.

Fig 6.5 compares the Oil RF vs. time for MT-A1, MT-A2 and MT-A3 immersed in fresh water + nanoparticle additive 1, fresh water + nanoparticle additive 2 and fresh water + microemulsion (ME) solutions respectively. We can observe that MT-A2 immersed into fresh water with nanoparticle additive 2 has highest oil RF. The sample immersed fresh water with ME has lower oil RF than the sample immersed fresh water with nanoparticle additive 2, but higher than another one immersed fresh water with additive 1.

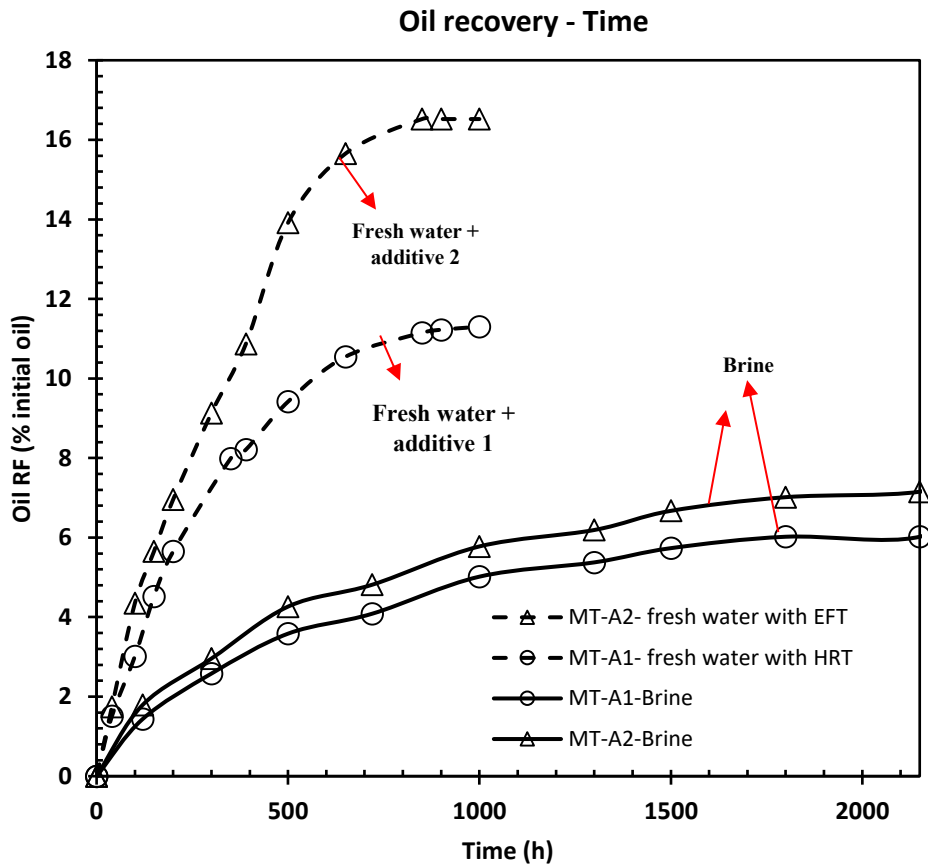


Figure 6.4 Oil RF vs. time for twin core plugs MT-A1 and MT-A2 immersed in brine and fresh water + nanoparticle solutions respectively.

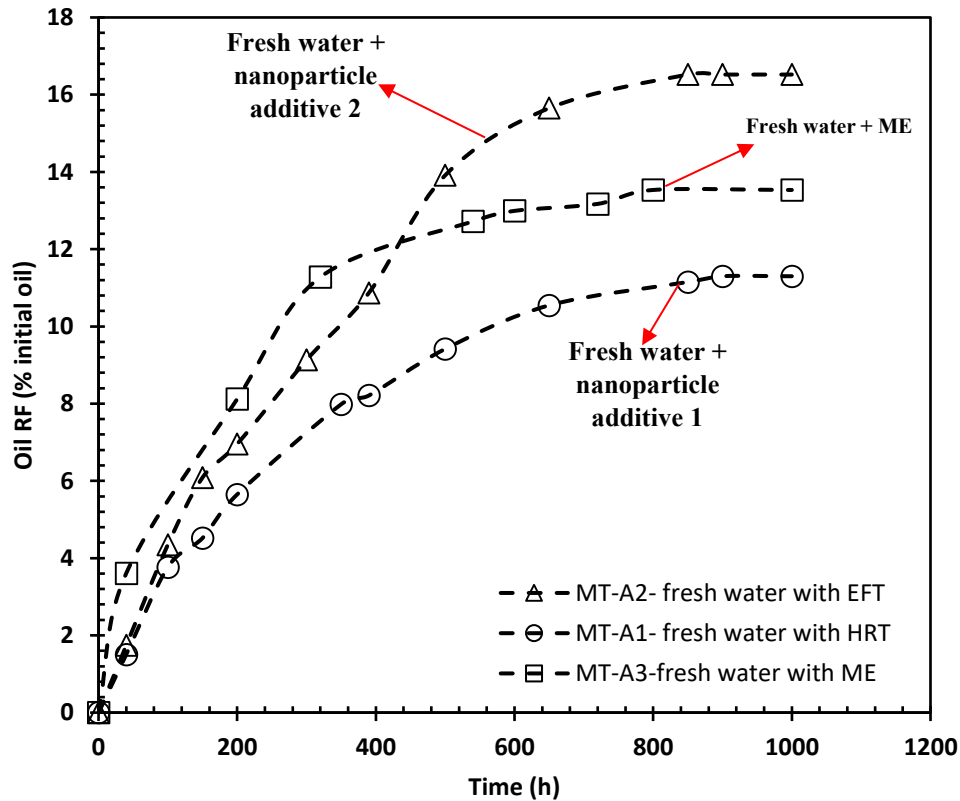


Figure 6.5 Oil RF vs. time for MT-A1, MT-A2 and MT-A3 immersed in fresh water + nanoparticle additive 1, water + nanoparticle additive 2 and water + microemulsion (ME) solutions respectively.

6.3.3 Effects of wettability on Imbibition Oil Recovery

Compared to base cases (brine or fresh water), ME solutions and nanoparticle solutions have lower IFT and the rock surface has higher wetting affinity towards ME solutions and nanoparticle solutions (higher oil CA). Here, we evaluate the effects of contact angle on oil recovery.

According to Eq 2.2, inverse bond number values can be calculated. **Table 6.4** lists the inverse bond number values for the fluids that we used for counter-current imbibition test. N_B^{-1} for all the soaking liquids is higher than 5, indicating capillary forces dominate the counter-current imbibition process. As we discussed before, P_c changes from negative to positive when adding nanoparticles in base cases (brine or tap water), and the wettability of rock alters from oil-wet to water-wet. The

wettability change may be able to explain the increased oil recovery when using nanoparticle solutions as soaking fluids.

According to **Table 6.2**, the average oil contact angle for base case is generally less than 90° while that for nanoparticle solutions is higher than 130° generally, which indicate the nanoparticles can alter the wettability of rock surface from oil-wet to water-wet compared to base case (brine or fresh water). From **Fig 6.4** we observe that the nanoparticle solutions can result in higher oil RF compared to base case (brine or fresh water). This can be explained by the stronger wetting affinity of core plugs to nanoparticle solutions, suggesting more fluid can be imbibed into core plugs and consequently result in higher oil RF. The wettability alternation of nanoparticles may be one important reason for the oil recovery enhancement.

From **Fig 6.5**, we observe that the core plug immersed into fresh water with nanoparticle additive 2 has highest oil RF (16.5%) while the core plug immersed fresh water with additive 1 has the lowest oil RF (11.2%). The oil RF of the other plug immersed fresh water with ME is in the middle (13.5%). For CA results, Here wettability alteration is more pronounced (oil CA is bigger) in the presence of nanoparticle additive 1. The wetting affinity of rock surface toward fresh water with additive 1 is higher than water with ME and fresh water with additive 2 which can increase the capillary pressure (Eq 2.1). Also, the IFT of fresh water with additive 1 is the highest in these three fluids which means the capillary pressure in presence of nanoparticle additive 1 should be the highest if we consider the same D for different tests. However the fresh water with nanoparticle additive 2 gave the highest oil production which is inconsistent with the oil recovery result. This may need further investigations in future study.

Table 6.4 Capillary Pressure Inverse Bond Number Values for Different Soaking Fluid Samples

Core	Fluid samples	N_b^{-1}
MT-A1	Fresh water with additive 1 (10 wt%)	70.50
MT-A2	Fresh water with additive 2 (3.78 cc/L)	40.70
MT-A3	Water with ME	19.20

Chapter 7 Conclusions and Recommendations for Future Study

7.1 Conclusions

(1) The results of air-liquid contact angle and spontaneous imbibition tests show that the natural wetting affinity of the core samples to oil is stronger than that to water, under dry conditions.

(2) The final imbibed volume of oil is higher than that of brine, and brine imbibition profiles reach to the equilibrium state earlier than oil profiles. Comparing oil and brine imbibition profiles suggests that oil imbibe into the entire pore network while brine cannot imbibe into small hydrophobic pores.

(3) The equilibrated normalized imbibed volume of oil (I_o^{eq}) is positively correlated to the volume fraction of small pores with pore-throat-size of less than 30 nm. This positive correlation suggests that the small pores tend to be dominantly oil-wet and explains the higher imbibed volume of oil compared with that of brine.

(4) The core plugs with higher imbibed water volume (under dry conditions) show higher oil RF in counter-current imbibition tests, suggesting that the produced oil is mainly from large hydrophilic pores.

(5) Fresh water with lower salinity imbibe more into the core plugs leading to higher oil recovery factor compared with reservoir brine with higher salinity. This observation can be explained by osmotic potential which provides an additional driving force for water imbibition.

(6) Soaking the core plugs in microemulsion solution after soaking in fresh water or brine leads to an incremental oil recovery of up to 2%. When the oil-saturated plug is immediately soaked in ME solution (without first soaking in water) the oil recovery rate is considerably higher compared with

the cases when the oil-saturated plugs are first immersed in water and then in microemulsion solution.

(7) Nanoparticle additive 1 and additive 2 may change the wettability of oil-saturated rock surface to make it more water-wet. The extent of wettability alteration is more pronounced in the presence of fresh water compared with reservoir brine. The oil-recovery imbibition tests show faster and higher oil recovery by the two nanoparticle additives compared with the reference cases of brine and fresh water and diluted brine, consistent with the results of contact-angle tests.

7.2 Recommendations for Future Work

(1) We observe water imbibition into oil-saturated core plugs to expel oil out. Adding ME and nanoparticle solutions can enhance oil recovery. However, the mechanism behind ME and nanoparticle EOR is still not very clear. In future, we consider to utilize Derjaguin, Landau, Verwey, and Overbeek (DLVO) theory to calculate disjoining pressure to investigate the stability of oil film covering the rock surface in presence of different soaking fluids (ME solutions and nanoparticle solutions).

(2) We evaluated wetting affinity of core plugs to oil and brine by measuring spontaneous imbibition of reservoir oil and brine. However, we did not evaluate the wettability of the core plugs to other fluids like surfactant solutions. For future study, we are supposed to do co-current imbibition tests by using different fluids including surfactant solutions and nanoparticle solutions to evaluate and compare the wettability of different fluids.

(3) We measured the oil effective permeability at residual water saturation in this thesis. However, we did not do insight investigations on the effects of surfactant soaking on oil regain permeability.

In our next study, we are supposed to do coreflooding tests to measure and compare oil effective permeability before and after soaking the oil-saturated plugs in the surfactant solution.

(4) We observe higher oil RF for plugs immersed in fresh water compared with those in brine. The main mechanism responsible for this observation may be osmotic effect due to the existence of clay minerals which can behave as semipermeable membrane. In our future study, we will calculate the value of osmotic pressure caused to quantify the osmotic effect during soaking process.

(5) For nanoparticle solutions, we need to further study on evaluating the possibility of pore-throat blockage by comparing the size distribution of the self-assembled particles using dynamic light scattering method with pore size distribution of the core plugs obtained from SEM and MICP analyses.

References

- Alvarez, J. O., and Schechter, D. S. (2017). Wettability alteration and spontaneous imbibition in unconventional liquid reservoirs by surfactant additives. *SPE Reservoir Evaluation & Engineering*, 20(01), 107-117. <https://doi.org/10.2118/177057-PA>
- Al Hinai, A., Rezaee, R., Esteban, L., and Labani, M. (2014). Comparisons of pore size distribution: a case from the Western Australian gas shale formations. *Journal of Unconventional Oil and Gas Resources*, 8, 1-13. <https://doi.org/10.1016/j.juogr.2014.06.002>
- Bustin, R. M., Bustin, A. M., Cui, A., Ross, D., and Pathi, V. M. (2008). Impact of shale properties on pore structure and storage characteristics, SPE shale gas production conference, Society of Petroleum Engineers. <https://doi.org/10.2118/119892-MS>.
- Berg, R. R. (1975). Capillary pressures in stratigraphic traps, *AAPG bulletin* 59(6), 939-956.
- Bobek, J. E., Mattax, C. C., and Denekas, M. O. (1958). Reservoir rock wettability-its significance and evaluation.
- Brown, R. J., and Fatt, I. (1956, January). Measurements of fractional wettability of oil fields' rocks by the nuclear magnetic relaxation method. In *Fall Meeting of the Petroleum Branch of AIME*. Society of Petroleum Engineers. <https://doi.org/10.2118/743-G>.
- Begum, M., Yassin, M.R., and Dehghanpour, H. (2017, February). Rock-Fluid Interactions in the Duvernay Formation: Measurement of Wettability and Imbibition Oil Recovery. In *SPE Unconventional Resources Conference*. Society of Petroleum Engineers.
- Clarkson, C. R., Freeman, M., He, L., Agamalian, M., Melnichenko, Y., Mastalerz, M., Bustin, R., Radliński, A., and Blach, T. (2012). Characterization of tight gas reservoir pore structure using USANS/SANS and gas adsorption analysis, *Fuel* 95, 371-385. <https://doi.org/10.2118/155537-MS>.
- Chalmers, G. R., Bustin, R. M., and Power, I. M. (2012). Characterization of gas shale pore systems by porosimetry, pycnometry, surface area, and field emission scanning electron microscopy/transmission electron microscopy image analyses: Examples from the Barnett, Woodford, Haynesville, Marcellus, and Doig units, *AAPG bulletin* 96(6), 1099-1119.
- Cui, A., Wust, R., Nassichuk, B., Glover, K., Brezovski, R., and Twemlow, C. (2013). A nearly complete characterization of permeability to hydrocarbon gas and liquid for unconventional reservoirs: a challenge to conventional thinking, *Unconventional Resources Technology Conference*, Society of Exploration Geophysicists, American Association of Petroleum Geologists, Society of Petroleum Engineers, pp. 1716-1732. <https://doi.org/10.15530/URTEC-1578611-MS>.

Davies, G. R. (1997). The Triassic of the Western Canada Sedimentary Basin: tectonic and stratigraphic framework, paleogeography, paleoclimate and biota. *Bulletin of Canadian Petroleum Geology*, 45(4), 434-460.

Donaldson, E. C., Thomas, R. D., and Lorenz, P. B. (1969). Wettability determination and its effect on recovery efficiency. *Society of Petroleum Engineers Journal*, 9(01), 13-20. <https://doi.org/10.2118/2338-PA>.

Dehghanpour, H., Lan, Q., Saeed, Y., Fei, H., and Qi, Z. (2013). Spontaneous imbibition of brine and oil in gas shales: effect of water adsorption and resulting microfractures, *Energy & Fuels* 27(6), 3039-3049.

Dehghanpour, H., Xu, M., and Habibi, A. (2015). Wettability of gas shale reservoirs, *Fundamentals of Gas Shale Reservoirs*, 341-359.

de Gennes, P. G. (1985). Wetting static and dynamics. *Rev. Mod. Phys.* 57, 827-863.

Gruener, S., Hermes, H. E., Schillinger, B., Egelhaaf, S. U., and Huber, P. (2016). Capillary rise dynamics of liquid hydrocarbons in mesoporous silica as explored by gravimetry, optical and neutron imaging: Nano-rheology and determination of pore size distributions from the shape of imbibition fronts. *Colloids Surf. A Physicochem. Eng. Asp.* 496, 13-27.

Greenberg, J. A., Mitchell, J. K., and Witherspoon, P. A. (1973). Coupled salt and water flows in a groundwater basin. *Journal of Geophysical Research*, 78(27), 6341-6353.

Gruener, S., Sadjadi, Z., Hermes, H. E., Kityk, A. V., Knorr, K., Egelhaaf, S. U., Rieger, H., and Huber, P. (2012). Anomalous front broadening during spontaneous imbibition in a matrix with elongated pores, *Proceedings of the National Academy of Sciences* 109(26), 10245-10250.

Handy, L. L. (1960). Determination of effective capillary pressures for porous media from imbibition data.

Hoar, T. P., and J. H. Schulman. (1943). *Nature*, (152), 102-103.

Handwerger, D. A., Keller, J., and Vaughn, K. (2011). Improved Petrophysical Core Measurements on Tight Shale Reservoirs Using Retort and Crushed Samples. Presented at the SPE Annual Technical Conference and Exhibition, Denver, 30 October–2 November. SPE-147456-MS. <https://doi.org/10.2118/147456-MS>.

Hendraningrat, L., Li, S., and Torsæter, O. (2013). A coreflood investigation of nanofluid enhanced oil recovery. *Journal of Petroleum Science and Engineering*, 111, 128-138.

- Habibi, A., Dehghanpour, H., Binazadeh, M., Bryan, D., and Uswak, G., (2016). Advances in Understanding Wettability of Tight Oil Formations: A Montney Case Study, SPE Reservoir Evaluation & Engineering 19(04) 583-603. <https://doi.org/10.2118/175157-PA>.
- Hurst, A., and Nadeau, P. H. (1995). Clay microporosity in reservoir sandstones: an application of quantitative electron microscopy in petrophysical evaluation, AAPG bulletin 79(4), 563-573.
- Javaheri, A., Dehghanpour, H., and Wood, J. (2017). Tight rock wettability and its relationship to other petrophysical properties: A Montney case study. Journal of Earth Science, 28(2), 381-390.
- Johnson, R. E., Dettre, and R. H. (1969). Wettability and contact angles. Surface and colloid science, 2(1):85-154.
- Khlaifat, A. L., Qutob, H., and Barakat, N. (2011). Tight gas sands development is critical to future world energy resources, SPE-142049-MS presented at SPE Middle East Unconventional Gas Conference and Exhibition, Muscat, Oman.
- Keller, W. D., Reynolds, R. C., and Inoue Atsuyuki. (1986). Morphology of clay minerals in the smectite-to-illite conversion series by scanning electron microscopy. Clays and Clay Minerals, Vol, 34, No. 2, 187-197.
- Kemper, W. D., and Van Schaik, J. C. (1966). Diffusion of Salts in Clay-Water Systems 1. Soil Science Society of America Journal, 30(5), 534-540.
- Kendall, D. R. (1999). Sedimentology and stratigraphy of the lower triassic Montney Formation, Peace River basin, subsurface of northwestern Alberta. University of Calgary.
- Kathel, P., and Mohanty, K. K. (2013). Wettability alteration in a tight oil reservoir. Energy & Fuels, 27(11), 6460-6468. <https://doi.org/10.1021/ef4012752>
- Kamari, A., Nikookar, M., Hemmati-Sarapardeh, A., Sahranavard, L., and Mohammadi, A. H. (2014). Screening Of Potential Application of Eor Processes in a Naturally Fractured Oil Reservoir. Enhanced Oil Recovery: Methods, Economic Benefits and Impacts on the Environment, Nova Science Publishers Inc., NY, USA.
- Lan, Q., Dehghanpour, H., Wood, J., and Sanei, H. (2015). Wettability of the Montney tight gas formation, SPE Reservoir Evaluation & Engineering 18(03) 417-431. <https://doi.org/10.2118/171620-PA>.
- Law, C. A. (1999). Evaluating source rocks. AAPG Special Volumes. Treatise of Petroleum Geology/Handbook of Petroleum Geology, 3, 6-1.
- Lucas, R. (1918). Rate of capillary ascension of liquids. Kolloid Z, 23(15), 15-22.

Lan, Q., Xu, M., Dehghanpour, H., and Wood, J. (2014, October). Advances in understanding wettability of tight and shale gas formations. In SPE Annual Technical Conference and Exhibition. Society of Petroleum Engineers. <https://doi.org/10.2118/170969-MS>.

Lager, A., Webb, K. J., and Black, C. J. J. (2007, April). Impact of brine chemistry on oil recovery. In IOR 2007-14th European Symposium on Improved Oil Recovery.

Morrow, N., and Buckley, J. (2011). Improved oil recovery by low-salinity waterflooding. *Journal of Petroleum Technology*, 63(05), 106-112.

Mohan, K., Gupta, R., and Mohanty, K. K. (2011). Wettability altering secondary oil recovery in carbonate rocks. *Energy & Fuels*, 25(9), 3966-3973. <https://doi.org/10.1021/ef200449y>.

Sharma, G., and Mohanty, K. (2013). Wettability alteration in high-temperature and high-salinity carbonate reservoirs. *SPE Journal*, 18(04), 646-655. <https://doi.org/10.2118/147306-PA>.

Ma, S. M., Zhang, X., Morrow, N. R., and Zhou, X. (1999). Characterization of wettability from spontaneous imbibition measurements. *Journal of Canadian Petroleum Technology*, 38(13). <https://doi.org/10.2118/99-13-49>.

Neuzil, C. E. (2000). Osmotic generation of 'anomalous' fluid pressures in geological environments. *Nature*, 403(6766), 182.

NEB, A., OGC, B., & MNGD, B. (2013). The Ultimate Potential for Unconventional Petroleum from the Montney Formation of British Columbia and Alberta. Energy Briefing Note.

Saraji, S., and Piri, M. (2015). The representative sample size in shale oil rocks and nano-scale characterization of transport properties, *International Journal of Coal Geology* 146, 42-54.

Sanei, H., Wood, J. M., Ardakani, O. H., Clarkson, C. R., and Jiang, C. (2015). Characterization of organic matter fractions in an unconventional tight gas siltstone reservoir. *International Journal of Coal Geology*, 150, 296-305. <https://doi.org/10.1016/j.coal.2015.04.004>

Shi, Y., Yassin, M. R., and Dehghanpour, H. (2018). A modified model for spontaneous imbibition of wetting phase into fractal porous media. *Colloids and Surfaces A: Physicochemical and Engineering Aspects*, 543, 64-75.

Shi, Y., Yassin, M. R., Yuan, L., and Dehghanpour, H. (2019). Modelling imbibition data for determining size distribution of organic and inorganic pores in unconventional rocks. *International Journal of Coal Geology*, 201, 26-43.

Salathiel, R. A. (1973). Oil recovery by surface film drainage in mixed-wettability rocks. *Journal of Petroleum Technology*, 25(10), 1-216. <https://doi.org/10.2118/4104-PA>.

Smith, D. A. (1966). Theoretical considerations of sealing and non-sealing faults, *AAPG Bulletin* 50(2), 363-374.

- Salehi, M., Johnson, S. J., & Liang, J. T. (2008). Mechanistic study of wettability alteration using surfactants with applications in naturally fractured reservoirs. *Langmuir*, 24(24), 14099-14107. <https://doi.org/10.1021/la802464u>
- Schembre, J., Akin, S., Castanier, L., and Kovscek, A. (1998). Spontaneous water imbibition into diatomite. Paper presented at the SPE Western Regional Meeting.
- Satter, A., and Iqbal, G. M. (2015). *Reservoir Engineering: The fundamentals, simulation, and management of conventional and unconventional recoveries*. Gulf Professional Publishing.
- Van Krevelen, D. W. (1950). Graphical-statistical method for the study of structure and reaction processes of coal. *Fuel*, 29, 269-284.
- Wu, Y. S., and Pruess, K. (1998). Gas flow in porous media with Klinkenberg effects. *Transport in porous Media*, 32(1), 117-137.
- Washburn, E. W. (1921). The dynamics of capillary flow. *Physical review*, 17(3), 273.
- Wang, D., Butler, R., Zhang, J., and Seright, R. (2012). Wettability survey in Bakken shale with surfactant-formulation imbibition. *SPE Reservoir Evaluation & Engineering*, 15(06), 695-705. <https://doi.org/10.2118/153853-PA>
- Wasan, D. T., and Nikolov, A. D. (2003). Spreading of nanofluids on solids. *Nature*, 423(6936), 156.
- Wasan, D., Nikolov, A., and Kondiparty, K. (2011). The wetting and spreading of nanofluids on solids: Role of the structural disjoining pressure. *Current Opinion in Colloid & Interface Science*, 16(4), 344-349.
- Whitaker, S. (1986). Flow in porous media I: A theoretical derivation of Darcy's law. *Transport in porous media*, 1(1), 3-25.
- Webb, K. J., Black, C. J. J., and Edmonds, I. J. (2005, April). Low salinity oil recovery—The role of reservoir condition corefloods. In *IOR 2005-13th European Symposium on Improved Oil Recovery*. <https://doi.org/10.2118/149077-MS>.
- Xu, M., and Dehghanpour, H. (2014). Advances in understanding wettability of gas shales, *Energy & Fuels* 28(7), 4362-4375.
- Young, T. (1805). III. An essay on the cohesion of fluids. *Philosophical transactions of the royal society of London*, (95), 65-87.
- Yassin, M. R., Begum, M., and Dehghanpour, H. (2017) Organic shale wettability and its relationship to other petrophysical properties: A Duvernay case study, *International Journal of Coal Geology* 169, 74-91.

Yassin, M. R., Dehghanpour, H., Wood, J., and Lan, Q. (2016). A theory for relative permeability of unconventional rocks with dual-wettability pore network, SPE Journal. <https://doi.org/10.2118/178549-PA>.

Yassin, M. R., Begum, M., Dehghanpour, H., and Dunn, L. (2018). Evaluation of Imbibition Oil Recovery in the Duvernay Formation. SPE Reservoir Evaluation & Engineering, 21(02), 257-272. <https://doi.org/10.2118/185065-PA>.

Yarveicy, H., and Haghtalab, A. (2018). Effect of amphoteric surfactant on phase behavior of hydrocarbon-electrolyte-water system-an application in enhanced oil recovery. Journal of Dispersion Science and Technology, 39(4), 522-530.

Zolfaghari, A., Dehghanpour, H., and Xu, M. (2017). Water sorption behaviour of gas shales: II. Pore size distribution, International Journal of Coal Geology.

Zhang, Y., Xie, X., and Morrow, N. R. (2007, January). Waterflood performance by injection of brine with different salinity for reservoir cores. In SPE annual technical conference and exhibition. Society of Petroleum Engineers. <https://doi.org/10.2118/109849-MS>.

Appendix A: Dynamic Contact-Angle Measurements of Nanoparticle Solutions

1. The CA measurement for oil-saturated end piece immersed into *brine*.

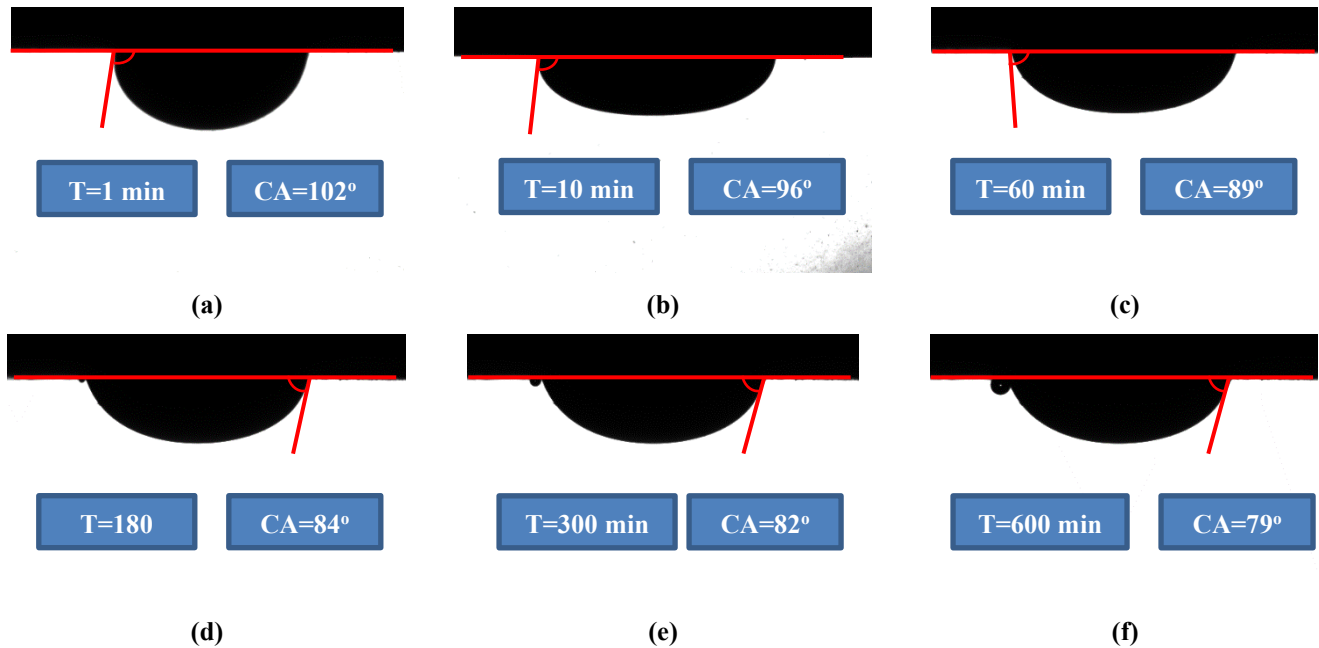


Figure A.1 The CA changes of oil droplet with time on the surface of oil-saturated end piece immersed into brine. a) CA at 1 min; b) CA at 10 min; c) CA at 60 min; d) CA at 180 min; e) CA at 300min; a) CA at 600 min.

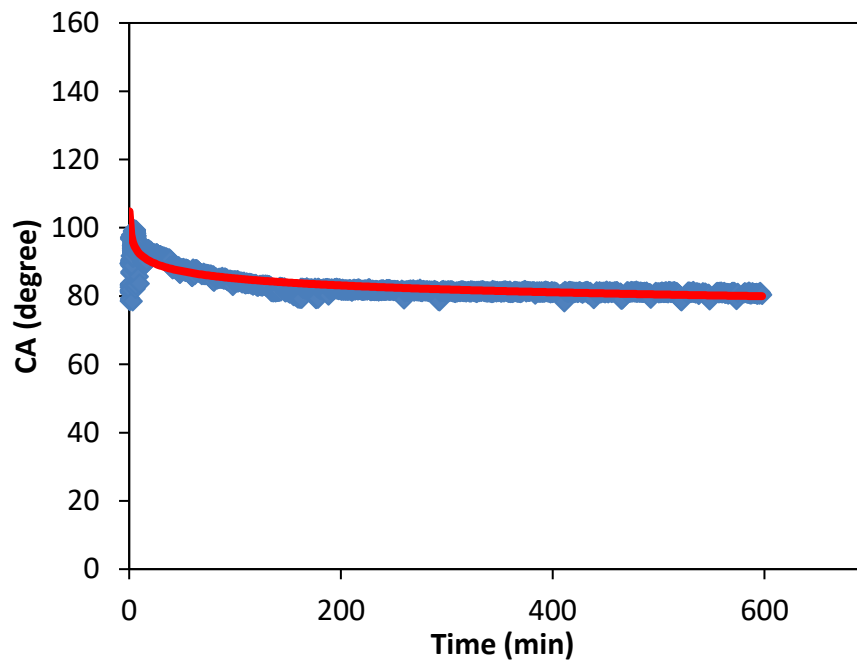


Figure A.2 The CA changes oil droplet versus experimental time for oil-saturated end piece immersed into brine.

2. The CA measurement for oil-saturated end piece immersed into *fresh water*

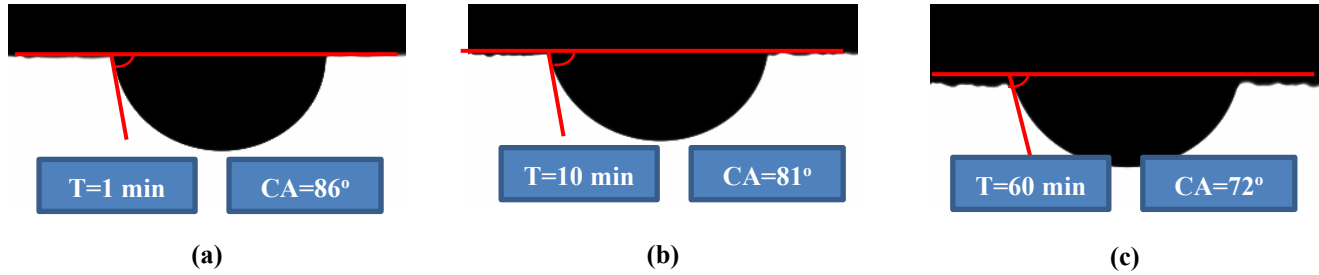


Figure A.3 The CA changes of oil droplet with time on the surface of oil-saturated end piece immersed into fresh water. a) CA at 1 min; b) CA at 10 min; c) CA at 60 min.

3. The CA measurement for oil-saturated end piece immersed into *fresh water with additive 1 (5 wt%)*.

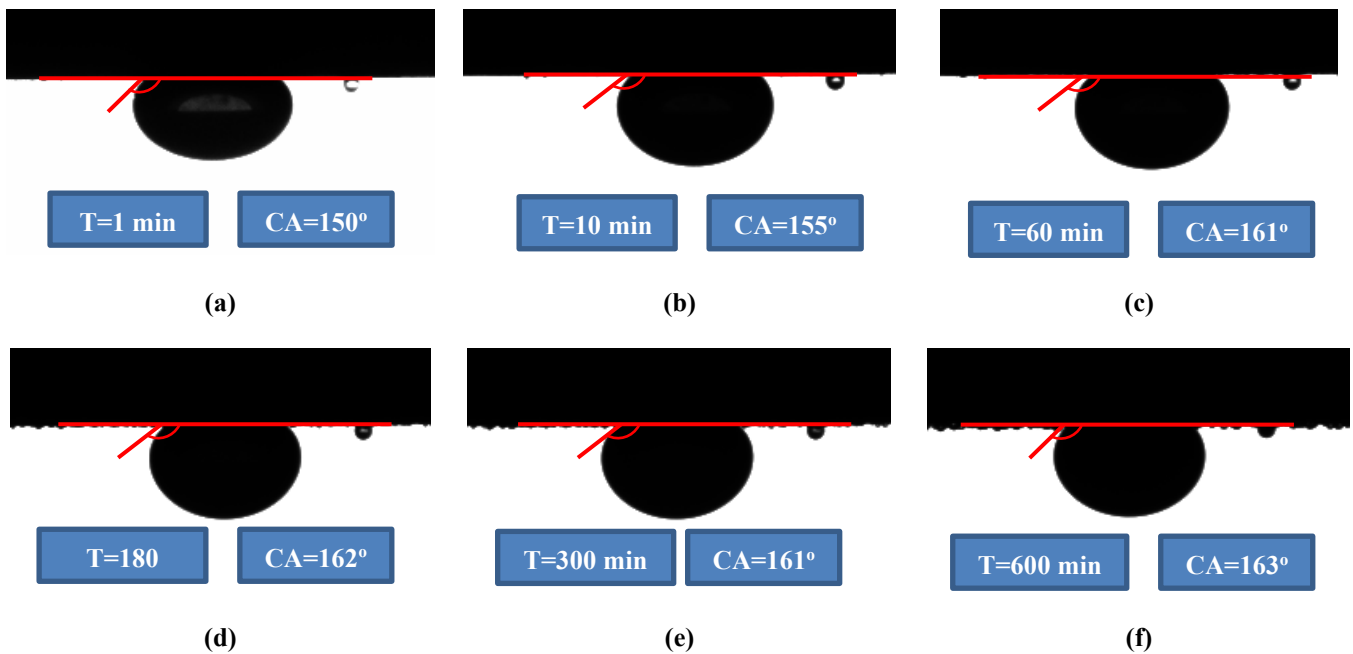


Figure A.4 The CA changes of oil droplet with time on the surface of oil-saturated end piece immersed into fresh water with additive 1 (5 wt%). a) CA at 1 min; b) CA at 10 min; c) CA at 60 min; d) CA at 180 min; e) CA at 300min; a) CA at 600 min.

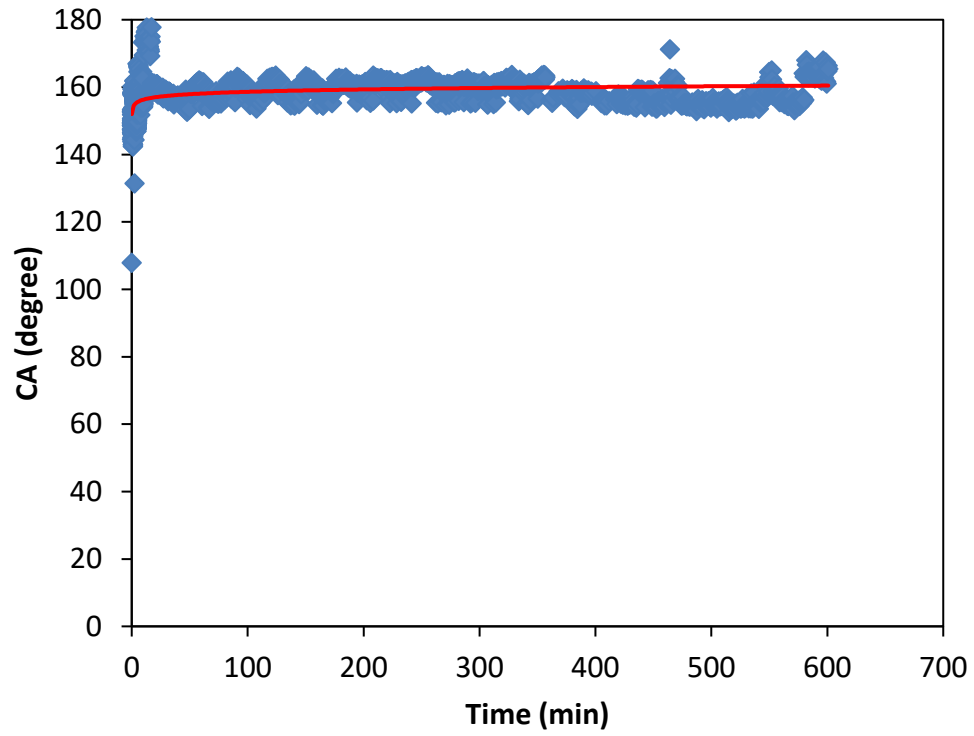


Figure A.5 The CA changes oil droplet versus experimental time for oil-saturated end piece immersed into fresh water with additive 1 (5 wt%).

4. The CA measurement for oil-saturated end piece immersed into *fresh water with additive 1 (10 wt%)*.

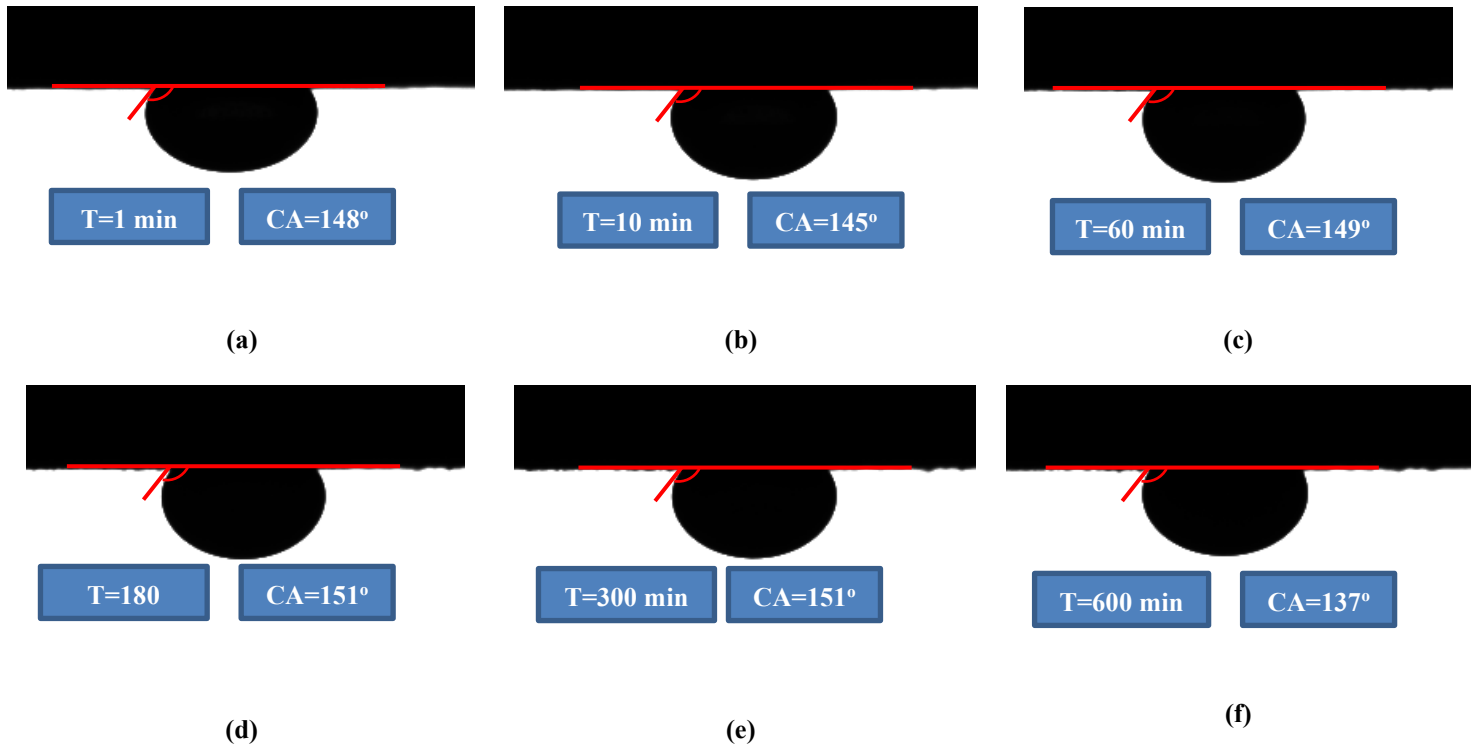


Figure A.6 The CA changes of oil droplet with time on the surface of oil-saturated end piece immersed into fresh water with additive 1 (10 wt%). a) CA at 1 min; b) CA at 10 min; c) CA at 60 min; d) CA at 180 min; e) CA at 300min; a) CA at 600 min.

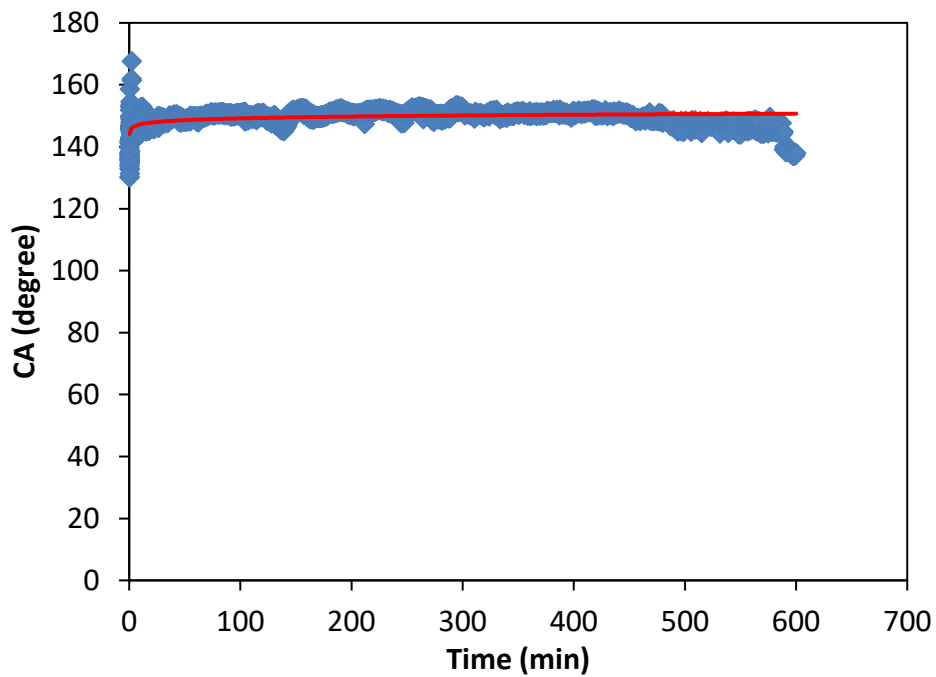


Figure A.7 The CA changes oil droplet versus experimental time for oil-saturated end piece immersed into fresh water with additive 1 (10 wt%).

5. The CA measurement for oil-saturated end piece immersed into *fresh water with additive 1 (35 wt%)*.

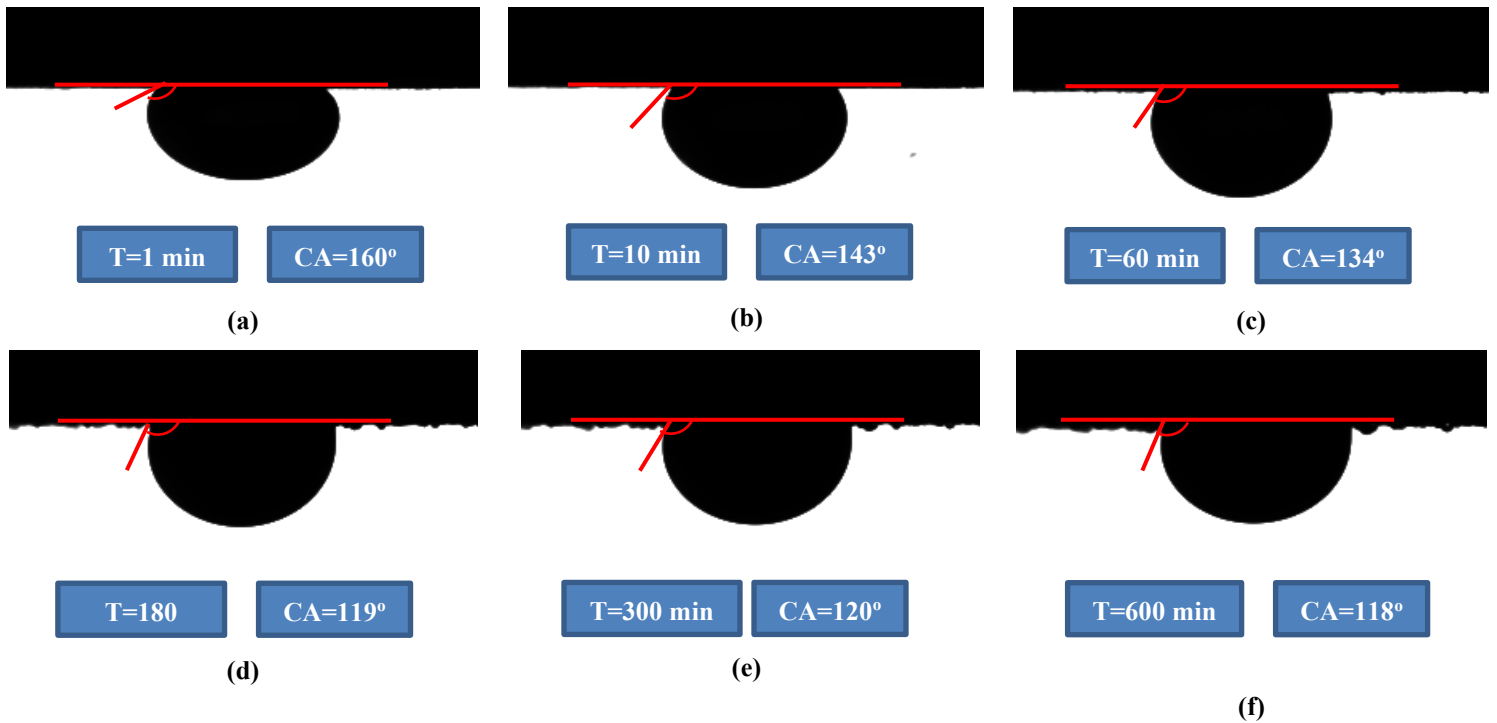


Figure A.8 The CA changes of oil droplet with time on the surface of oil-saturated end piece immersed into fresh water with additive 1 (35 wt%). a) CA at 1 min; b) CA at 10 min; c) CA at 60 min; d) CA at 180 min; e) CA at 300min; a) CA at 600 min.

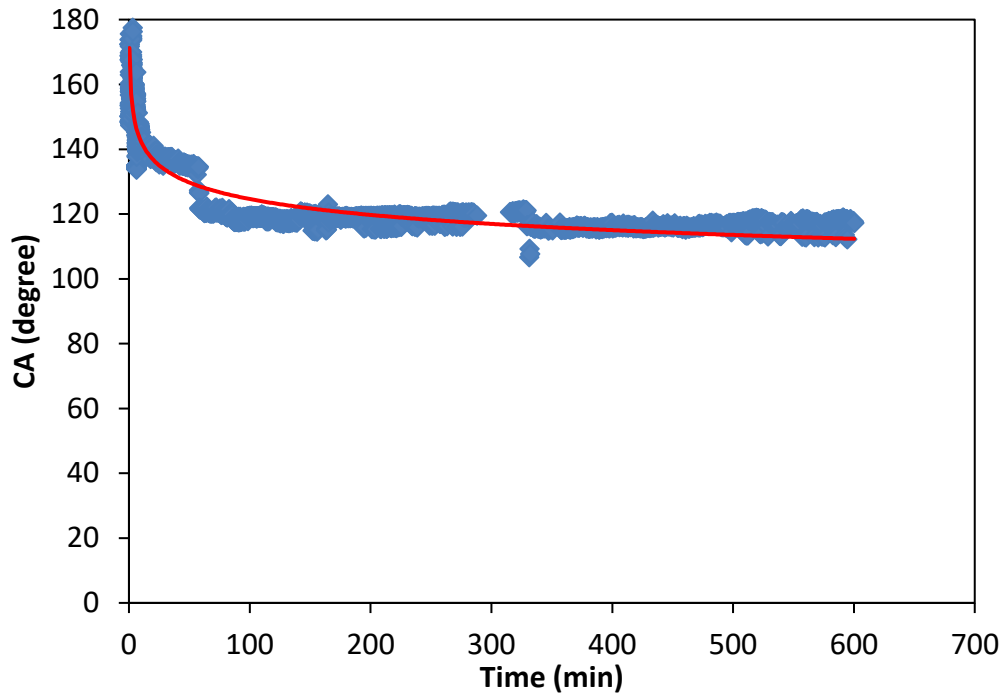


Figure A.9 The CA changes oil droplet versus experimental time for oil-saturated end piece immersed into fresh water with additive 1 (35 wt%).

6. The CA measurement for oil-saturated end piece immersed into *brine with additive 1 (5 wt%)*.

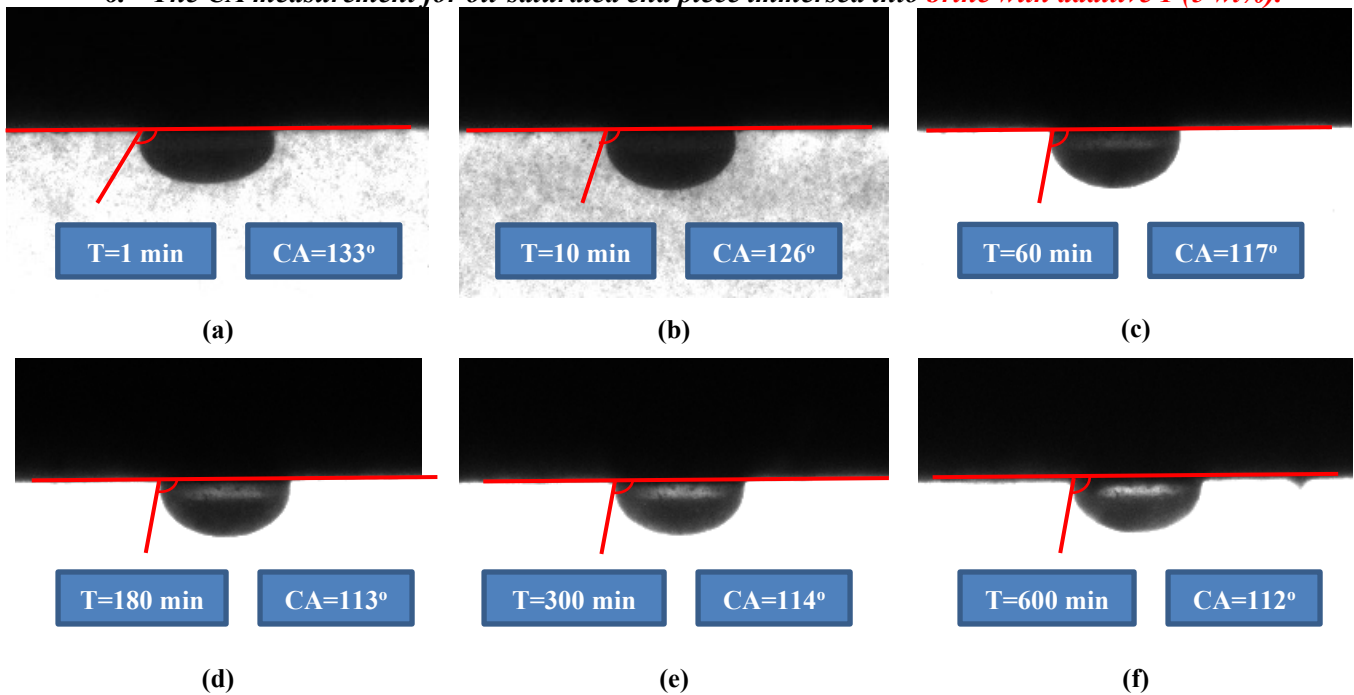


Figure A.10 The CA changes of oil droplet with time on the surface of oil-saturated core sample MT-A1 immersed into brine with nanoparticle additive 1 (5%wt). a) CA at 1 min; b) CA at 10 min; c) CA at 60 min; d) CA at 180 min; e) CA at 300min; a) CA at 600 min.

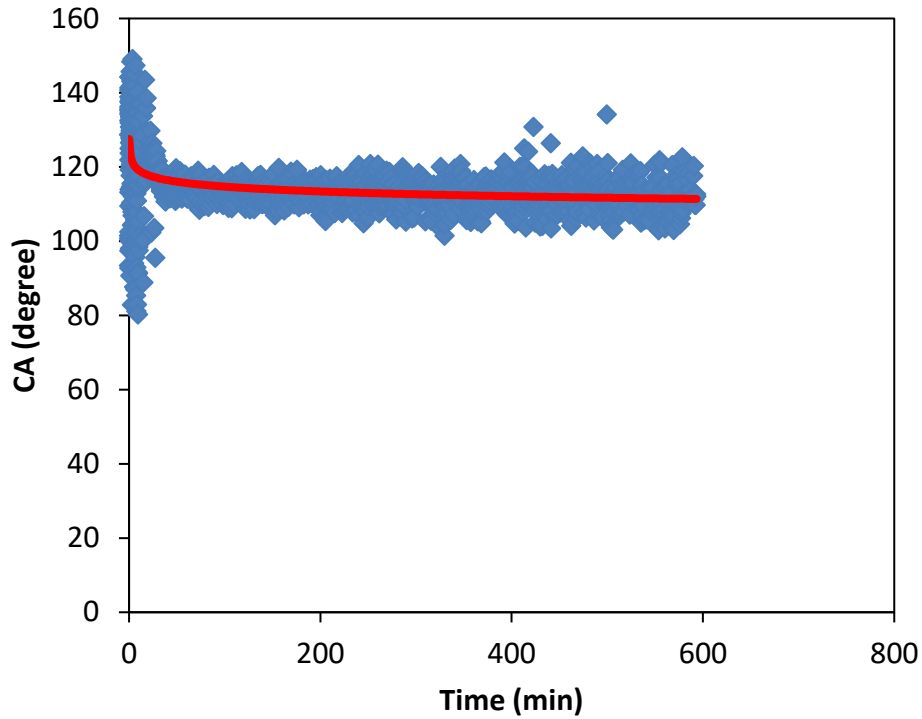


Figure A.11 The CA changes oil droplet versus experimental time for oil-saturated end piece immersed into brine with additive 1 (5 wt%).

7. The CA measurement for oil-saturated end piece immersed into brine with additive 1 (10wt%).

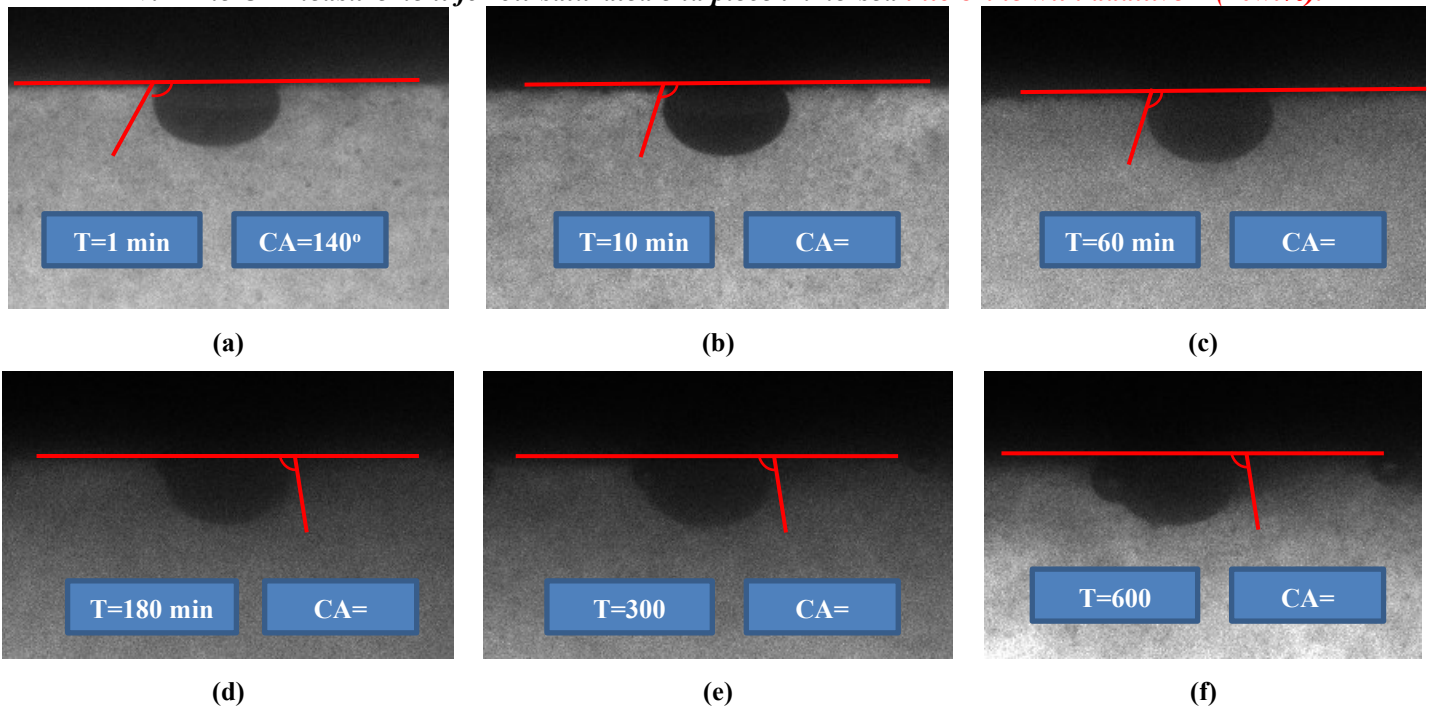


Figure A.12 The CA changes of oil droplet with time on the surface of oil-saturated core sample MT-A1 immersed into brine with additive 1 (10%wt). a) CA at 1 min; b) CA at 10 min; c) CA at 60 min; d) CA at 180 min; e) CA at 300min; a) CA at 600 min.

9. The CA measurement for oil-saturated end piece immersed into *fresh water with additive 2 (1.89 cc/L)*.

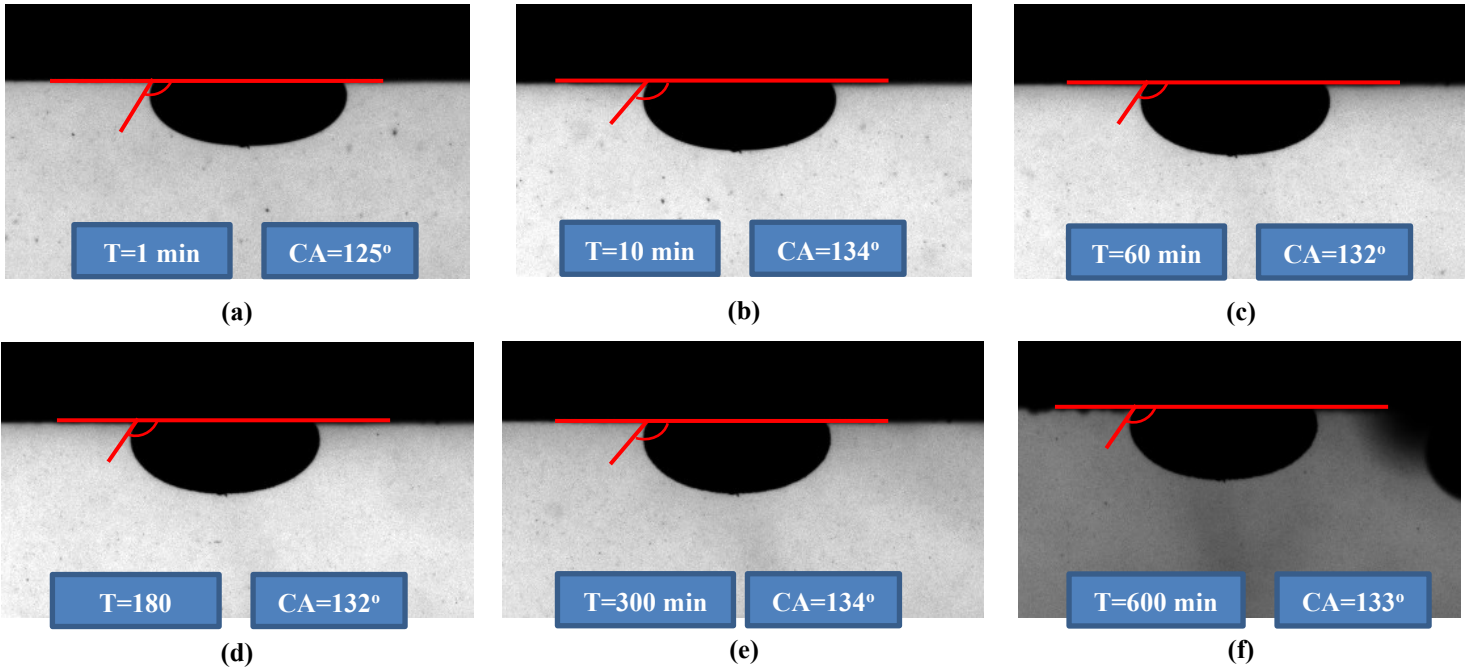


Figure A.15 The CA changes of oil droplet with time on the surface of oil-saturated end piece immersed into fresh water with additive 2 (1.89 cc/L). a) CA at 1 min; b) CA at 10 min; c) CA at 60 min; d) CA at 180 min; e) CA at 300min; a) CA at 600 min.

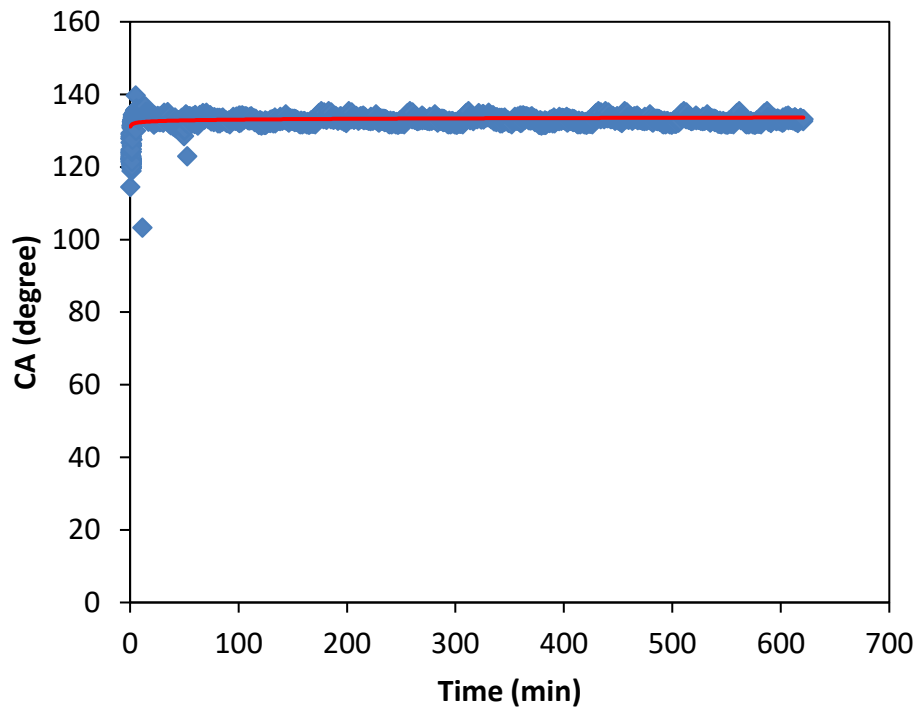


Figure A.16 The CA changes oil droplet versus experimental time for oil-saturated end piece immersed into fresh water with additive 2 (1.89 cc/L).

10. The CA measurement for oil-saturated end piece immersed into *fresh water with additive 2 (3.78 cc/L)*.

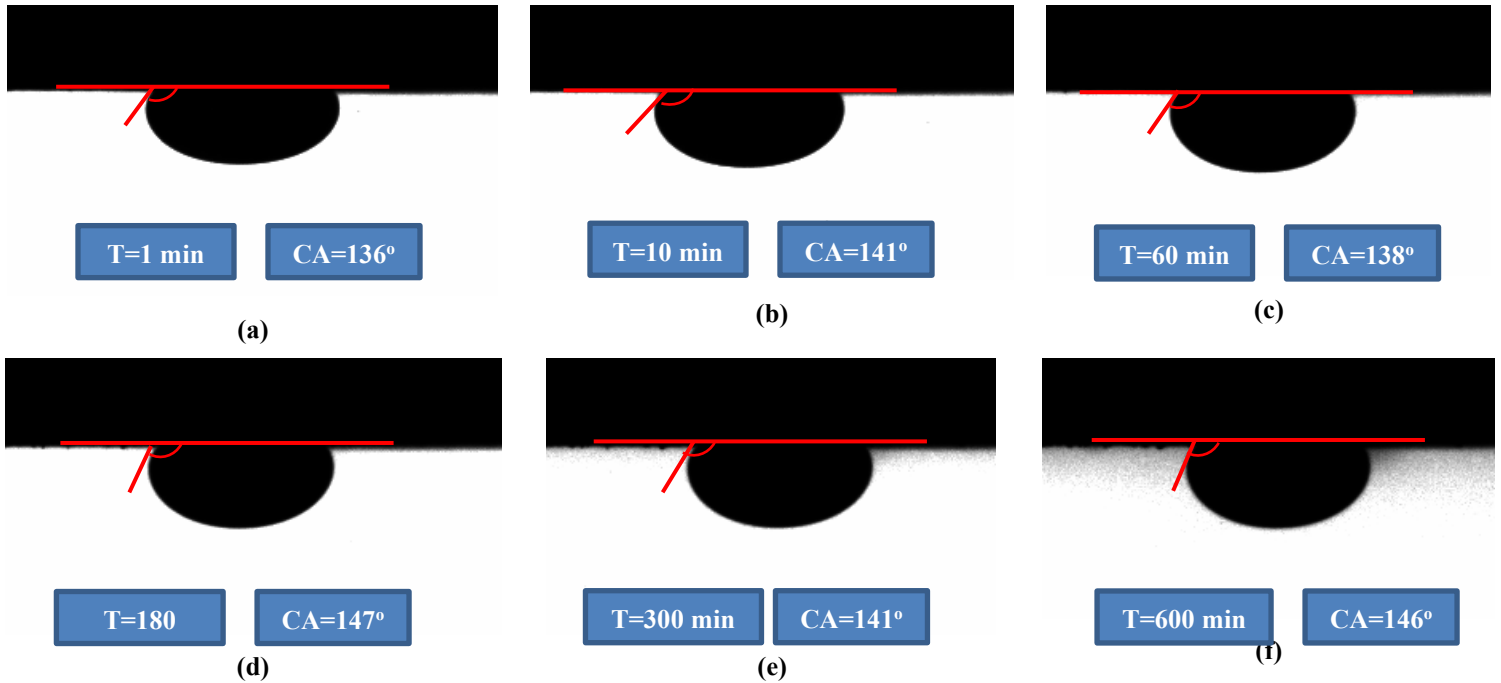


Figure A.17 The CA changes of oil droplet with time on the surface of oil-saturated end piece immersed into fresh water with additive 2 (3.78 cc/L). a) CA at 1 min; b) CA at 10 min; c) CA at 60 min; d) CA at 180 min; e) CA at 300min; a) CA at 600 min.

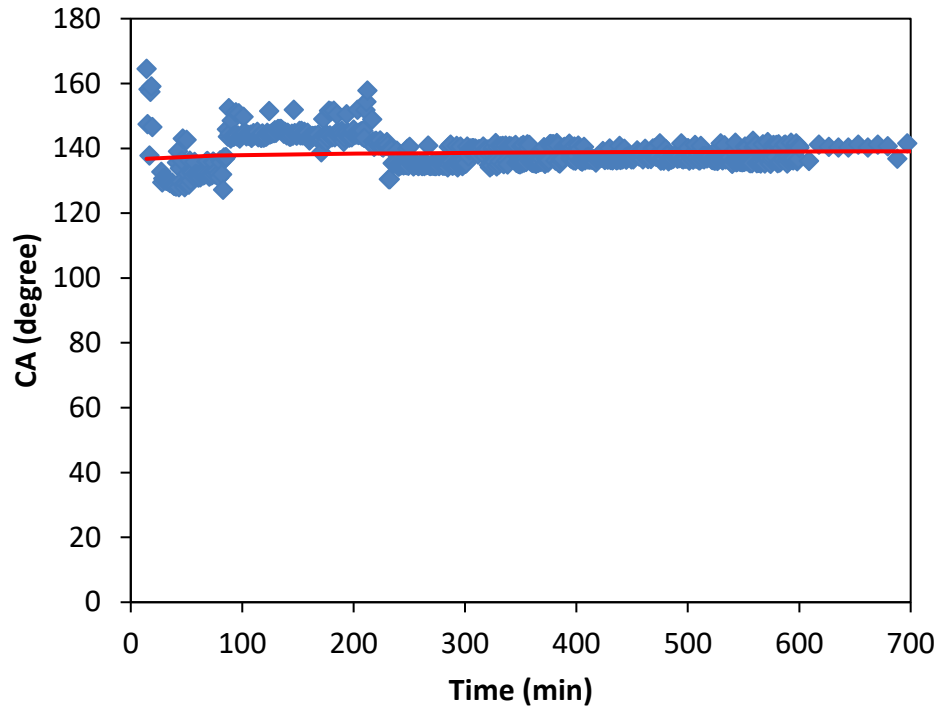


Figure A.18 The CA changes oil droplet versus experimental time for oil-saturated end piece immersed into fresh water with additive 2 (3.78 cc/L).

11. The CA measurement for oil-saturated end piece immersed into *fresh water with additive 2 (7.56 cc/L)*.

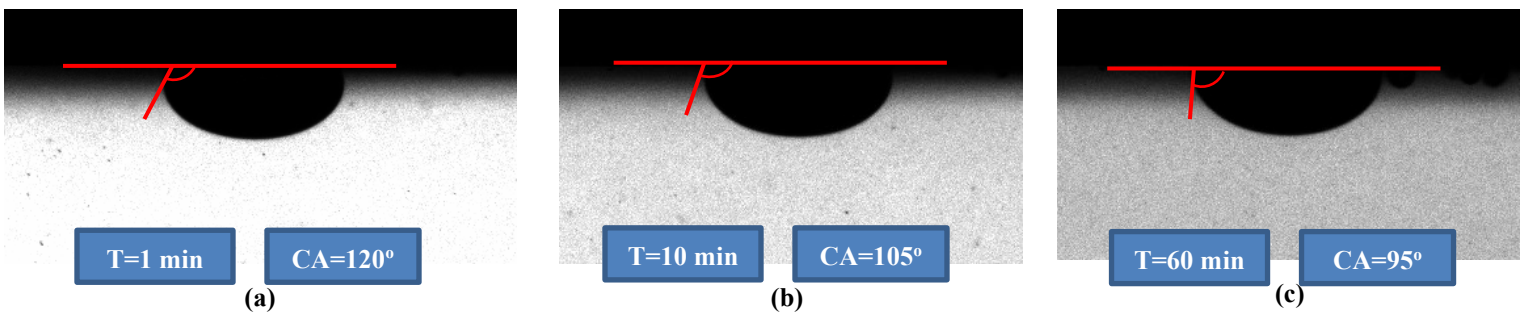


Figure A.19 The CA changes of oil droplet with time on the surface of oil-saturated end piece immersed into fresh water with additive 2 (7.56 cc/L). a) CA at 1 min; b) CA at 10 min; c) CA at 60 min; d) CA at 180 min; e) CA at 300min; a) CA at 600 min.

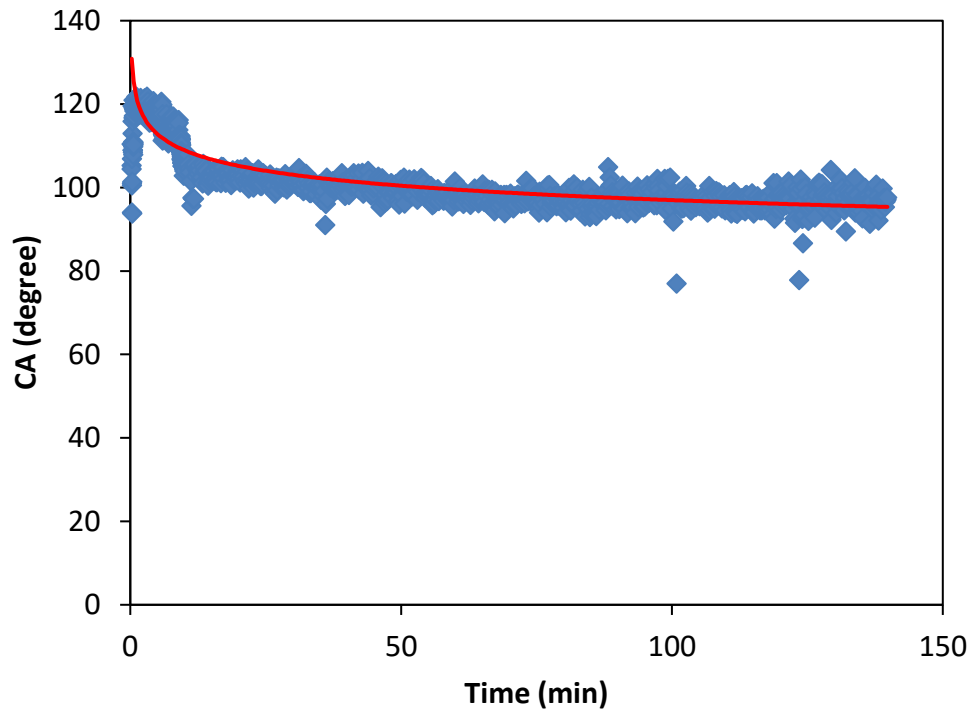


Figure A.20 The CA changes oil droplet versus experimental time for oil-saturated end piece immersed into fresh water with additive 2 (7.56 cc/L).

Appendix B: Capillary-driven Imbibition Model

For imbibition results, we observe that oil imbibes faster than brine into core plugs. In order to explain this observation, we plot the normalized imbibed volume of oil and brine (for twin core plugs) vs. square root of time in **Fig B.1**. Each imbibition profile on these plots could be divided into three regions: region 1 (initial linear part), region 2 (nonlinear transition part) and region 3 (final equilibrated part). The slope of region 1 represents the initial liquid imbibition rate. Handy (1960) proposed a 1D imbibition model for liquid/air systems. He showed that the imbibed volume of wetting phase is proportional to the square root of time:

$$V = \sqrt{\frac{2A_c^2 \phi K S_f P_c}{\mu}} \sqrt{t} \quad (\text{C.1})$$

where V is the imbibed wetting fluid volume, K is fluid effective permeability, A_c is the cross-sectional area of the core plug, ϕ is the core porosity, ρ is the fluid density, P_c is capillary pressure, S_f is the fluid saturation behind the imbibition front and t is the imbibition time. The slope of imbibition curve should be $\sqrt{\frac{2A^2 \phi K S_f P_c}{\mu}}$.

We refer to the imbibition slope of oil and brine to m_o and m_b respectively. The ratio between the oil imbibition slope and brine imbibition slope is given by

$$R = \frac{m_o}{m_b} = \sqrt{\frac{A_c^2 \phi_o K_o S_{fo} P_{co} \mu_w}{A_c^2 \phi_b K_b S_{fb} P_{cb} \mu_o}} \sqrt{t} \quad (\text{C.2})$$

Assuming that the twin core plugs have similar petrophysical properties such as ϕ , K , A , and S_f , the ratio between oil capillary and brine capillary pressure after rearranging Eq C.2 is:

$$\left(\frac{P_{co}}{P_{cw}}\right)_{imbibition} = \left(\frac{m_o}{m_w}\right)^2 \frac{\mu_o}{\mu_w} \quad (C.3)$$

m_o and m_b could be obtained from the imbibition data and then the effective capillary ratio could be calculated by using Eq C.3.

We can also calculate capillary pressure ratio using Young-Laplace equation ($P_c = \frac{2\sigma\cos\theta}{r}$). Here, we assume that the average pore radius for oil imbibition flow is equal to that for brine imbibition flow ($r_o = r_w$). Therefore, the capillary pressure is given by:

$$\left(\frac{P_{co}}{P_{cw}}\right)_{Young-Laplace} = \frac{\sigma_o \cos\theta_o}{\sigma_w \cos\theta_w} \quad (C.4)$$

where σ is the surface tension and θ is the contact angle of oil or brine droplet on the polished rock surface. Table 4.8 lists the capillary pressure ratio from imbibition data and that from Young-Laplace equation. In **Fig B.2**, we plot $\left(\frac{P_{co}}{P_{cw}}\right)_{imbibition}$ versus $\left(\frac{P_{co}}{P_{cw}}\right)_{Young-Laplace}$ and compare the difference between them. Then we observe that $\frac{P_{co}}{P_{cb}}$ calculated based on Young-Laplace equation is around 0.5 (from 0.46 to 0.55). This means that the capillary pressure for oil imbibition is only half of that for brine imbibition. On the other hand, $\frac{P_{co}}{P_{cw}}$ calculated based on imbibition data is higher than 1 (from 1.68 to 6.78). The discrepancy between $\left(\frac{P_{co}}{P_{cw}}\right)_{imbibition}$ and $\left(\frac{P_{co}}{P_{cw}}\right)_{Young-Laplace}$ is possibly due to the assumptions we made in Eq C.2 (i.e. twin core plus having the same petrophysical properties). Additionally, we also assume that the only drive mechanism for imbibition is capillary pressure. In our experiments, all the core plugs have strong oil uptake compared with brine uptake. Therefore, oil sorption caused the presence of organic matters may be an additional driving force that is not accounted in our assumptions. In rock

samples which have a pore network of organic matters, oil can imbibe faster (Lan et al., 2014c) and therefore the we can observe higher oil imbibition rate in our results.

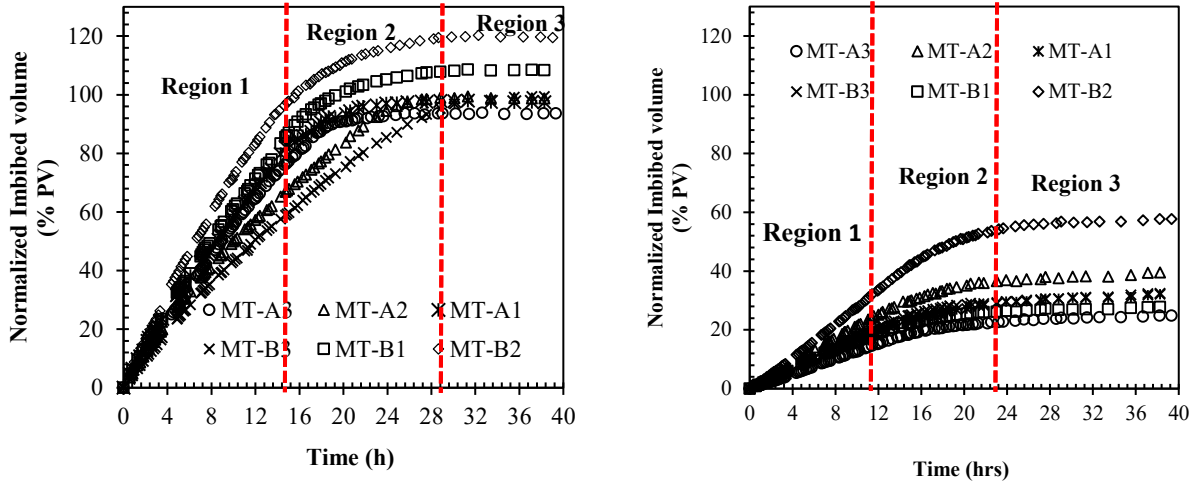


Figure B.1 Normalized imbibed volume of oil (a) and brine (b) into 6 pairs of twin core plugs vs. square root of time

Table B.1 The ratio of oil capillary pressure to water capillary pressure for each twin core plug from imbibition data and Young-Laplace equation.

Sample ID	Slope ratio (m_o/m_w)	$\left(\frac{P_{co}}{P_{cw}}\right)_{\text{imbibition}}$	$\left(\frac{P_{co}}{P_{cw}}\right)_{\text{Young-Laplace}}$
MTA-1	3.12313326	3.79	0.46
MTA-2	2.07730699	1.68	0.47
MTA-3	4.17605094	6.78	0.47
MTB-1	3.93073755	6.01	0.47
MTB-2	3.07559304	3.68	0.49
MTB-3	2.36539623	2.17	0.55

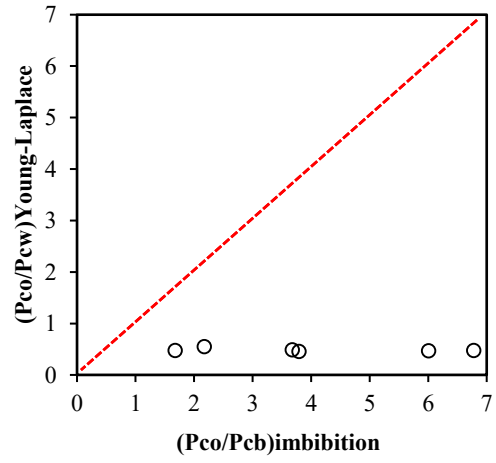


Figure B.2 $(P_{co}/P_{cw})_{Young-Laplace}$ vs. $(P_{co}/P_{cb})_{imbibition}$